Lecture Notes 414.341

선 박 해 양 유 체 역 학

MARINE HYDRODYNAMICS

2019년 6월 28일

Suh, Jung-Chun
서 정 천

Seoul National Univ., Dept. NAOE
서울대학교 공과대학 조선해양공학과

2

MODEL TESTING

2.1 Introduction

2.1.1 Dimensional Analysis

- Buckingham's Pi Theorem
  - With problems where 3 fundamental units are mass (M), length (L) and time (T), the unknown Q and the significant parameters can be expressed in terms of these units.
  - If the unkown Q depends on $N-1$ significant parameters, there will be a total of N interrelated dimensional quantities including Q.
  - The number of independent nondimensional parameters will be reduced by the same number. A total of $N-3$ nondimensional quantities must be interrelated.
- Example: Falling Body in a Vacuum
  - Vertical position y might depend on time t, mass m, the gravitational acceleration g.
    - Vertical position y can not be affected by size and and shape of a falling body.
  - Since neither g nor t contains the units of mass, there is no way of forming the parameters t, m, g into nondimensional parameters

$$\frac{y}{g\,t^2} = C \tag{2.1}$$

    where C is a constant. It is known to be equal to 1/2 from mechanics.
- Example: Pendulum
  - Period of a simple pendulum T: pendulum length l, mass m, gravitational acceleration g, maximum angle of its swing motion θ_0
  - Suitable combination with time units: $T(g/l)^{1/2} = f(\theta_0)$

– If the maximum swing angle is assumed to be small, then the period T tends to a finite limit:

$$T(g/l)^{1/2} = f(0) \tag{2.2}$$

where $f(0)$ is known from mechanics to be 2π.

– In terms of frequency (angular velocity) $\omega = 2\pi/T$, the form is

$$\omega(l/g)^{1/2} = 2\pi/f(\theta_0) \simeq 2\pi/f(0) = 1 \tag{2.3}$$

- Dimensions of Fluid Properties: See Table 2.1.

Table 2.1 Dimensions of fluid properties

Quantities		Dimensions (MLT)	Quantities		Dimensions (MLT)
Angle	θ	None	Mass flow rate	Q	MT^{-1}
Mass	m	M	Strain	ϵ	None
Length	L, l	L	Pressure	p	$ML^{-1}T^{-2}$
Area	A, S	L^2	Stress	$\underline{\tau}$	$ML^{-1}T^{-2}$
Volume	V	L^3	Surface tension	σ	MT^{-2}
Time	t	T	Force	$\underline{F}$	MLT^{-2}
Velocity	$\underline{V}, \underline{q}, \underline{u}$	LT^{-1}	Moment, Torque	$\underline{M}, \underline{Q}$	ML^2T^{-2}
Acceleration	$\underline{a}$	LT^{-2}	Energy, Work	E, W	ML^2T^{-2}
Angular velocity	$\underline{\Omega}, \underline{\alpha}$	T^{-1}	Power	P	ML^2T^{-3}
Angular acceleration	$\dot{\underline{\Omega}}, \dot{\underline{\alpha}}$	T^{-2}	Modulus of elasticity	E	$ML^{-1}T^{-2}$
Density	ρ	ML^{-3}	Dynamic viscosity	μ	$ML^{-1}T^{-1}$
Momentum	$\underline{L}$	MLT^{-1}	Kinemtaic viscosity	ν	L^2T^{-1}
Angular momentum	$\underline{H}$	ML^2T^{-1}	Moment of inertia(area)	I	L^4
Volume flow rate	Q	L^3T^{-1}	Moment of inertia(mass)	I	ML^4

2.1.2 Flow Similarity and Model Studies

- Geometric Similarity

  - Model and prototype have same shape.
  - Linear dimensions on model and prototype correspond within constant scale factor.

- Kinematic Similarity
  - Velocities at corresponding points on model and prototype differ only by a constant scale factor.

- Dynamic Similarity
  - Forces on model and prototype differ only by a constant scale factor.

- Incomplete Similarity
  - Sometimes complete similarity cannot be obtained, but phenomena may still be successfully modelled.

2.1.3 Nature of Dimensional Analysis: Example

- Drag on a Sphere
  - Drag depends on 4 parameters: sphere size, speed, fluid density, fluid viscosity
$$F = f(D, V, \rho, \mu) \tag{2.4}$$
  - Difficult to know how to set up experiments to determine dependencies
  - Difficult to know how to present results (four graphs?)

- Take the dimensional analysis for $F = f(D, V, \rho, \mu)$

$$\boxed{\frac{F}{\rho V^2 D^2} = f_1\left(\frac{\rho V D}{\mu}\right)} \tag{2.5}$$

– If dynamic similarity $\left(\frac{\rho V D}{\mu}\right)_{\text{model}} = \left(\frac{\rho V D}{\mu}\right)_{\text{full scale}}$ is satisfied, $\left(\frac{F}{\rho V^2 D^2}\right)_{\text{model}} = \left(\frac{F}{\rho V^2 D^2}\right)_{\text{full scale}}$ would hold. [1]

– Only one dependent and one independent variable

– Easy to set up experiments to determine dependency

– Easy to present results (one graph) (See Figure 2.1)

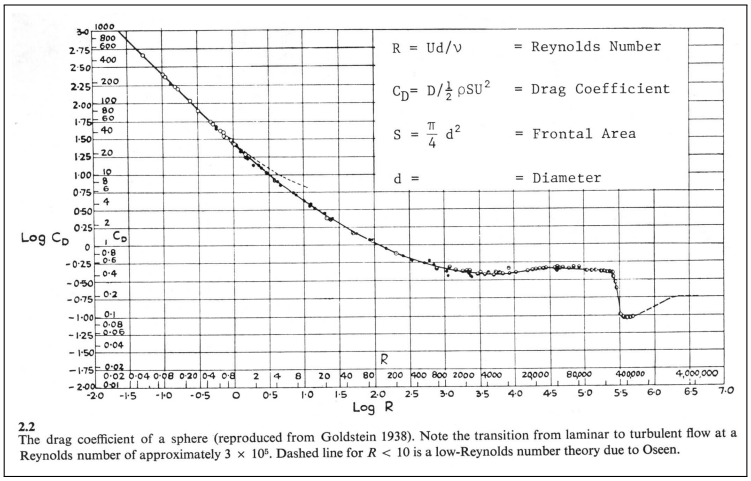

Figure 2.1 The drag coefficient of a sphere. (From Newman 1977)

2.1.4 Significant Dimensionless Numbers

- Reynolds Number $Re = \frac{\rho V L}{\mu} = \frac{V L}{\nu}$
- Froude Number $Fr = \frac{V}{\sqrt{gL}}$
- Cavitation Number $Ca = \frac{p - p_v}{\frac{1}{2}\rho V^2}$
- Mach Number $M = \frac{V}{c}$

[1] Movie: Dimensional analysis for drag on sphere
./mmfm_movies/542.mov ./mmfm_movies/540.mov ./mmfm_movies/541.mov

- Strouhal Number $S = \dfrac{fL}{V}$
- Weber Number $We = \dfrac{\rho V^2 L}{\sigma}$

2.1.5 Error Estimates in Uncertainty Analysis

- Error = Measured Value – True Value
  True Value: How to know?
  Known in calibration systems? (or still unknown?)

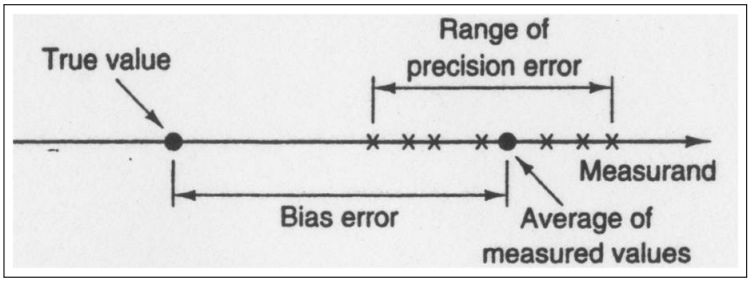

Figure 2.2 Definition of bias and precision error.

- Total error = Bias error + Precision error
  Bias error (fixed or systematic error) = average of measured values – true value
  Precision error (random error) = measured values – average of measured values

- Measurement Error and Population

2.1.6 Flow Visualization

- Smoke, Dye [2]

[2] Movie: 2-D Cavity Flow, Juncture Flow, Finite Cyliner, Airplane Tip Vortex Flow
./mmfm_movies/166.mov ./mmfm_movies/1.mov ./mmfm_movies/468.mov
./mmfm_movies/4275.mov ./mmfm_movies/4292.mov

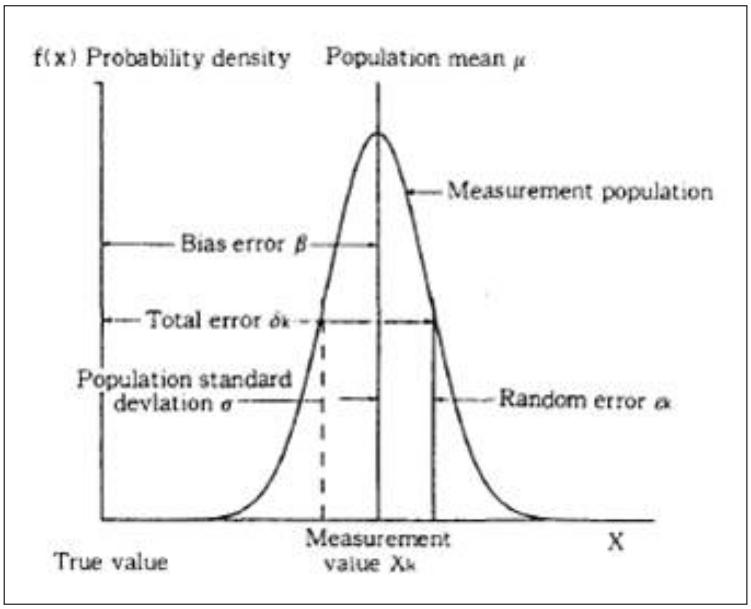

Figure 2.3 Probability error estimates.

- Laser: Laser Doppler Velocimetry (LDV), Particle Image Velocimetry (PIV) [3]
  - Example: Stereoscopic PIV system for cavitation tunnel at SNU

2.2 Drag Force on a Sphere

2.2.1 Dimensional Analysis

- The drag force D must be a function of the diameter (d), the sphere velocity (U), the fluid density (ρ), and the kinematic viscosity (ν):

$$D = f(d, U, \rho, \nu) \tag{2.6}$$

- Nondimensionalization these 5 parameters yields 2 nondimensional quantities, which can be expressed in the form

$$\frac{D}{\rho U^2 d^2} = f\left(\frac{Ud}{\nu}\right) \tag{2.7}$$

[3] Movie: Concept of PIV system
./mmfm_movies/4582.mov

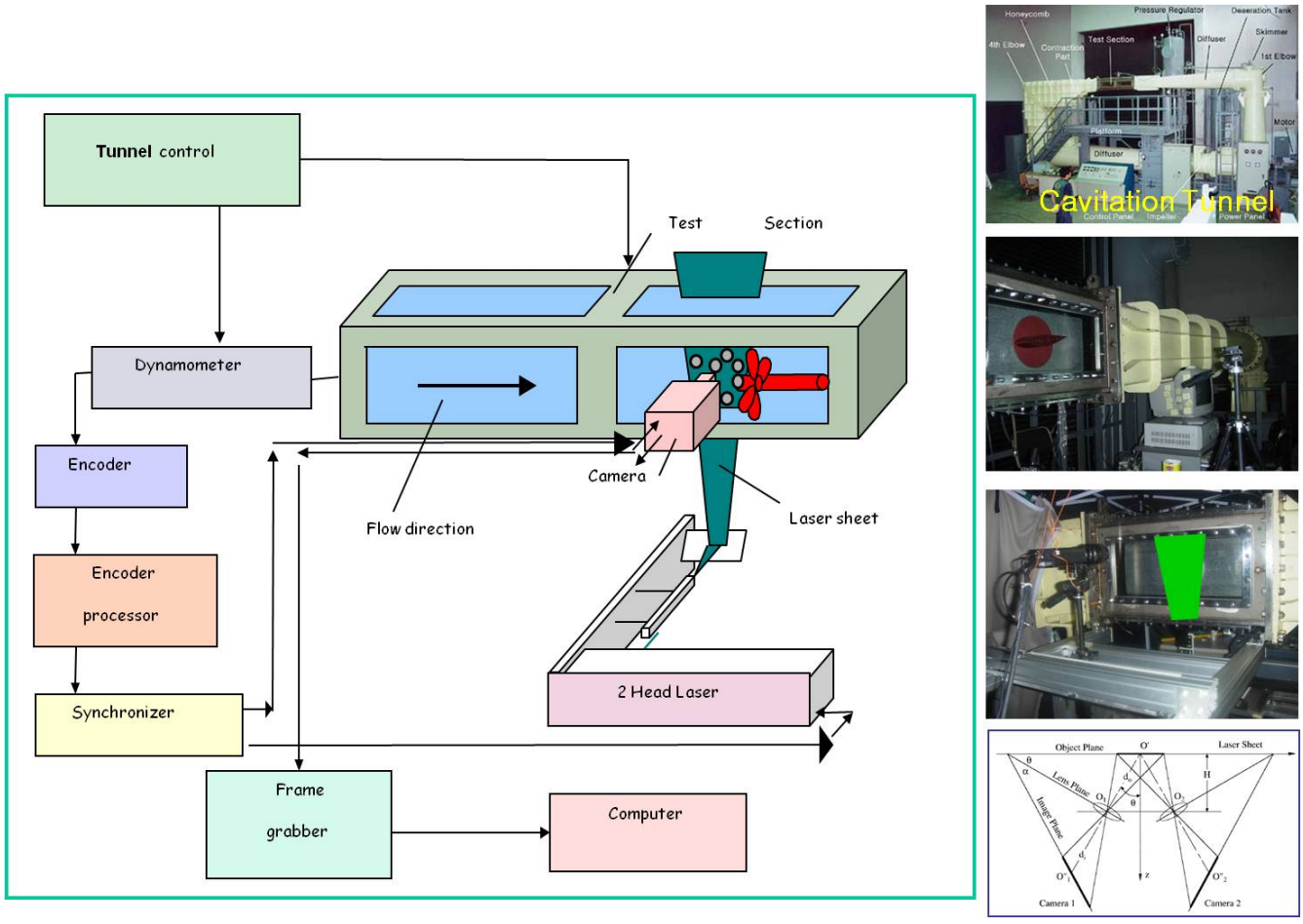

Figure 2.4 Typical PIV system for cavitation tunnel.

where $R = \dfrac{Ud}{\nu}$ is the Reynolds number based on the sphere diameter.

- The drag coefficient C_D can be written in a more conventional form:

$$\frac{D}{\frac{1}{2}\rho U^2 S} = C_D(R) \tag{2.8}$$

where $S = \pi d^2/4$ is the frontal area of the sphere.

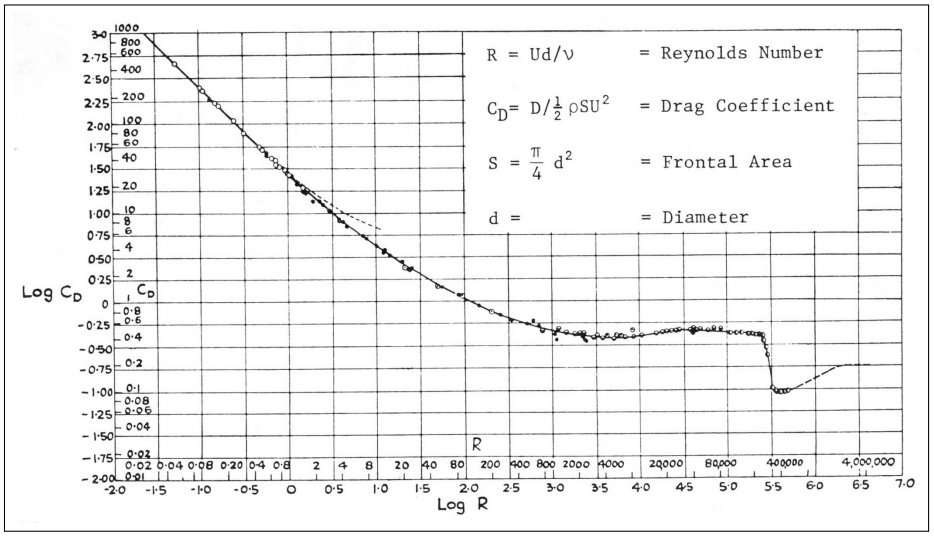

Figure 2.5 The drag coefficient of a sphere. (From Newman 1977)

2.2.2 Pressure Drag Variation with Reynolds Numbers

- For moderate Reynolds number ($10^3 \sim 3\times10^5$), the dominant contribution to the drag force is due to separation, which occurs near the midplane of the sphere.
  - A substantial pressure difference between the forebody and afterbody contributes to the drag force:

$$\text{Drag} \sim \text{Projected(Frontal) area} \times (p_s - p_\infty) = \left(\frac{1}{2}\rho U^2\right) S\, C_D \tag{2.9}$$

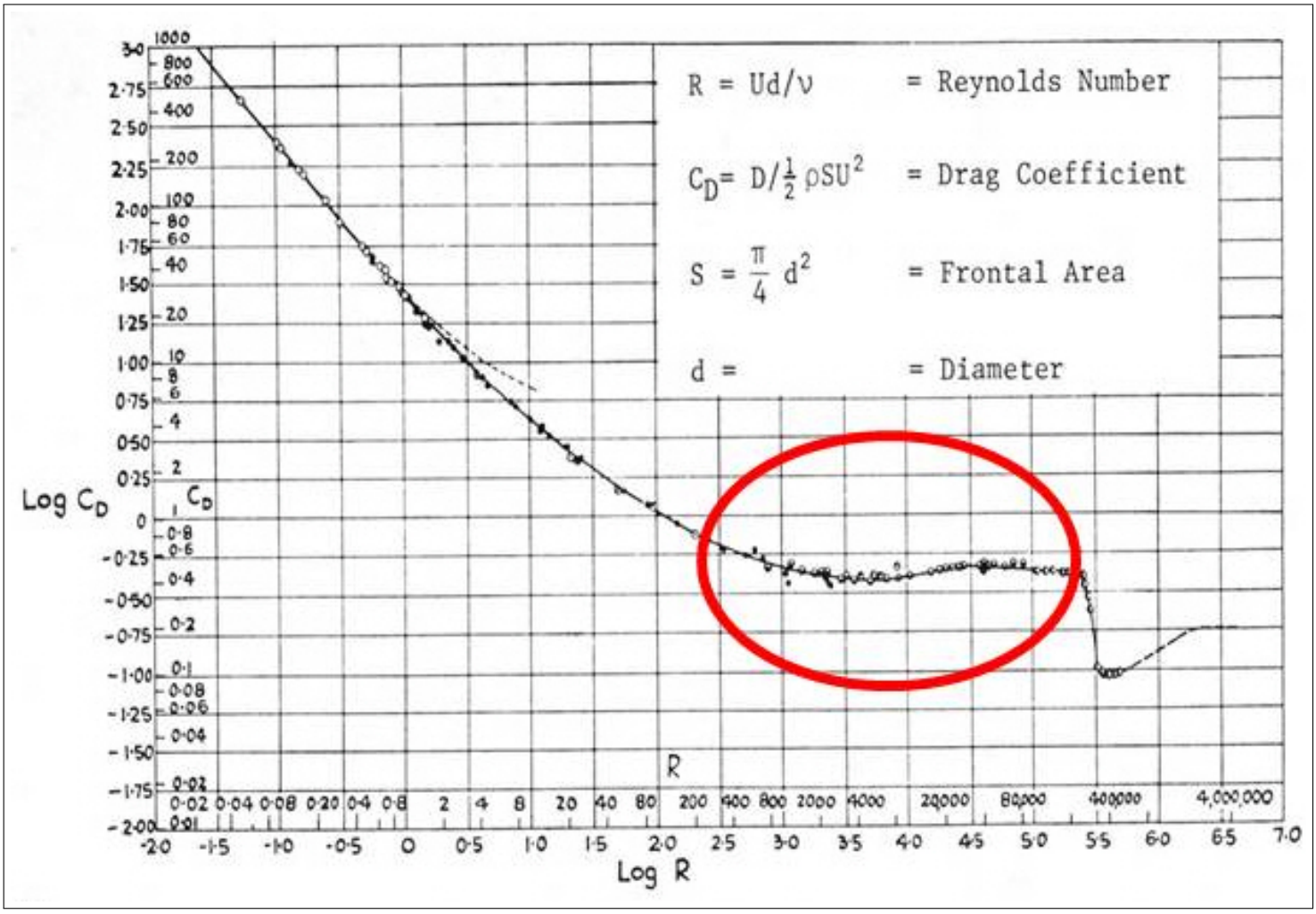

Figure 2.6 The drag coefficient of a sphere for moderate Reynolds number.

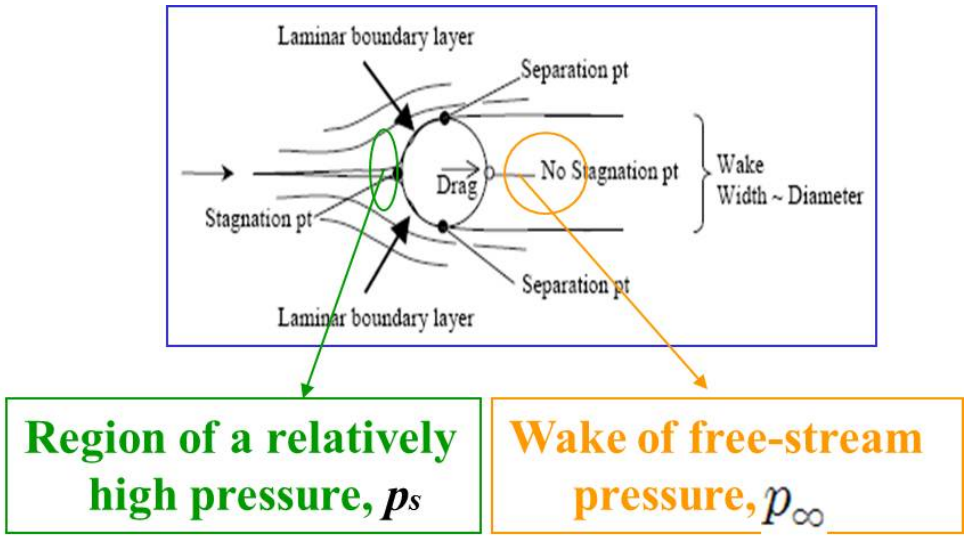

Figure 2.7 Wake of a sphere for moderate Reynolds number.

- At a critical Reynolds number (3×10^5), the boundary layer becomes turbulent, and the increase of momentum convection delays separation.

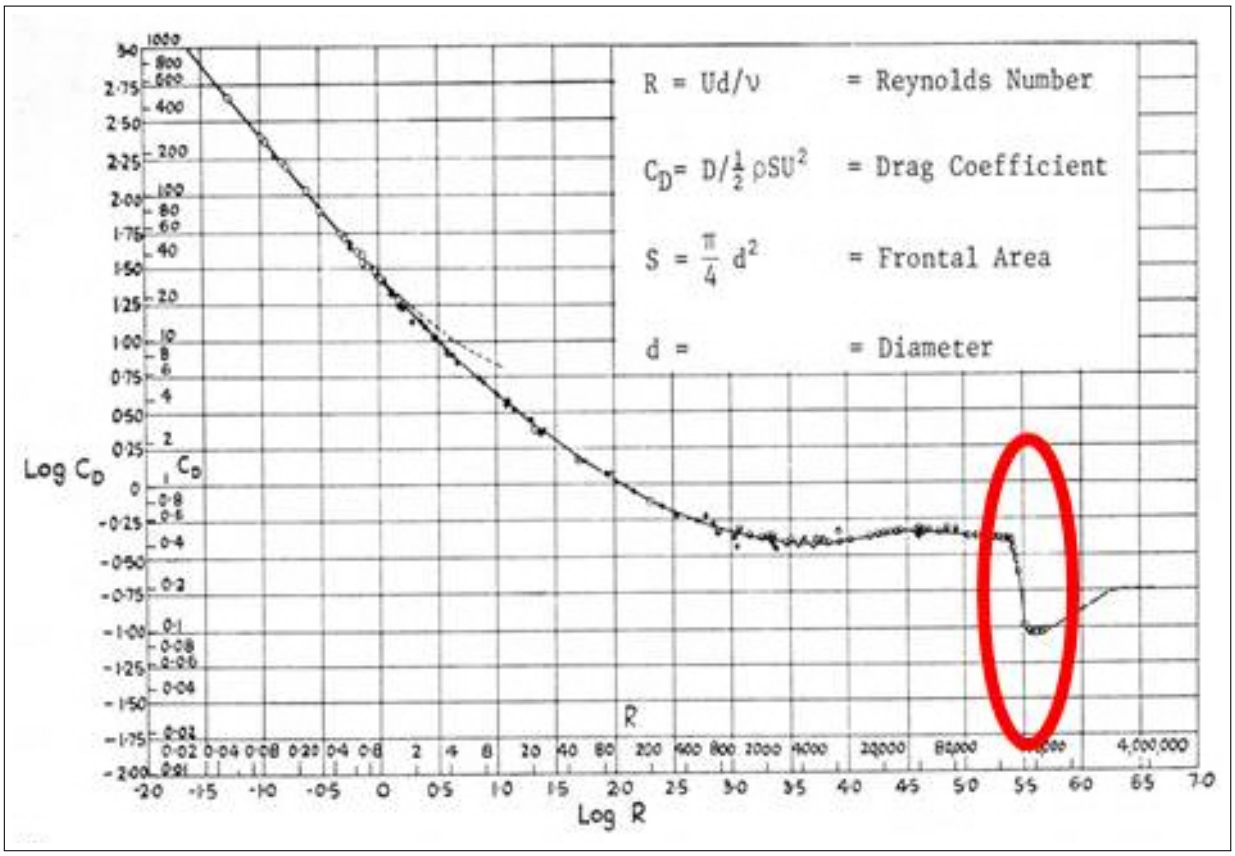

Figure 2.8 The drag coefficient of a sphere at critical Reynolds number.

  - The separated wake region is diminished and the drag is reduced dramatically.
  - Example: Golf ball and Turbulence simulator [4]

2.3 Viscous Drag on a Flat Plate

2.3.1 Dimensional Analysis for Frictional Drag

- Consider a flat plate of length l, breadth B, and negligible thickness, moving with velocity U in the longitudinal direction parallel to its length di-

[4] Movie: Laminar(without trip wire) and turbulent wake(with trip wire) of a sphere
./mmfm_movies/spheredragcombo2.mov

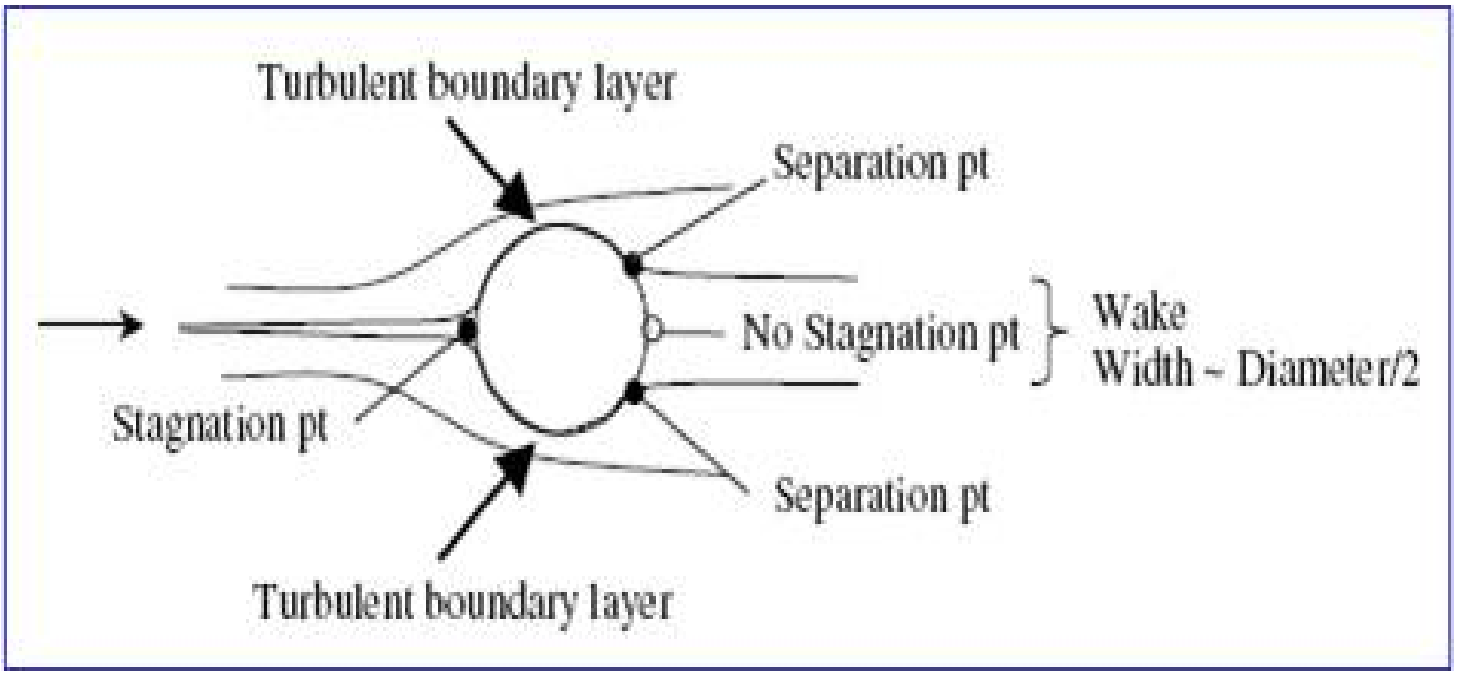

Figure 2.9 Wake of a sphere at critical Reynolds number.

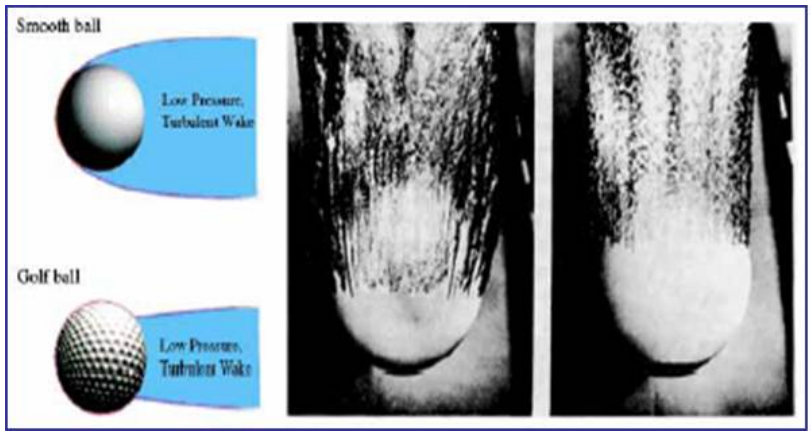

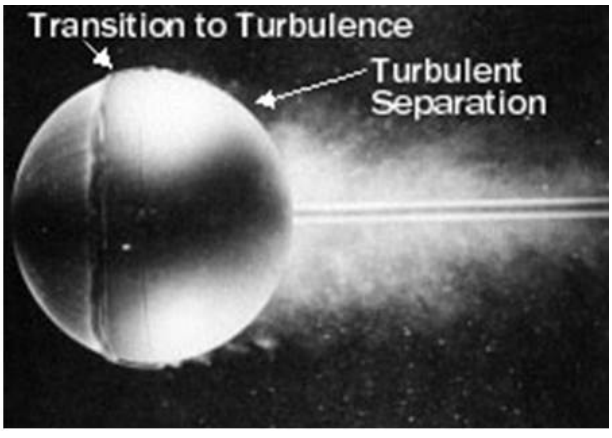

Figure 2.10 Wake of a sphere at critical Reynolds number.

mension.

- The drag coefficient is expressed as

$$\frac{D}{\frac{1}{2}\rho U^2 S} = C_D(R, B/l) \tag{2.10}$$

where S is the surface area of the plate.

- For Reynolds numbers on $O(10^5 \sim 10^{10})$, the drag coefficient is insensitive to the ratio B/l.

- Experimentally determined *frictional-drag* coefficients C_F for various flat plates are fitted with the semi empirical equation determined by Schoenherr (refer to p. 115 of Newman (1977) for details):

$$0.242/\sqrt{C_F} = \log_{10}(R\,C_F) \tag{2.11}$$

  - Validity of dimensional analysis is confirmed by the collapse of data from diverse experiments both in water and air.

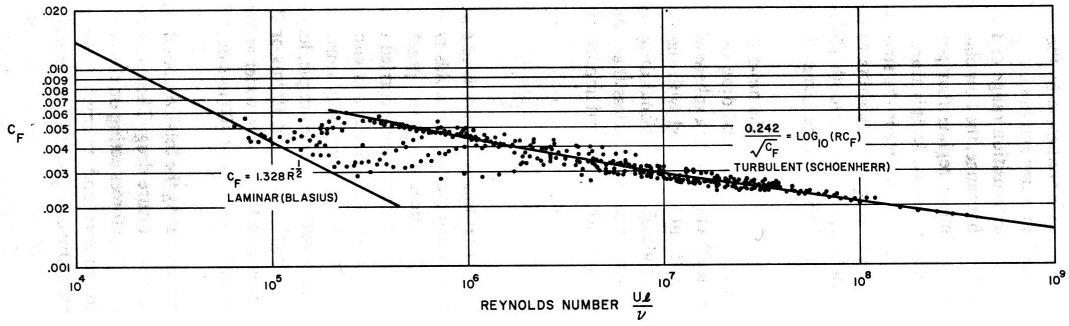

2.3
Schoenherr's flat-plate frictional drag coefficient, compared with various experimental results and the Blasius boundary-layer theory. Note that transition occurs between $R = 10^5$ and 2×10^6, depending on the plate roughness and ambient turbulence. For references to the experimental data see Todd (1967), figure 3.

Figure 2.11 Schoenherr's flat-plate frictional drag coefficient. (From Newman 1977)

2.3.2 Transition Range of Reynolds Numbers

- In the transition range of Reynolds numbers ($10^5 \sim 10^6$), there is a scatter data. [5]

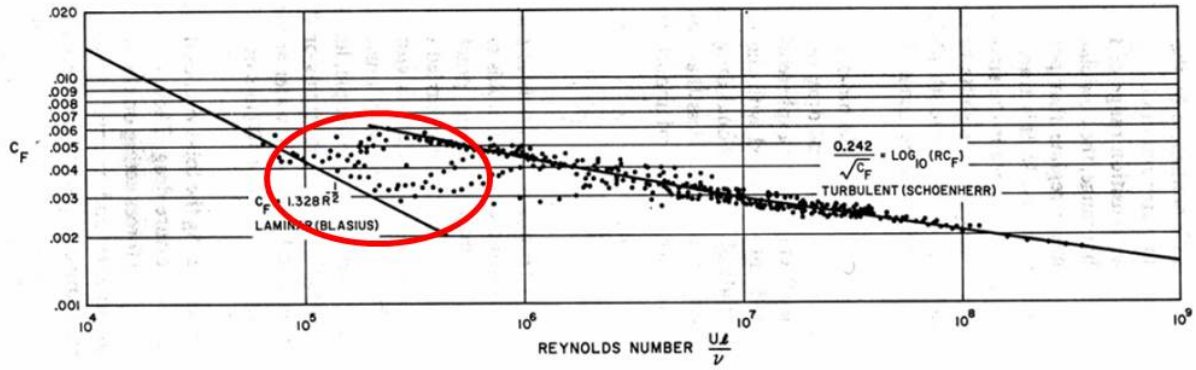

2.3
Schoenherr's flat-plate frictional drag coefficient, compared with various experimental results and the Blasius boundary-layer theory. Note that transition occurs between $R = 10^5$ and 2×10^6, depending on the plate roughness and ambient turbulence. For references to the experimental data see Todd (1967), figure 3.

Figure 2.12 Transition from laminar to turbulent flow for a flat plate drag coefficient. (From Newman 1977)

  - The flow changes from a smooth laminar regime to the turbulent regime.
  - An important mechanism that triggers turbulence is the smoothness of the body surface.
  - The drag of rough plates shifts to the turbulent value at lower Reynolds number.
  - For very smooth plates, laminar flow can be maintained longer.

- The consequence is to increase the momentum defect of the boundary layer and the resulting frictional drag on the flat plate.
  - Note: Opposite to the effects noted for a sphere where the dramatic decrease in drag is significant. (See Figure **2.8**)
  - The frictional drag coefficient is $O(1/100)$ of magnitude less than that of the drag coefficient for a sphere: the importance of streamlined body shape.

[5] Movie: Transition from laminar to turbulent flow
./mmfm_movies/5021.mov

2.4 Viscous Drag on General Bodies

2.4.1 Infeasible Tests of Geosims

- The drag on general bodies can be determined from tests of *geosims*, if Reynolds number for model and full-scale bodies is the same.
  - However it is difficult to find liquids less viscous than water.
  - The ratio of model velocity to full-scale velocity must be inversely proportional to the ratio of the lengths.
  - (Example) Let us consider a ship of 100 m length, moving at 10 m/s. If a 10 m model is to be tested in water at the same Reynolds number, it must move with a velocity of 100 m/s. **Not feasible in conventional facilities!**

2.4.2 Frictional Drag and Pressure Drag

- Usually the total drag is separated into 2 components, *frictional drag* and *pressure drag*: longitudinal components of forces acting on a body due to tangential shear stresses and normal pressure stresses, respectively.
  - Assumption 1: *The frictional drag* due to the tangential shear stress is affected by the Reynolds number only, and is equal to that of a flat plate of equal area and Reynolds number.

$$\boxed{D_f = \underline{i} \cdot \int_{\text{surface}} \tau \, \underline{t} \, dS} \tag{2.12}$$

  - Assumption 2: *The pressure drag* (also called *the form drag*) depends on the form of body. For a streamlined body, the pressure drag is independent of Reynolds number over the range where boundary layer is thin, typically for $Re > 10^5$.

$$\boxed{D_p = \underline{i} \cdot \int_{\text{surface}} (-p) \, \underline{n} \, dS} \tag{2.13}$$

– If the body has sharp edges not aligned with the flow, separation will occur at these edges irrespectively of Reynolds number.

– For example, a circular disc or a flat plate moving normal to the flow will experience separation at the periphery. [6]

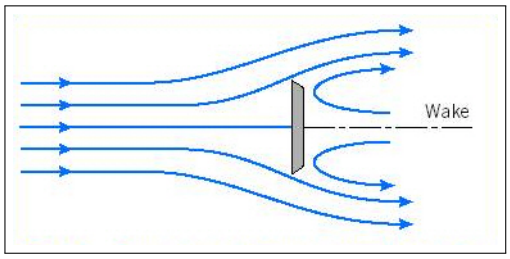

Figure 2.13 Flow over a flat plate normal to inflow. (From Fox, McDonald & Pritchard 2004)

- With these assumptions, the total drag coefficient can be written in the form $C_D(R) = C_F(R) + C_P$.

- For bodies with thickness-length ratio less than 0.2. the frictional drag is dominant.

- Conflicting roles of transition to turbulence: decrease of drag for bluff bodies and increase of drag for fined bodies.

- Contributions of frictional drag and pressure drag to total drag as a function of thickness-length ratio.

- Variation of drag coefficients of a cylinder and a sphere with Reynolds number. [7]

[6] Note: C. Mimeau, I. Mortazavi and G.-H. Cottet (2014), "Passive Flow Control Around a Semi-Circular Cylinder Using Porous Coatings," International Journal of Flow Control, 6, 43-50. *On a ground vehicle, the outside mirrors, due to their spanwise position, indeed generate a non-negligible wake which interferes with the flow past car sides. They are responsible of up to 10% of the total vehicle drag but they only represent 0.5% of the total projected surface.*

[7] Movie: Cylinder(CFD), Cylinder(Visualization), Sphere(Laminar & Turbulent)
./mmfm_movies/Cylinder.mov ./mmfm_movies/146.mov
./mmfm_movies/spheredragcombo2.mov

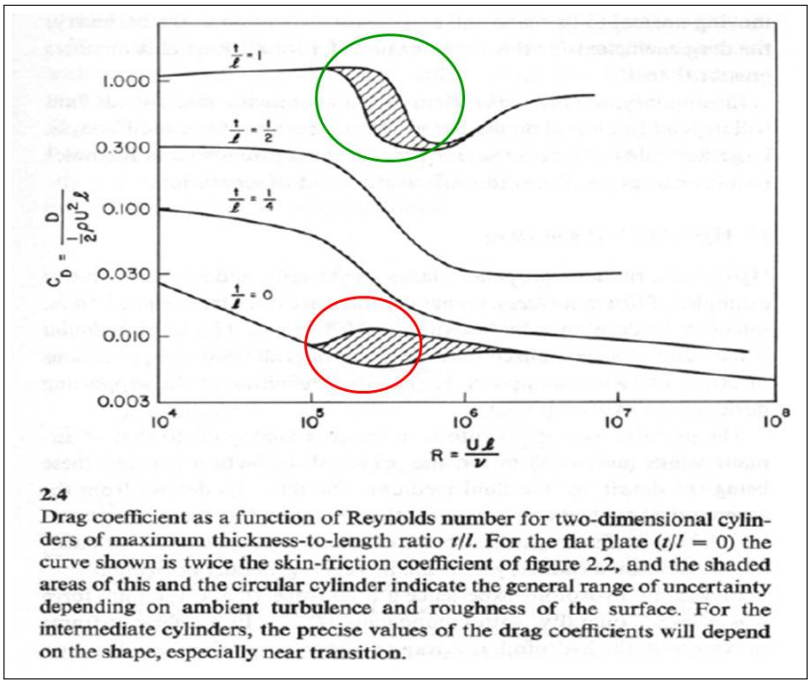

2.4
Drag coefficient as a function of Reynolds number for two-dimensional cylinders of maximum thickness-to-length ratio t/l. For the flat plate ($t/l = 0$) the curve shown is twice the skin-friction coefficient of figure 2.2, and the shaded areas of this and the circular cylinder indicate the general range of uncertainty depending on ambient turbulence and roughness of the surface. For the intermediate cylinders, the precise values of the drag coefficients will depend on the shape, especially near transition.

Figure 2.14 Drag coefficient for two-dimensional cylinders. (From Newman 1977)

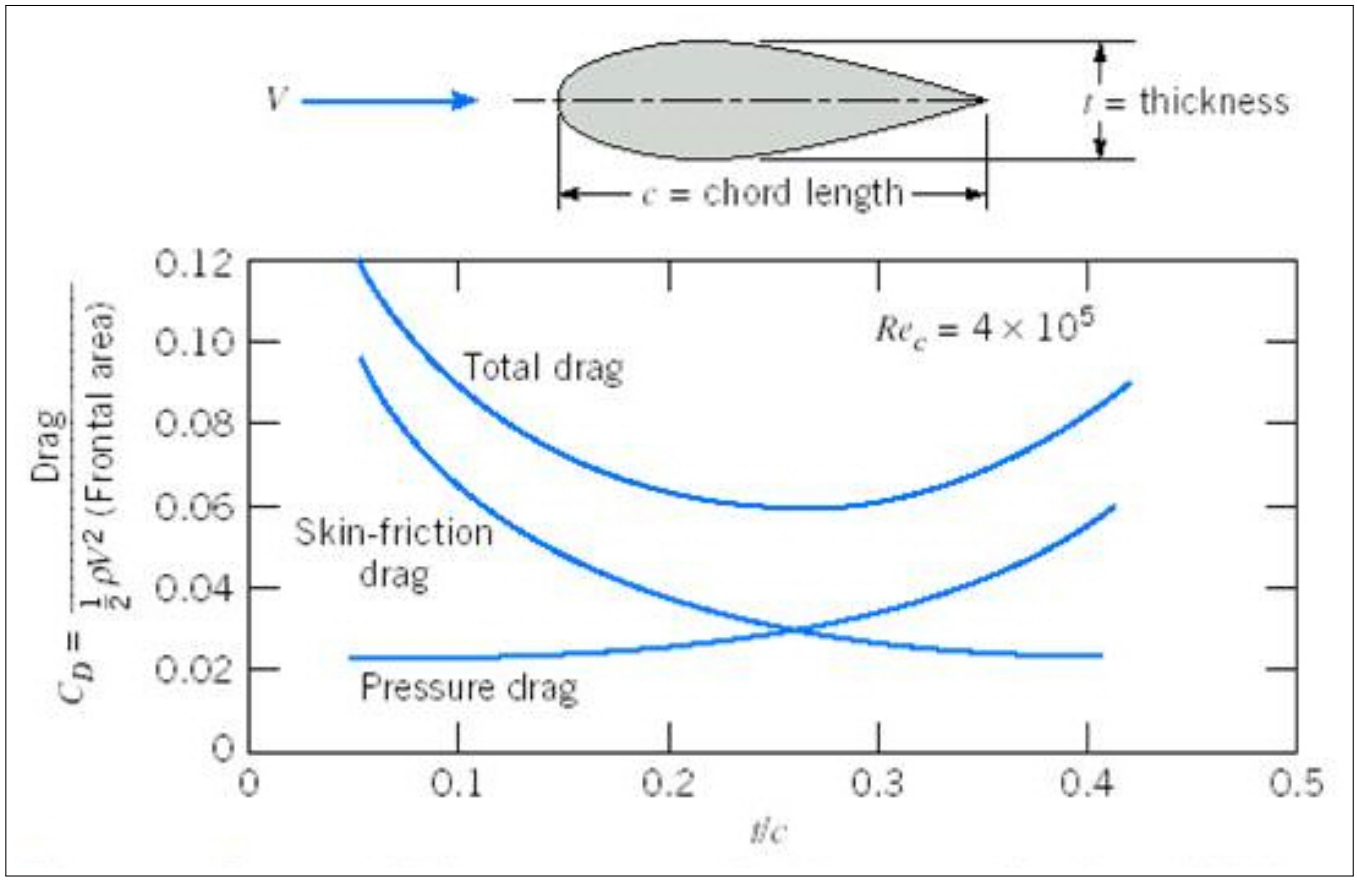

Figure 2.15 Drag on a strut: Contributions of frictional drag and pressure drag to total drag as a function of thickness-length ratio. (From Fox, McDonald & Pritchard 2004)

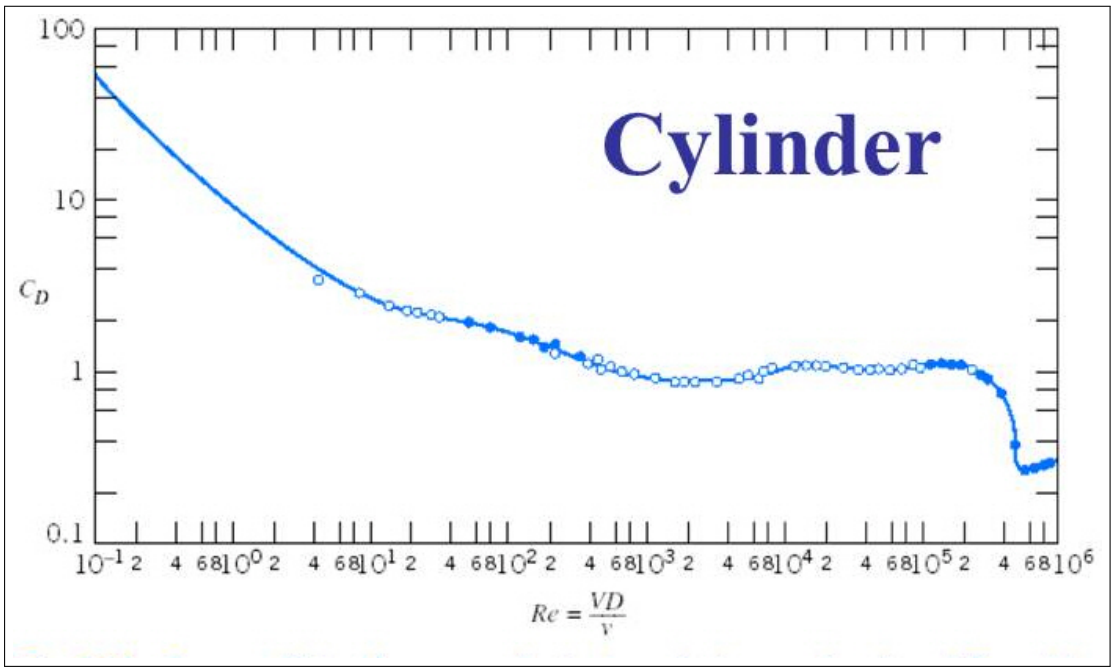

Figure 2.16 Drag coefficient for a circular cylinder. (From Fox, McDonald & Pritchard 2004)

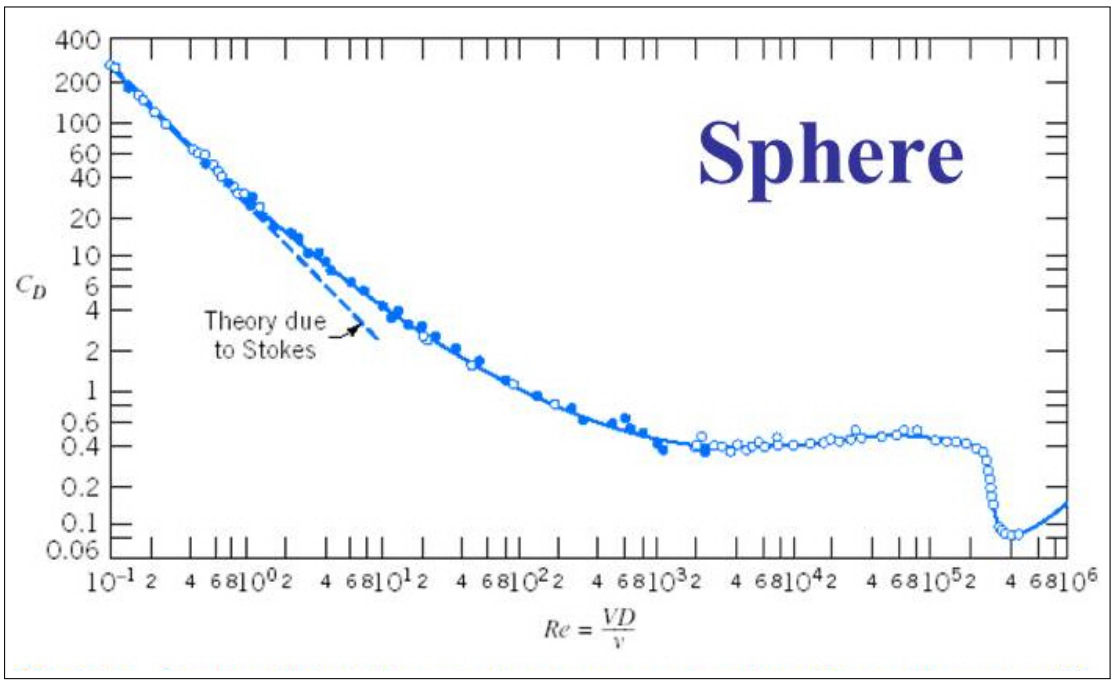

Figure 2.17 Drag coefficient for a sphere. (From Fox, McDonald & Pritchard 2004)

2.5 Hydrofoil Lift and Drag

2.5.1 Lifting Surfaces

- Streamlined planar bodies
  - Viscous effects to thin boundary layer
  - Characteristic length: chord length (in 3-dimensions, span as well)
  - Aspect ratio of span to mean chord,

$$A = s^2/S \tag{2.14}$$

where s = span; S = planform area (projected area on the plane $y = 0$) = (chord) x (span).

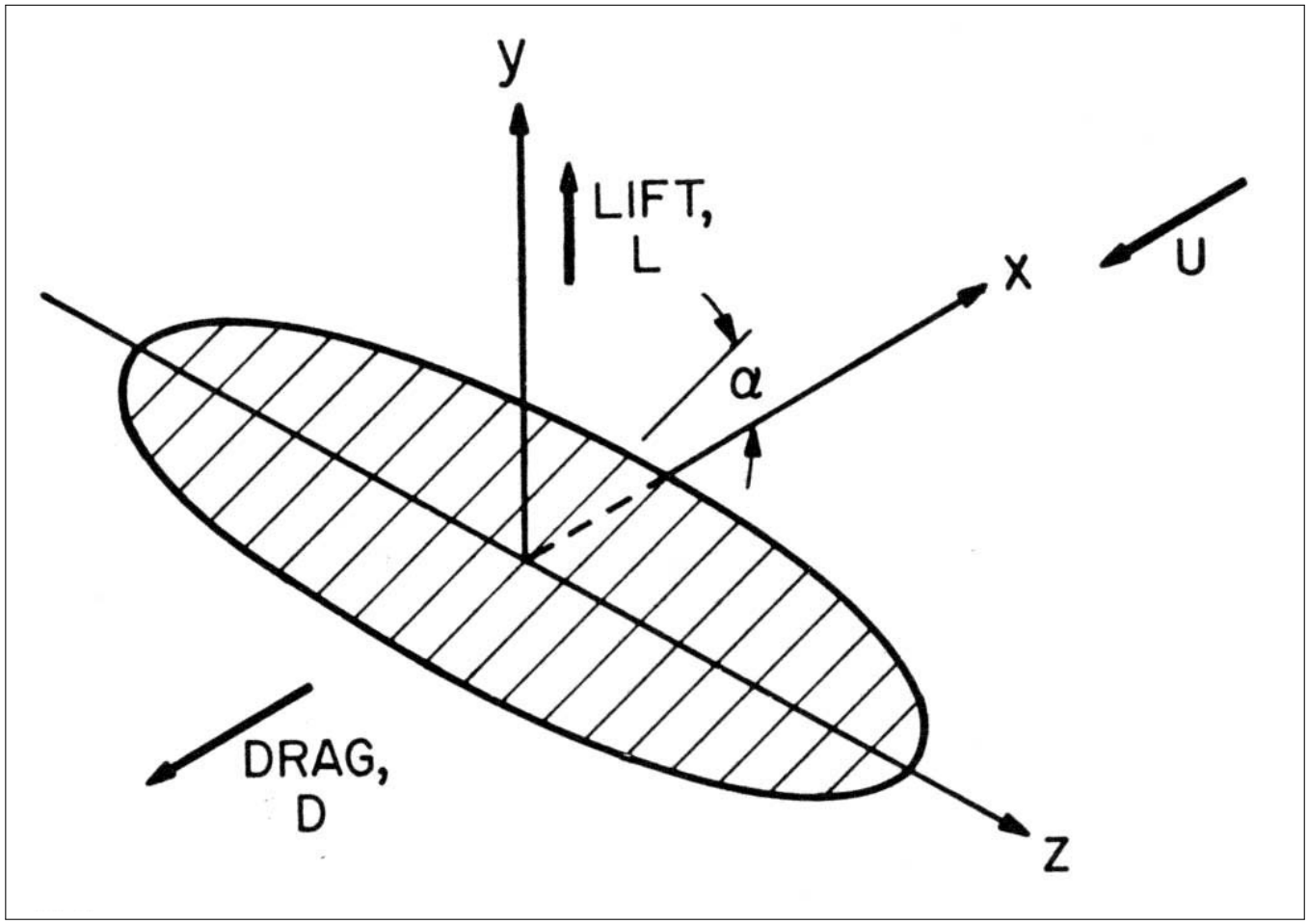

Figure 2.18 Three-dimensional lifting surface. (From Newman 1977)

- High aspect ratio: 2-D
  - 2-dimensional hydrofoil sections experience a drag force D, and lift force L.
  - Linearized thin-foil/wing theory for small angle of attacks

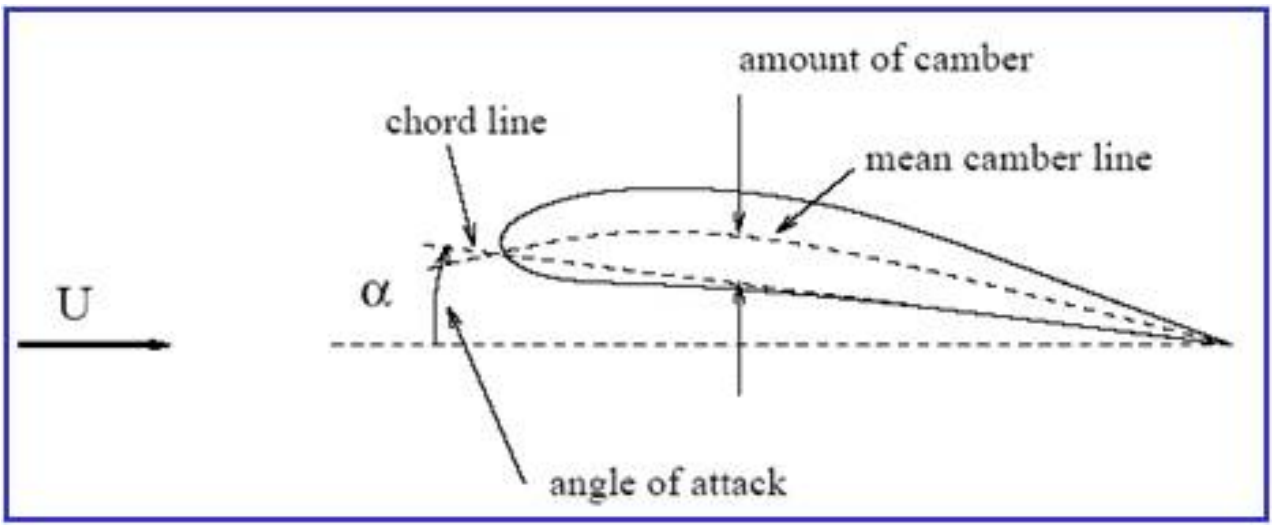

Figure 2.19 Geometry of a hydrofoil section.

- Lift Generation: Kutta Condition
  - Potential flow without circulation
  - Circulation around foil moves stagnation point back at the trailing edge(T.E.)

- Dimensional analysis for drag and lift forces with 5 parameters of planform ares S, velocity U, angle of attack α, fluid density ρ, and kinematic viscosity ν:

$$\frac{L}{\frac{1}{2}\rho U^2 S} = C_L(R,\alpha), \quad \frac{D}{\frac{1}{2}\rho U^2 S} = C_D(R,\alpha) \tag{2.15}$$

where l is used to define the Reynolds number $R = Ul/\nu$.

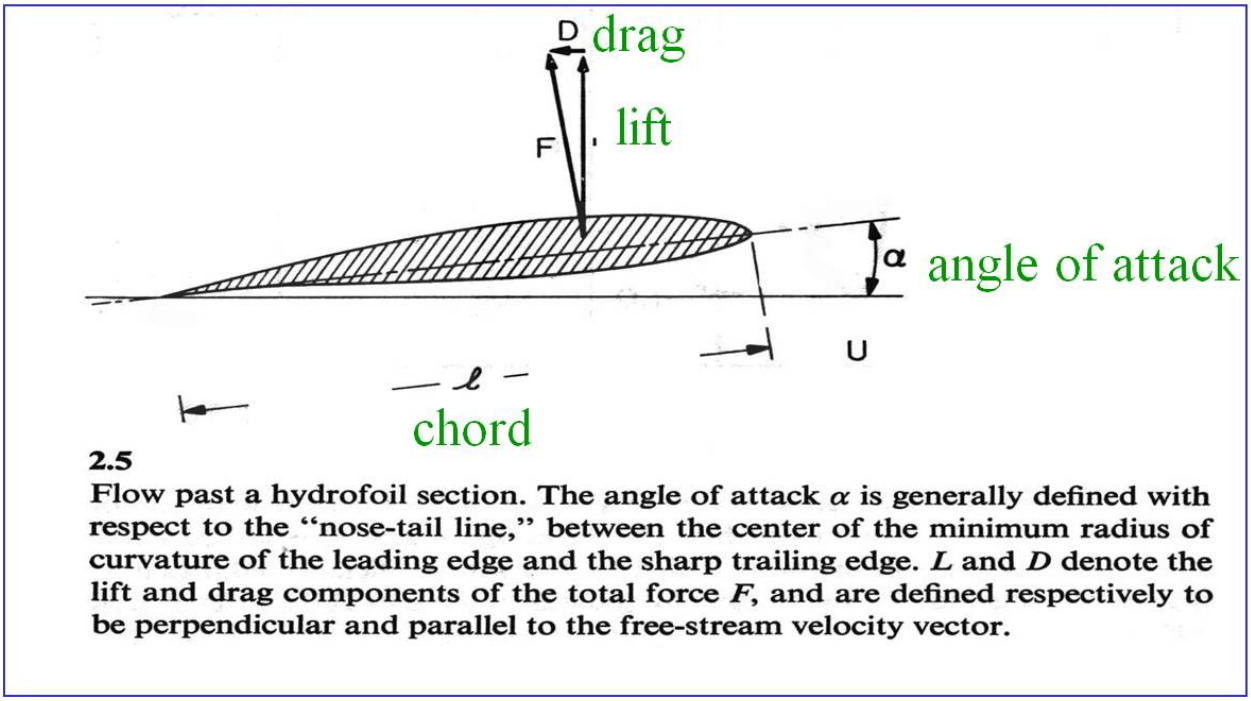

2.5
Flow past a hydrofoil section. The angle of attack α is generally defined with respect to the "nose-tail line," between the center of the minimum radius of curvature of the leading edge and the sharp trailing edge. L and D denote the lift and drag components of the total force F, and are defined respectively to be perpendicular and parallel to the free-stream velocity vector.

Figure 2.20 Flow past a hydrofoil section. (From Newman 1977)

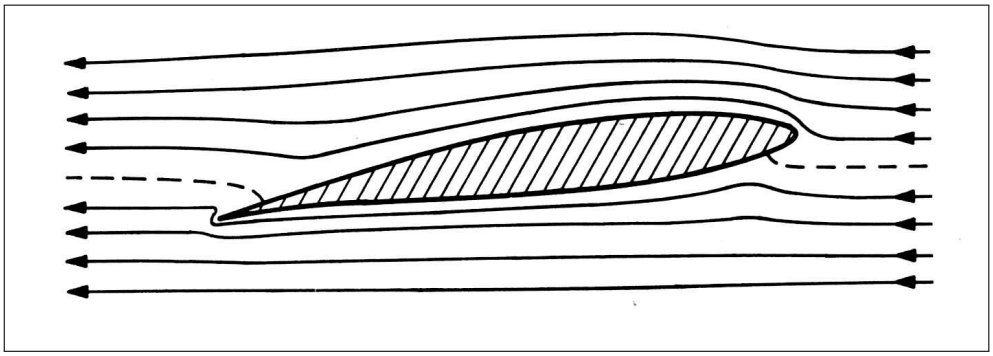

Figure 2.21 Flow past a foil without circulation. (From Newman 1977)

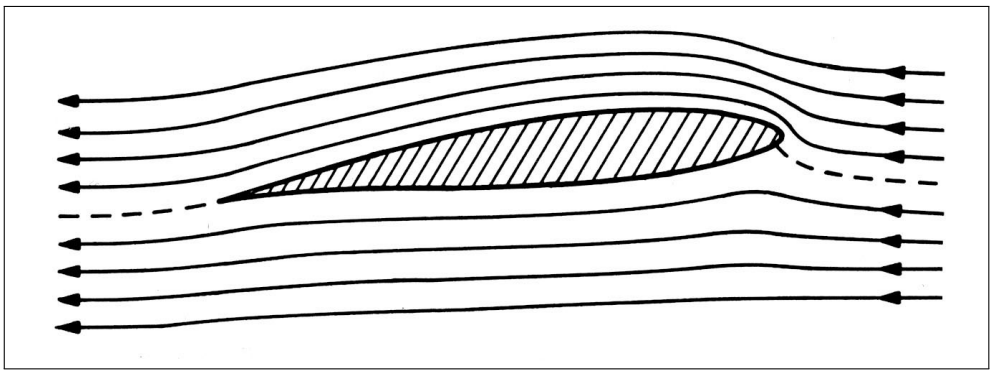

Figure 2.22 Assumed flow past a foil with circulation. (From Newman 1977)

2.5.2 Lift and Drag on Hydrofoil

- For hydrofoils with large aspect ratio (i.e., large span relative to chord), the total 3-D force can be estimated by integration of the *sectional* lift and drag along span.
- Lift coefficient is assumed to depend only on the angle of attack, and to be independent of the Reynolds number:
  - For small angles of attack, the lift coefficient is insensitive to the Reynolds number and increases in a linear manner with angle of attack.
  - As the angle of attack increases, the streamlined effect of diminishes and stall occurs with a dramatic reduction in the lift coefficient.
  - The stall position is sensitive to the Reynolds number, ambient turbulence, roughness of surface.

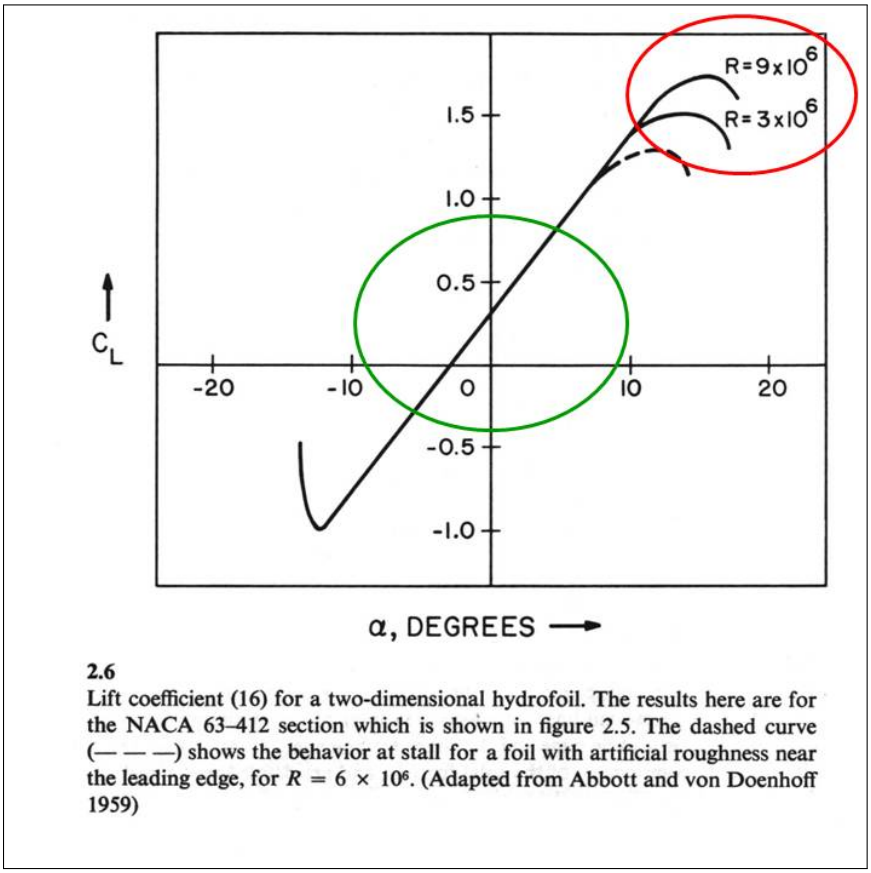

2.6
Lift coefficient (16) for a two-dimensional hydrofoil. The results here are for the NACA 63–412 section which is shown in figure 2.5. The dashed curve (— — —) shows the behavior at stall for a foil with artificial roughness near the leading edge, for $R = 6 \times 10^6$. (Adapted from Abbott and von Doenhoff 1959)

Figure 2.23 Lift coefficient for a two-dimensional hydrofoil. (From Newman 1977)

- Lift Characteristics of Hydrofoils [8]

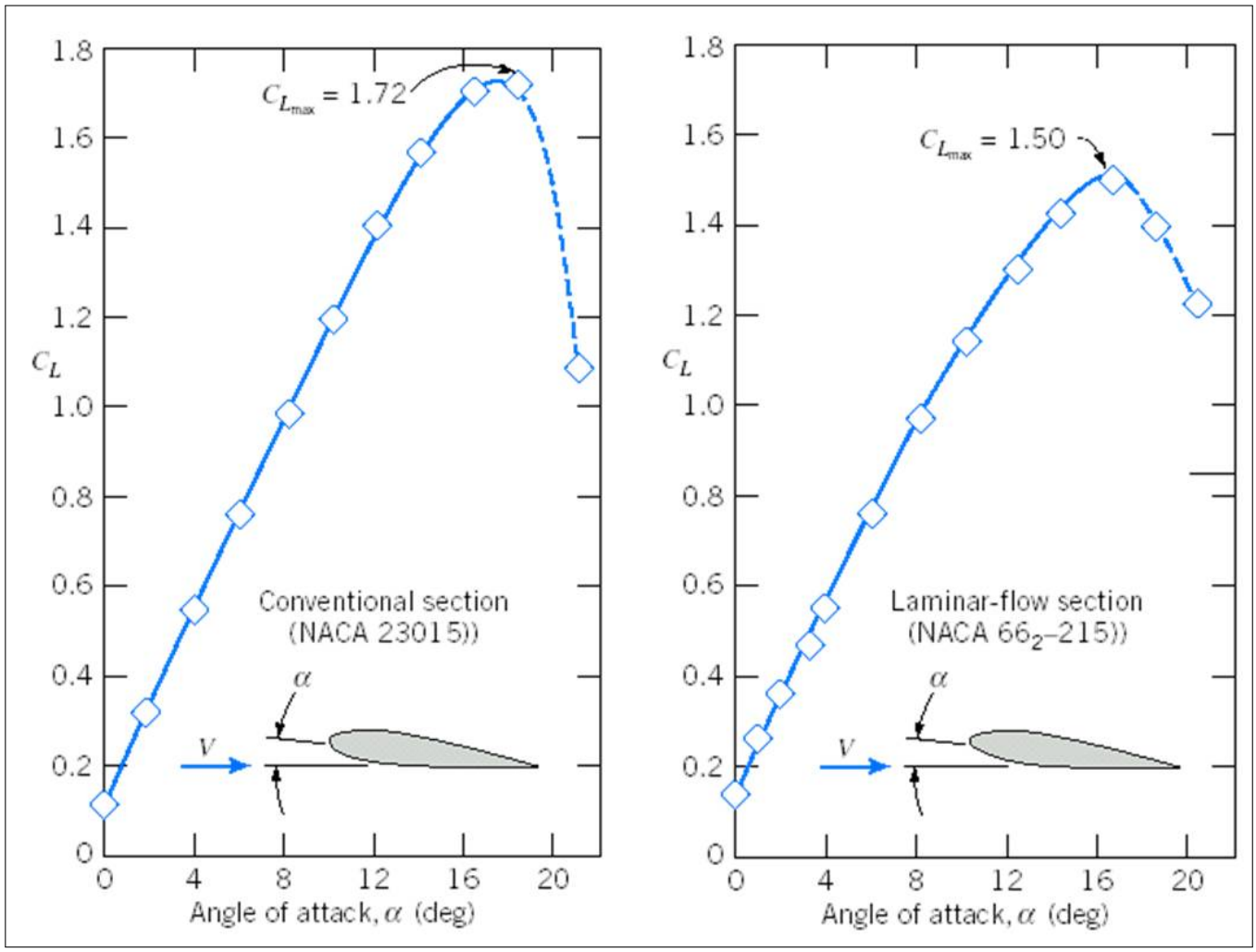

Figure 2.24 Lift characteristics of hydrofoils. (From Fox, McDonald & Pritchard 2004)

- The drag is assumed to be separated into 2 components: the frictional drag of a flat plate at zero angle of attack accounting for the Reynolds number dependence, and the pressure drag depending only on the angle of attack:

$$C_D(R, \alpha) = C_F(R) + C_P(\alpha) \tag{2.16}$$

[8] Movie: Lift Characteristics of Hydrofoils, CFD
./mmfm_movies/air_foil_00_deg.mov ./mmfm_movies/air_foil_05_deg.mov
./mmfm_movies/air_foil_10_deg.mov ./mmfm_movies/air_foil_15_deg.mov
./mmfm_movies/air_foil_20_deg.mov ./mmfm_movies/air_foil_25_deg.mov
./mmfm_movies/air_foil_60_deg.mov ./mmfm_movies/Airfoil1.mov
./mmfm_movies/kunio_flow.mov

  - For small positive or negative angles of attack where the lift force is small, the drag coefficient is insensitive to the Reynolds number and takes a value comparable to the flat plate frictional drag coefficient.
  - As the stall approached, the drag goes up remarkably and very sensitive to the Reynolds number.
  - The magnitude of the drag is much smaller than the lift.

2.5.3 Remarks: Induced Drag for 3-D Lifting Surfaces

- Induced velocity by trailing vortex system [9]
- Downwash effect :
  - Effective angle of attack:

$$\boxed{\alpha_{\text{effective}} = \alpha - \alpha_{\text{induced}}} \tag{2.17}$$

  - Additional induced drag component:

$$D = D_f + D_p + \boxed{D_{\text{induced}}} \tag{2.18}$$

  - Drag components for lifting bodies:

$$\begin{aligned} \text{Total drag} &= \text{Profile drag} + \text{Induced drag} \\ &= \text{Frictional drag} + \text{Pressure drag} + \text{Induced drag} \end{aligned}$$

2.6 Screw Propeller

- Characteristics of Marine Propellers
  - Complex Geometry: low aspect ratio, skewed/raked geom, boss, compound devices

[9] Movie: Wing tip vortex of a plane and a car
./mmfm_movies/wingtip_vortex.mov ./mmfm_movies/3629.mov
./mmfm_movies/3618.mov

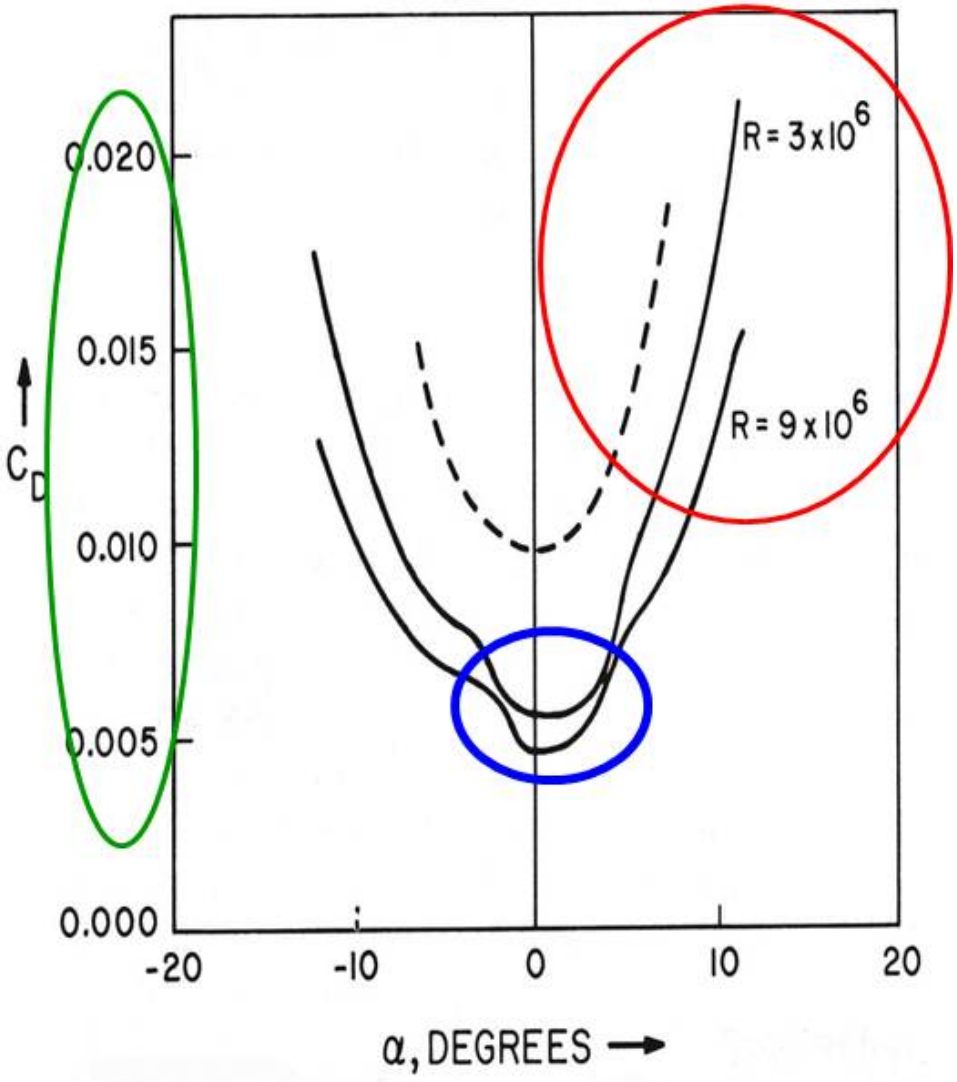

2.7
Drag coefficient (17) for the NACA 63–412 section as described in figure 2.6. (Adapted from Abbott and von Doenhoff 1959)

Figure 2.25 Drag coefficient for a two-dimensional hydrofoil. (From Newman 1977)

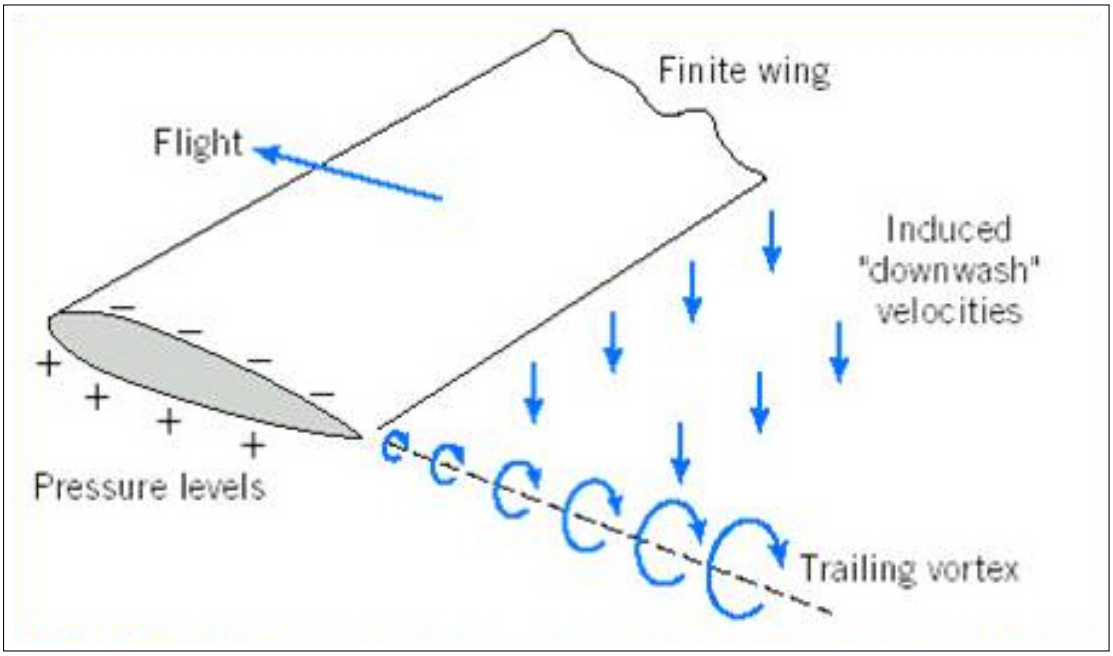

Figure 2.26 Trailing vortex system of a wing. (From Fox, McDonald & Pritchard 2004)

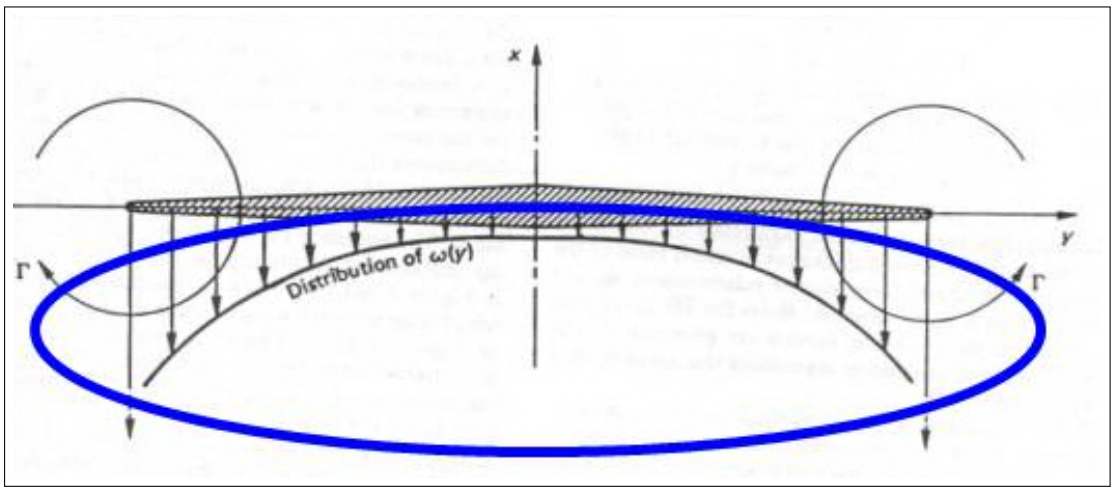

Figure 2.27 Downwash distribution for trailing vortex system on a wing. (From Carlton 1994)

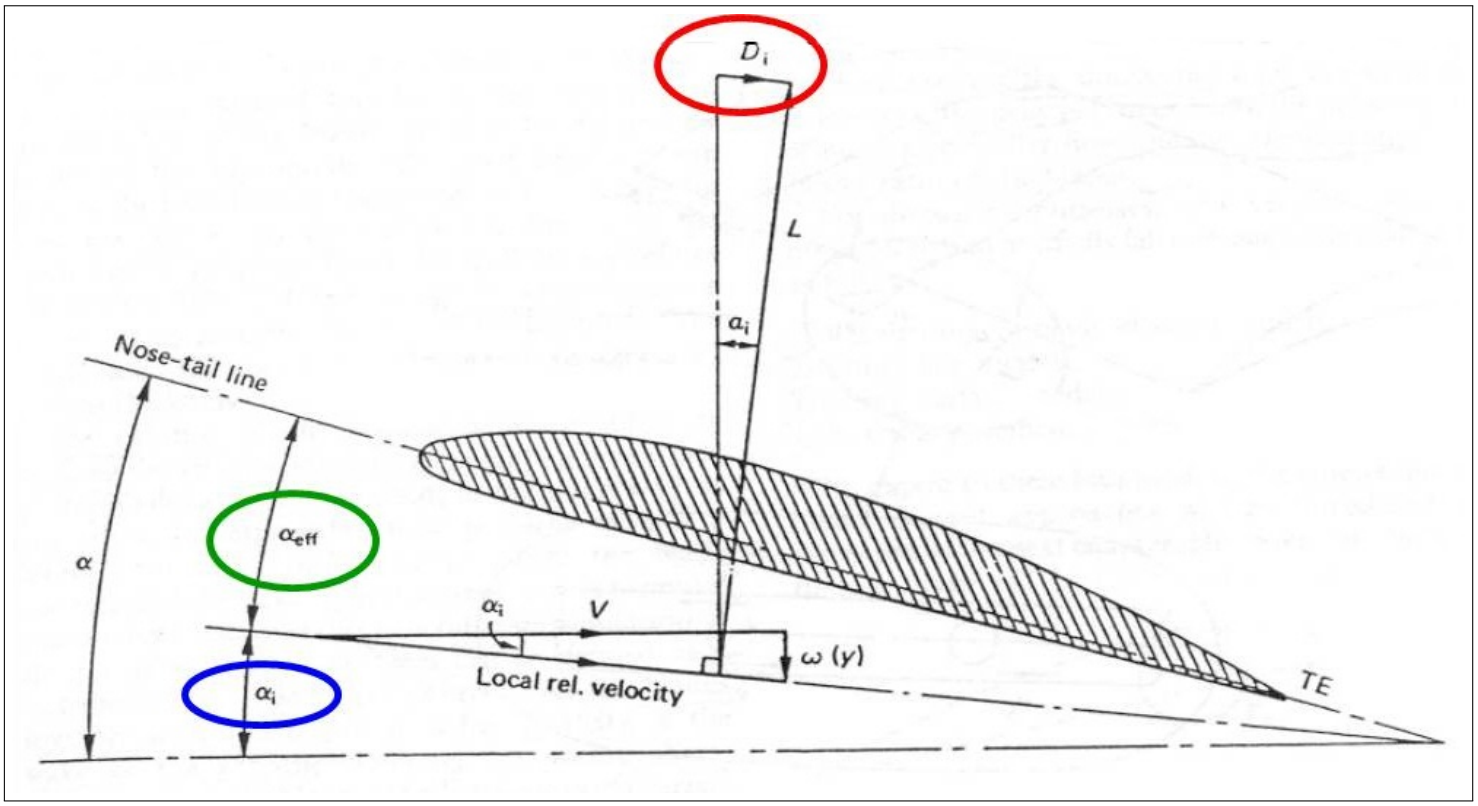

Figure 2.28 Derivation of induced drag on a wing. (From Carlton 1994)

  - Complicated Non-uniform Onset Flow: turbulence, unsteadiness, operation
  - Mutual Interaction: cavitation, hydroelasticity, free surface, hull, rudder

- Propeller Geometry
  - Propeller coordinate system
  - 3 coordinate systems: (1) Cartesian (2) Cylindrical (3) Helical coordinate system

- Propeller Open Water Test: Non-dimensional Numbers

$$\text{Reynolds number} \quad R = \frac{\rho V L}{\mu} = \frac{V L}{\nu} \tag{2.19}$$

$$\text{Froude number} \quad F_n = \frac{V}{\sqrt{gL}} \tag{2.20}$$

$$\text{Cavitation number} \quad C_a = \frac{p - p_v}{\frac{1}{2}\rho V^2} \tag{2.21}$$

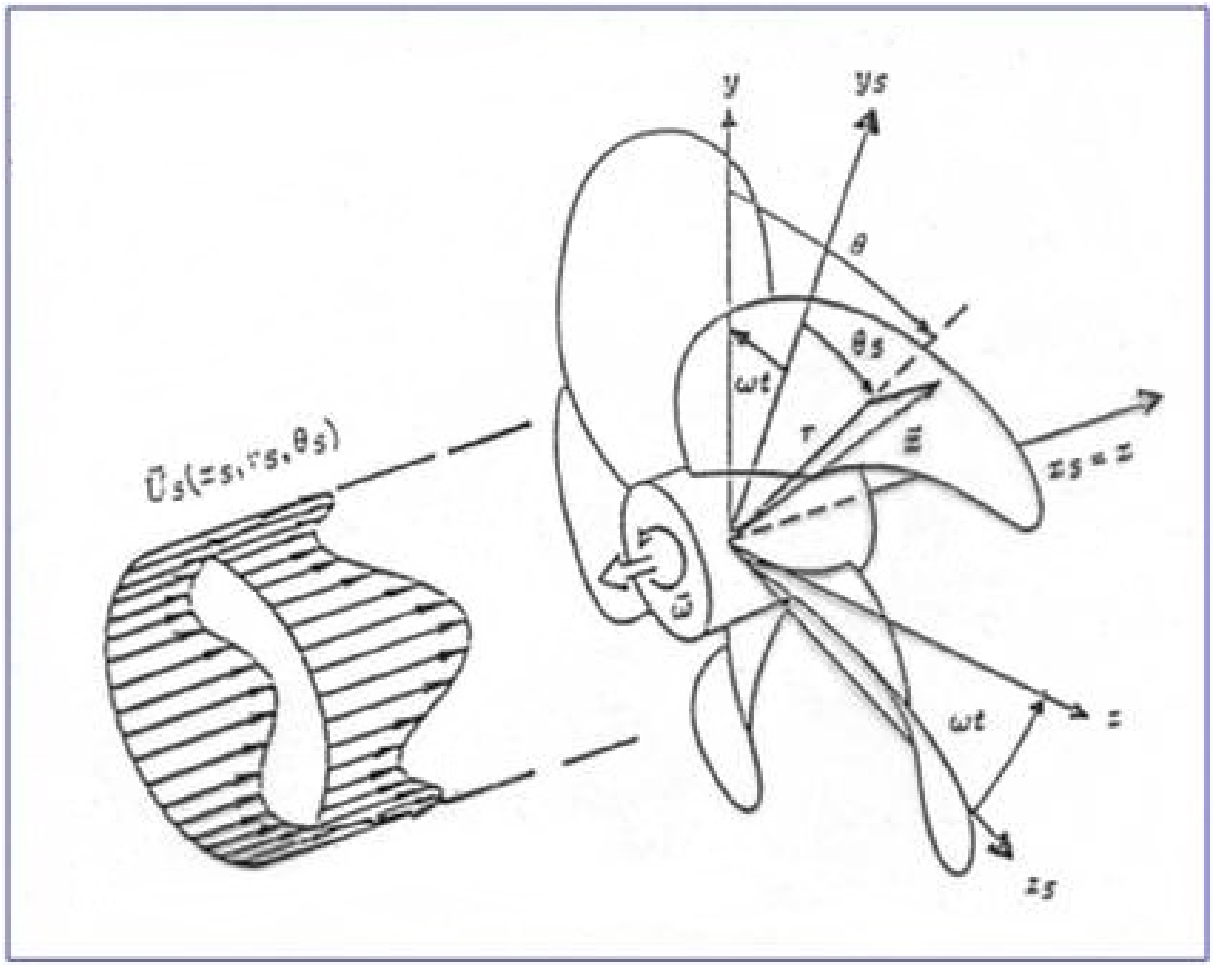

Figure 2.29 Propeller coordinate system.

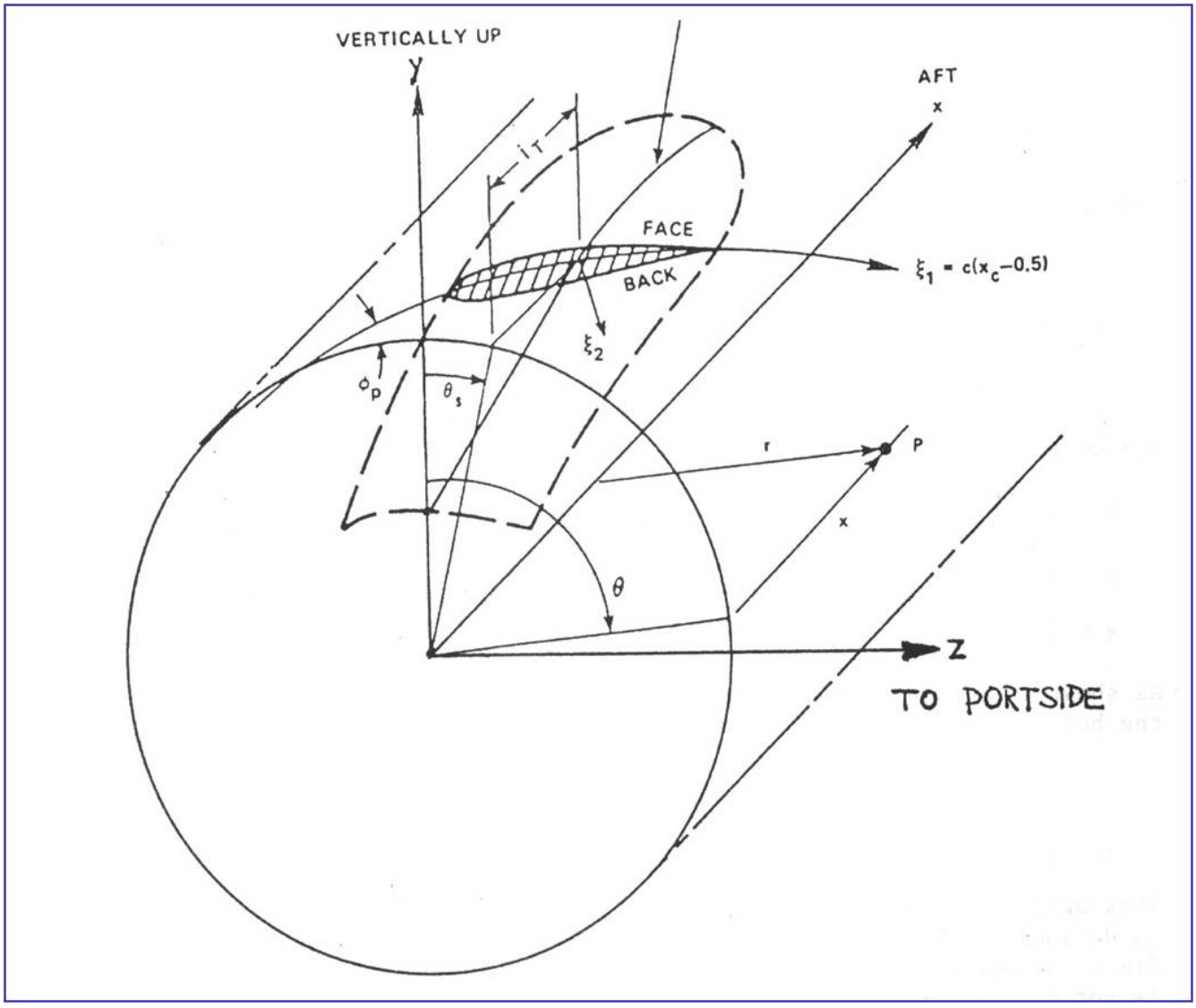

Figure 2.30 Propeller blade geometry in 3 coordinate systems.

- 3-D Perspective and 2-D view of a propeller blade section: Hydrodynamic forces

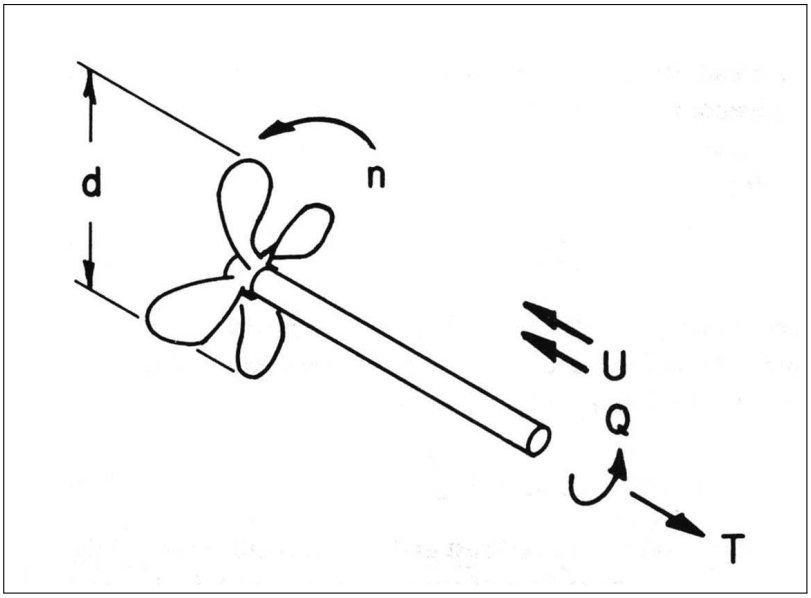

Figure 2.31 Perspective view of a propeller and its shaft. (From Newman 1977)

- Open Water Characteristics: Advance ratio J, Thrust/Torque coefficient K_T, K_Q, Propeller efficiency η_P

$$J = \frac{U}{n\,d} \tag{2.22}$$

$$K_T(J) = \frac{T}{\rho\, n^2\, d^4} \tag{2.23}$$

$$K_Q(J) = \frac{Q}{\rho\, n^2\, d^5} \tag{2.24}$$

$$\eta_P = \frac{UT}{2\pi n Q} = \frac{J}{2\pi}\frac{K_T}{K_Q} \tag{2.25}$$

- Components of Marine Propulsion System

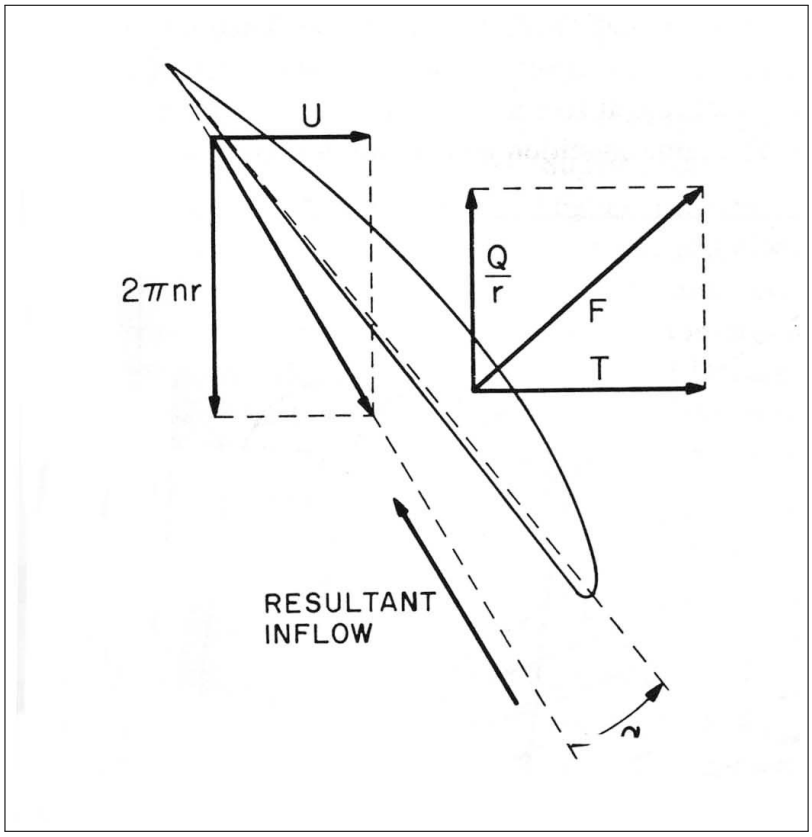

Figure 2.32 2-D view of a propeller blade section. (From Newman 1977)

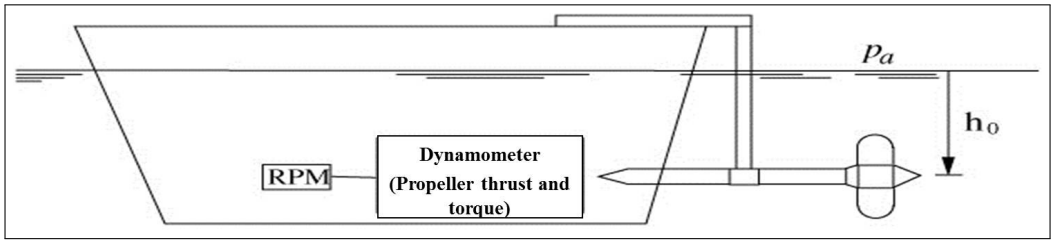

Figure 2.33 Experimental setup for propeller open water test in towing tank.

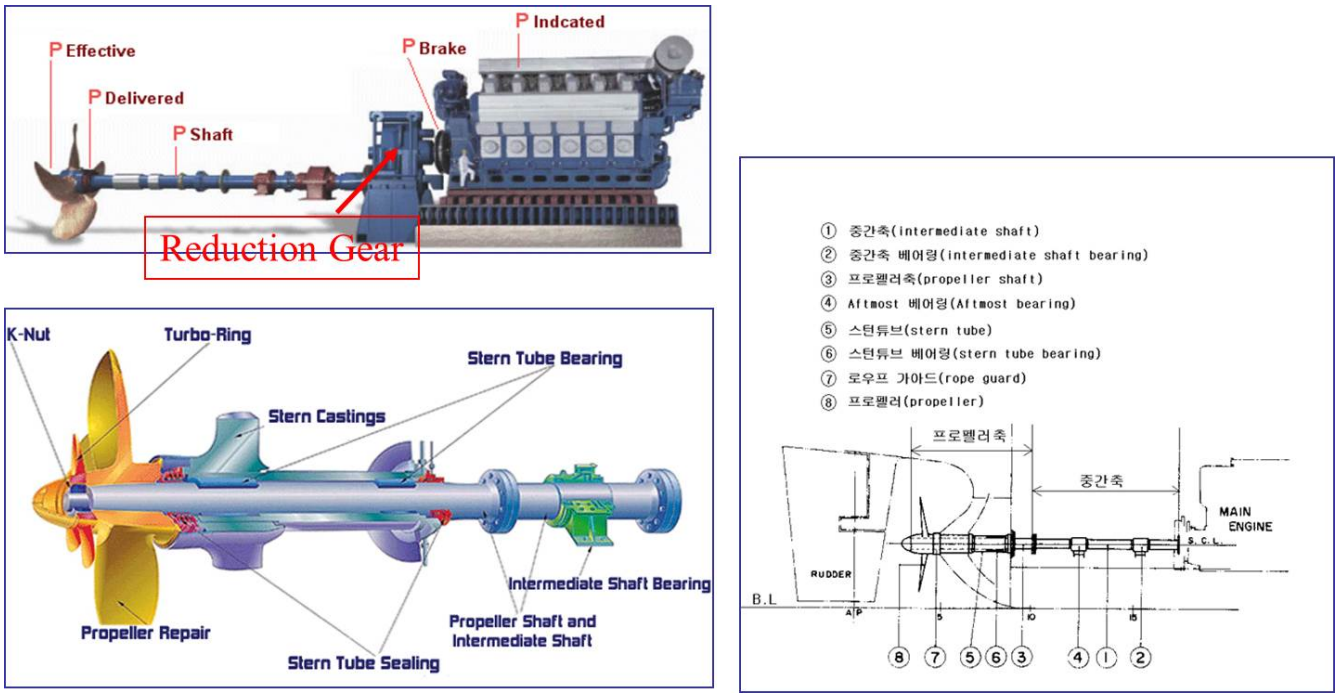

Figure 2.34 Components of a typical marine propulsion system. (출처: 삼성중공업 2004)

2.7 Drag on a Ship Hull

- In dimensional analysis, 6 dimensional quantities can be reduced to 3 nondimensional numbers.

$$\frac{D}{\frac{1}{2}\rho U^2 S} = C_D(R, F_n) \tag{2.26}$$

  where S is the wetted surface area of hull, and the Froude number $F_n = U/(gl)^{1/2}$ represents the effect of gravity.

- It is impossible to scale simultaneously both the Reynolds and Froude numbers.

- The residual drag is defined as, without the Froude's hypothesis,

$$C_R(R, F_n) = C_D(R, F_n) - C_F(R) \tag{2.27}$$

- Decomposition of Ship Resistance

- Froude's hypothesis The drag can be expressed as sum of a **frictional** drag

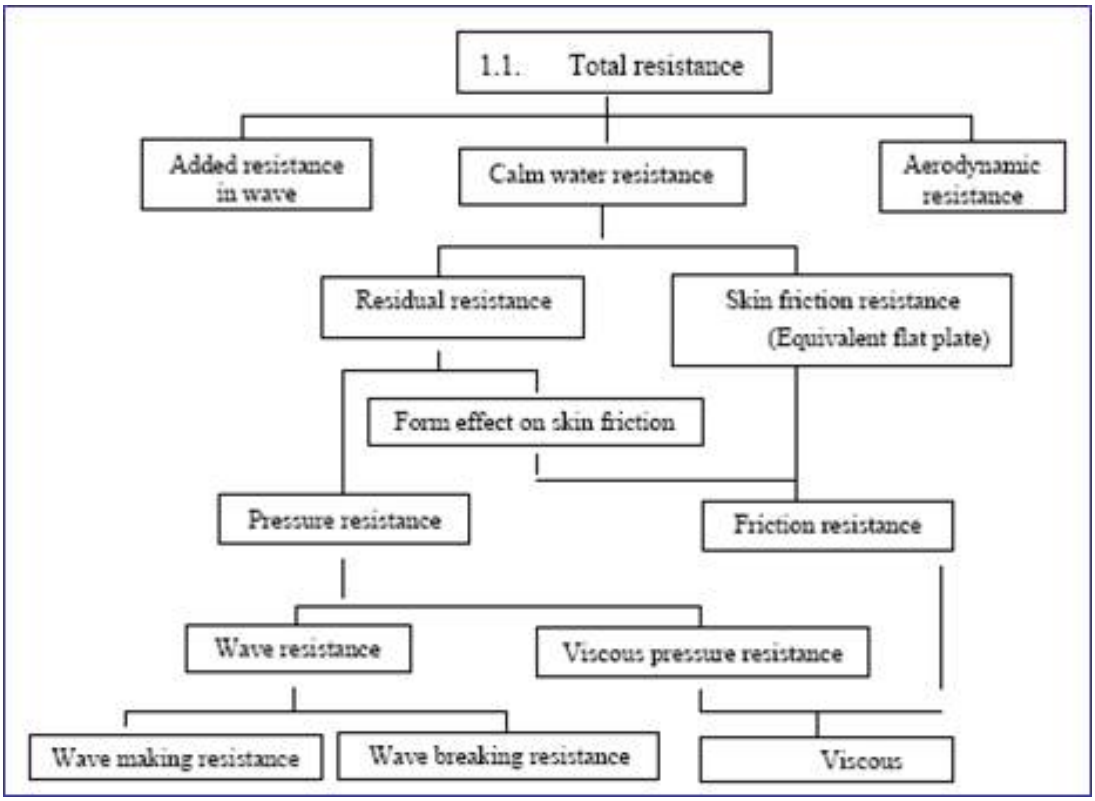

Figure 2.35 Decomposition of ship resistance.

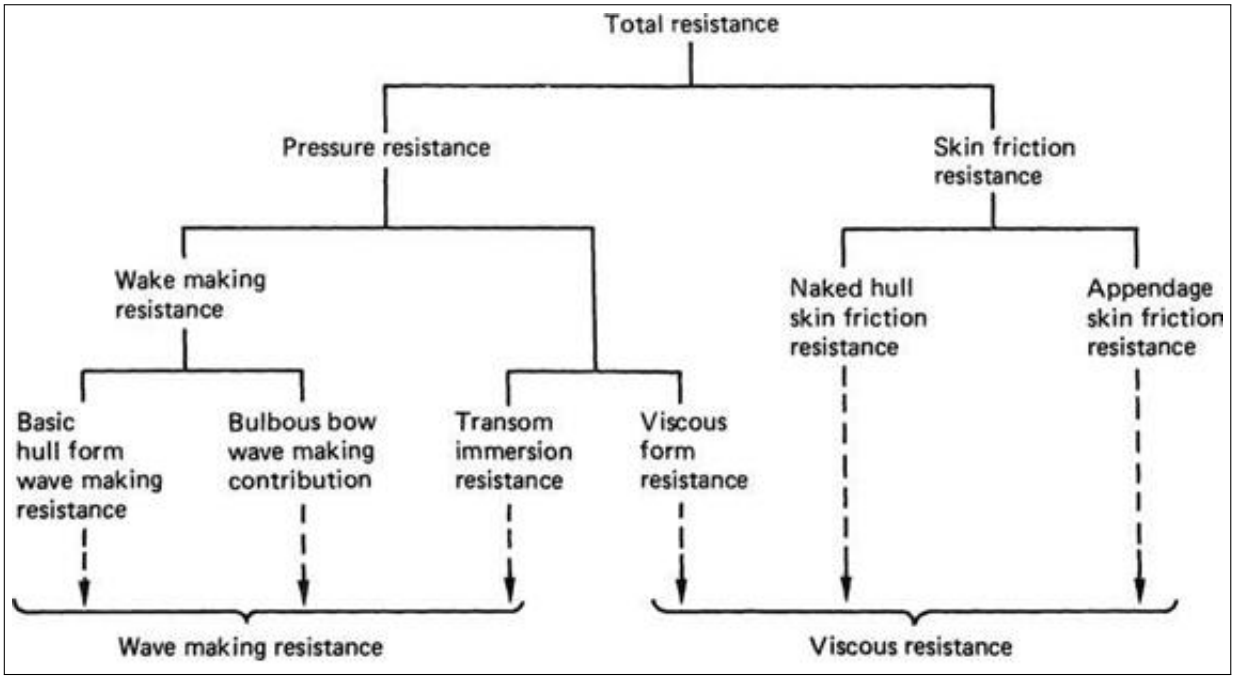

Figure 2.36 Components of ship resistance. (From Carlton 1994)

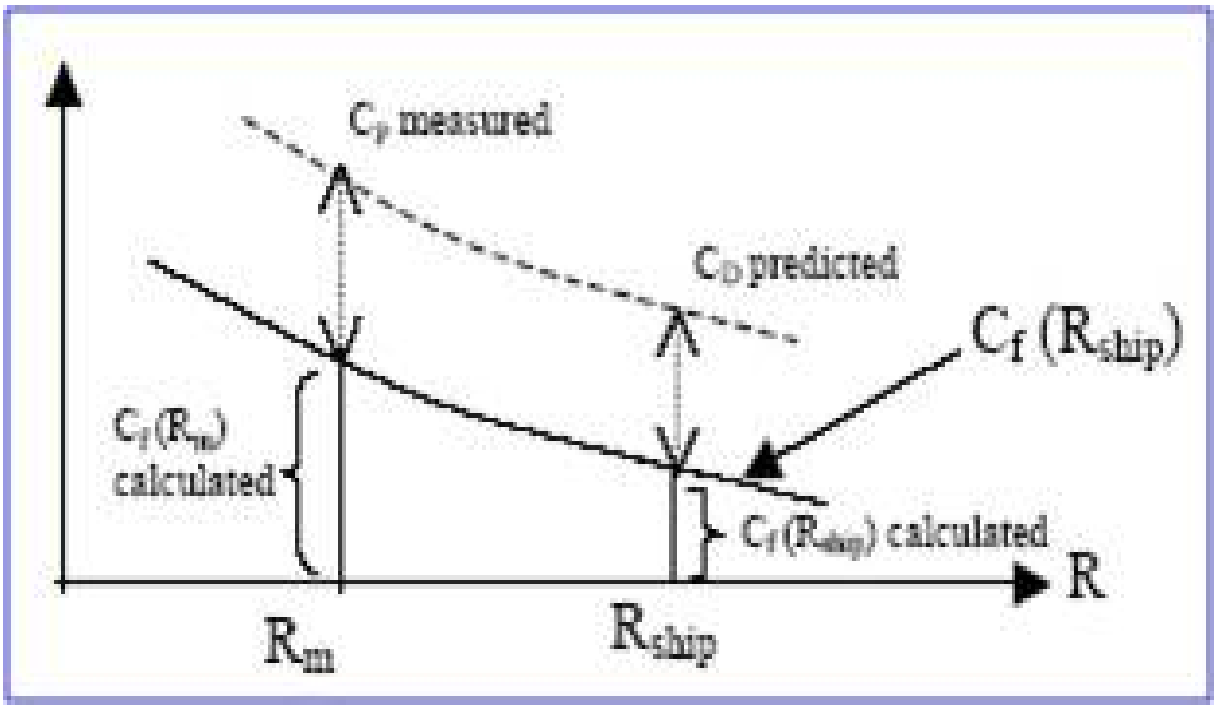

Figure 2.37 Froude's hypothesis for prediction of resistance of a full-scale ship. (From MIT website 2004)

depending on Reynolds number, plus a **residual** drag depending on Froude number.

$$\boxed{C_D(R,F) = C_F(R) + C_R(F)} \tag{2.28}$$

- Froude's hypothesis is an approximation to assume that the resulting C_R is independent of the Reynolds number.
- Extrapolator of model results to obtain full-scale resistance coefficients.

$$\boxed{(C_D)_{\text{ship}} = (C_D)_{\text{model}} - (C_F)_{\text{model}} + (C_F)_{\text{ship}}} \tag{2.29}$$

- Calculation of model and full-scale frictional drag

- Experimental validation of Froude's hypothesis
  - **Geosim models (length** $l = 4 \sim 30\, ft$ and **full-scale drag measurements** for several values of Froude number **(full-scale speed** $U = 4 \sim 15\, knots$**)**.

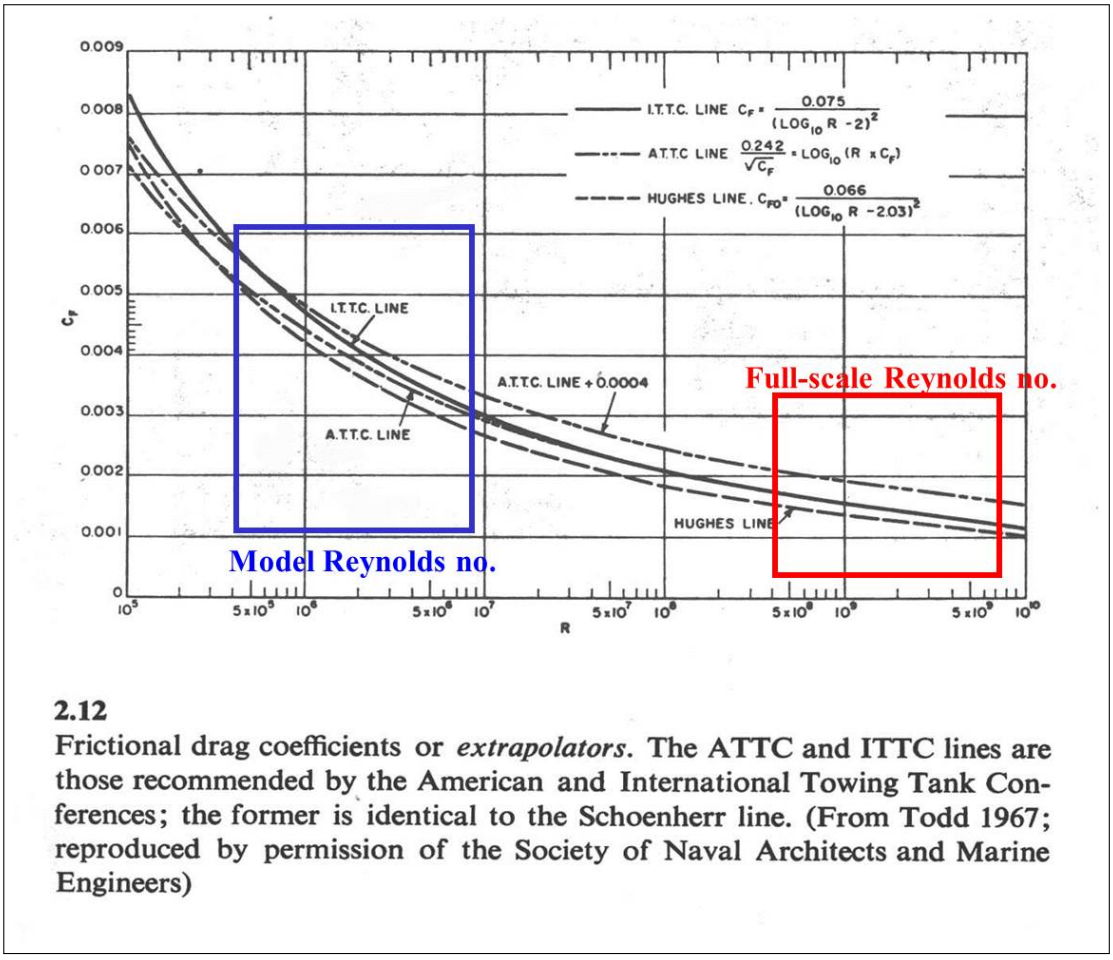

2.12
Frictional drag coefficients or *extrapolators*. The ATTC and ITTC lines are those recommended by the American and International Towing Tank Conferences; the former is identical to the Schoenherr line. (From Todd 1967; reproduced by permission of the Society of Naval Architects and Marine Engineers)

Figure 2.38 Calculation of model and full scale frictional drag coefficients. (From Newman 1977)

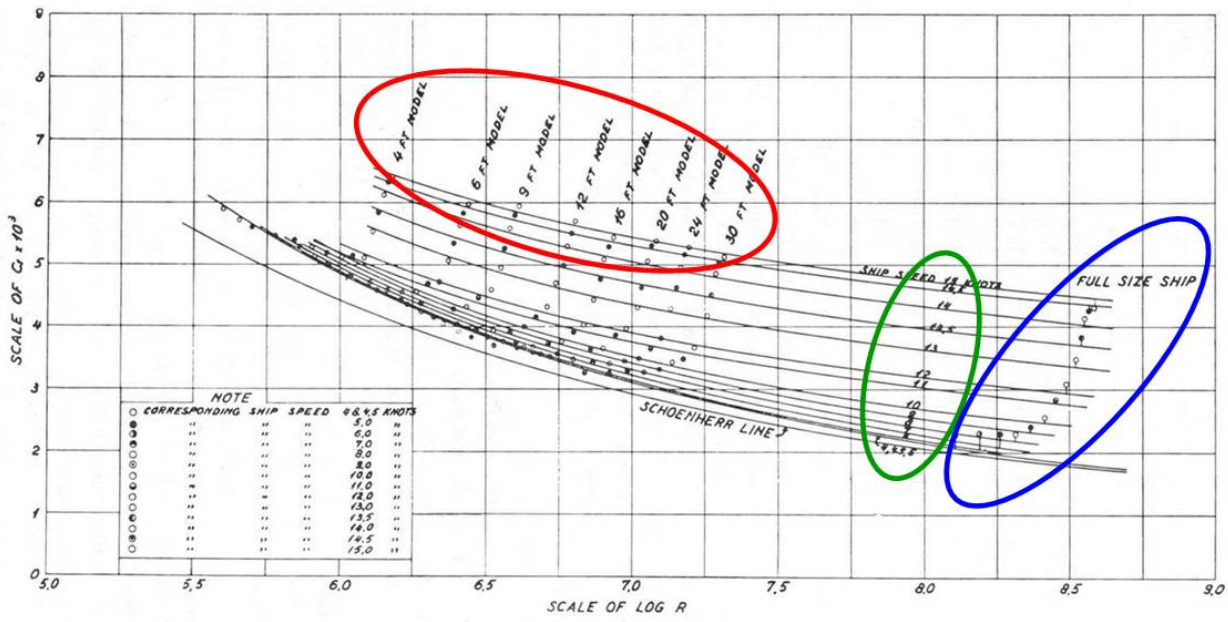

2.11
Total drag coefficients of the *Lucy Ashton* and several geosim models of the same vessel (from Troost and Zakay 1951). The faired curves represent constant values of the Froude number and, if Froude's hypothesis were strictly valid, these would be parallel with spacing independent of the Reynolds number. Note that, even for this small full-scale vessel (58 m long), there is a large gap between the largest model results and the full-scale results.

Figure 2.39 Total drag coefficients of geosim models. (From Newman 1977)

– The curves of constant values of Froude number are not strictly parallel to Schoenherr line of frictional drag, but Froude's hypothesis is acceptable to a considerable extent in correlating the resistance of several geosims.

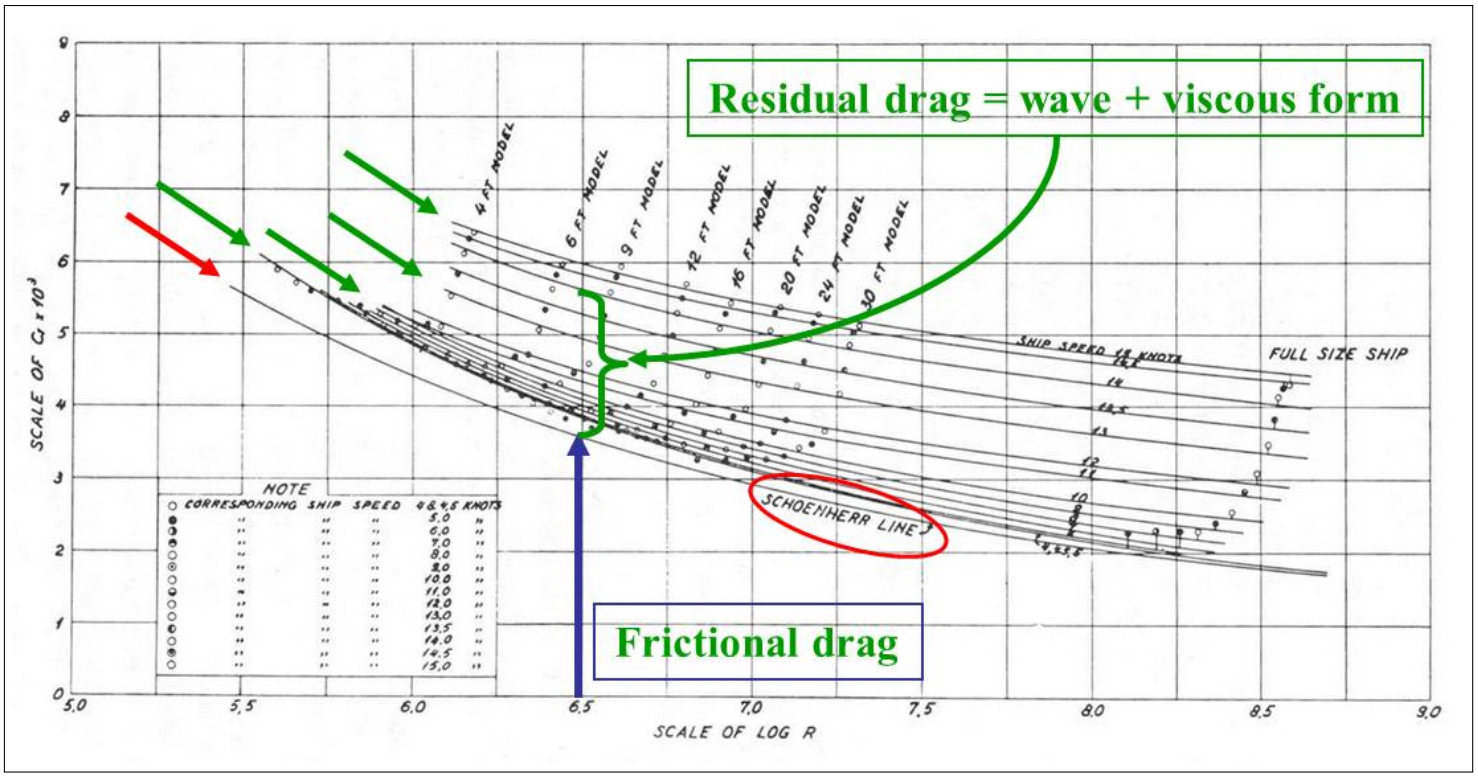

Figure 2.40 Total drag coefficients of geosim models: Validation check on Froude hypothesis. (From Newman 1977)

– The low Froude number asymptotic tendency is indicated by coalescence of the results for full-scale speeds of 4 5 knots. At these speeds, the wave resistance is negligible and the principal contribution to the residual drag is viscous form drag. The viscous form drag is not constant but decreases increasing Reynolds number.

– Suggestion: (1) The form drag should be assumed proportional to the friction drag or (2) the frictional drag curve should be more steeply sloped than the Schoenherr line (ATTC line): e.g. Hughes line/ITTC line.

– The viscous form drag coefficient increases with decreasing Reynolds number. The residual drag coefficient curves display the opposite tendency.

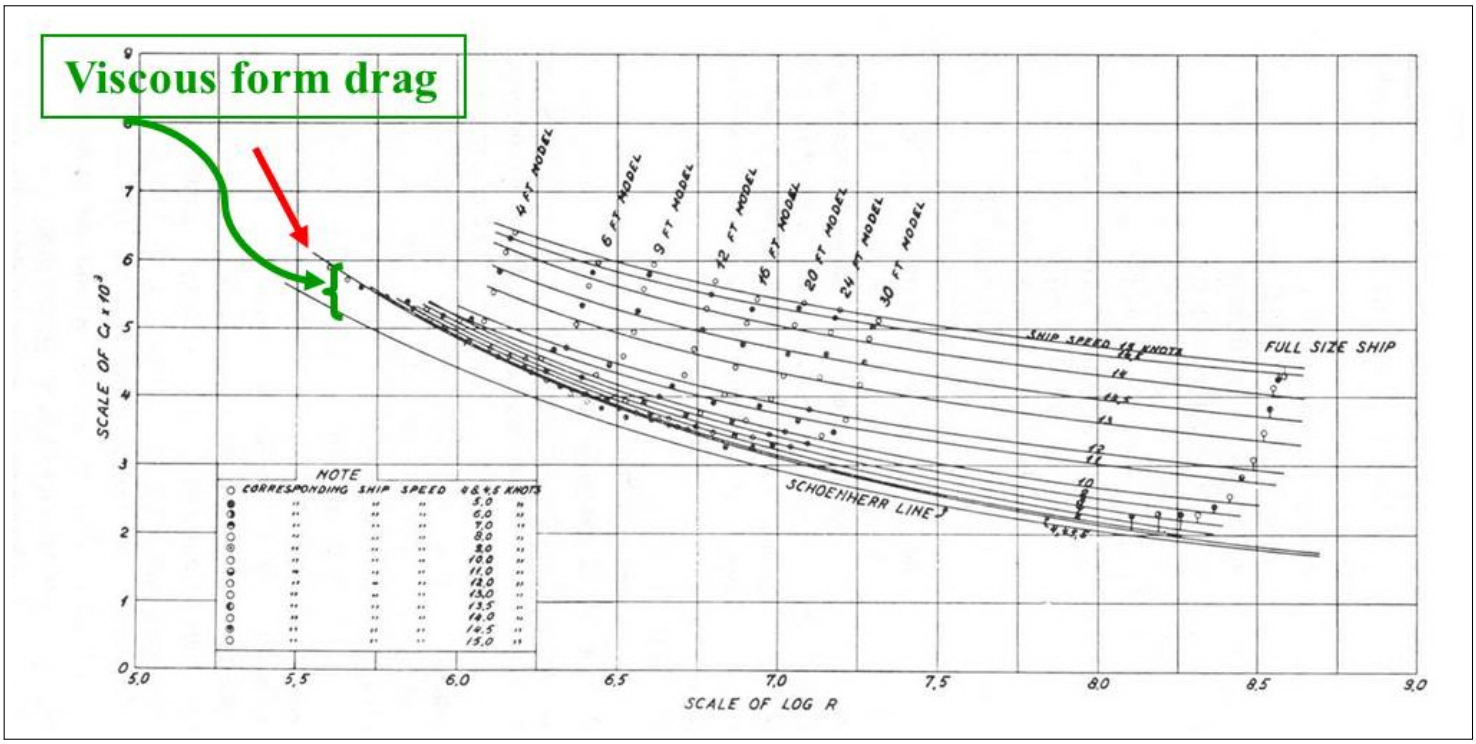

Figure 2.41 Total drag coefficients of geosim models: Viscous form drag. (From Newman 1977)

  - Both the wave drag and form drag depend separately on Reynolds number. These effects are small for the larger models.

- Extrapolation using form factor k

2.8 Propeller-Hull Interactions

- Individual analysis of hull and propeller, and interactions
- Self-propulsion factors: Wake fraction(w_T), thrust deduction factor(t), and relative rotative efficiency(η_R)

$$w_T = 1 - \frac{V_A}{V} \tag{2.30}$$

$$R_T = (1-t)T \tag{2.31}$$

$$\eta_R = \frac{(K_Q)_{OW}}{(K_Q)_{SP}} \tag{2.32}$$

$$V_A = n\,D\,J \tag{2.33}$$

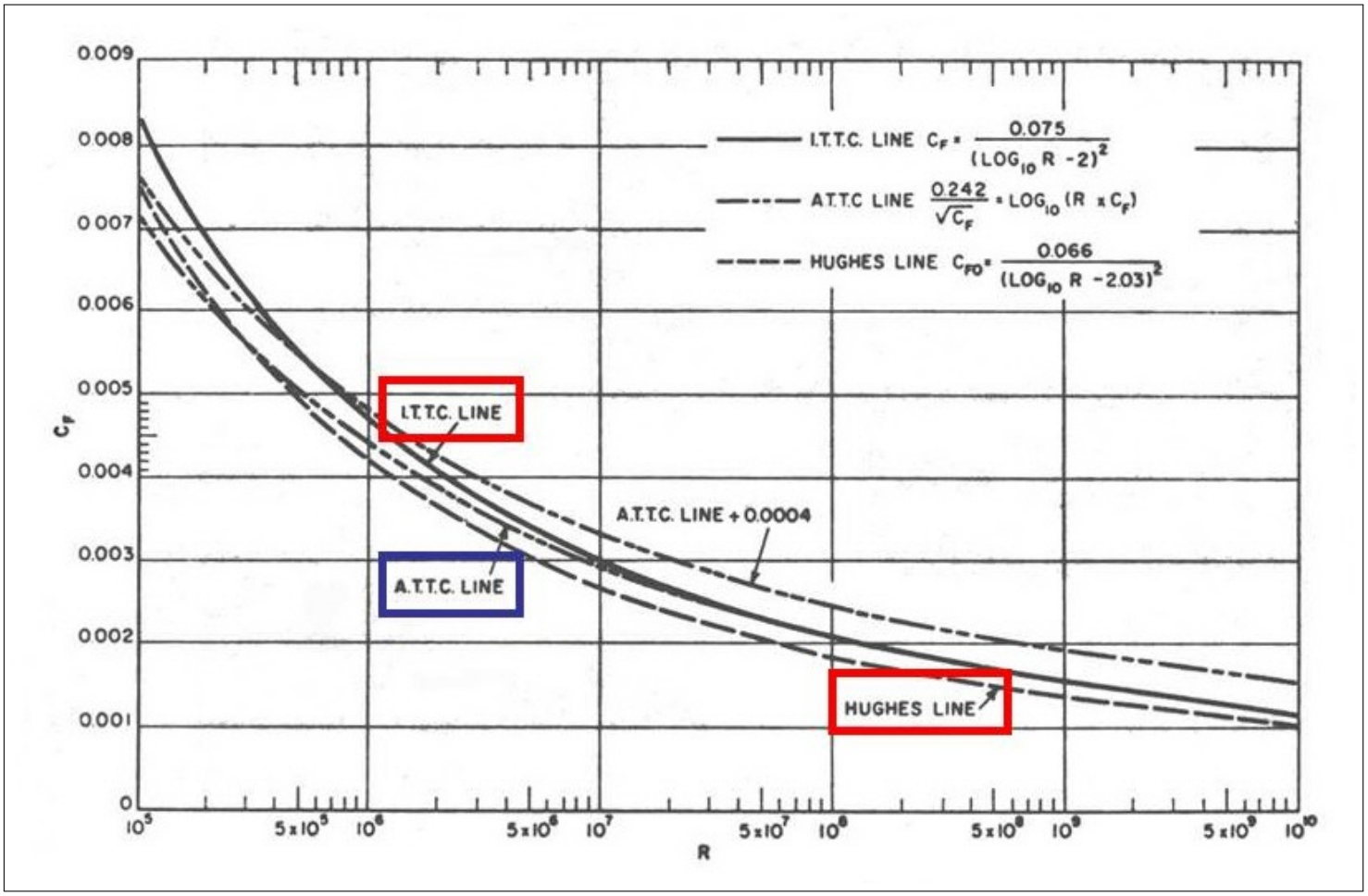

Figure 2.42 Frictional drag coefficients. (From Newman 1977)

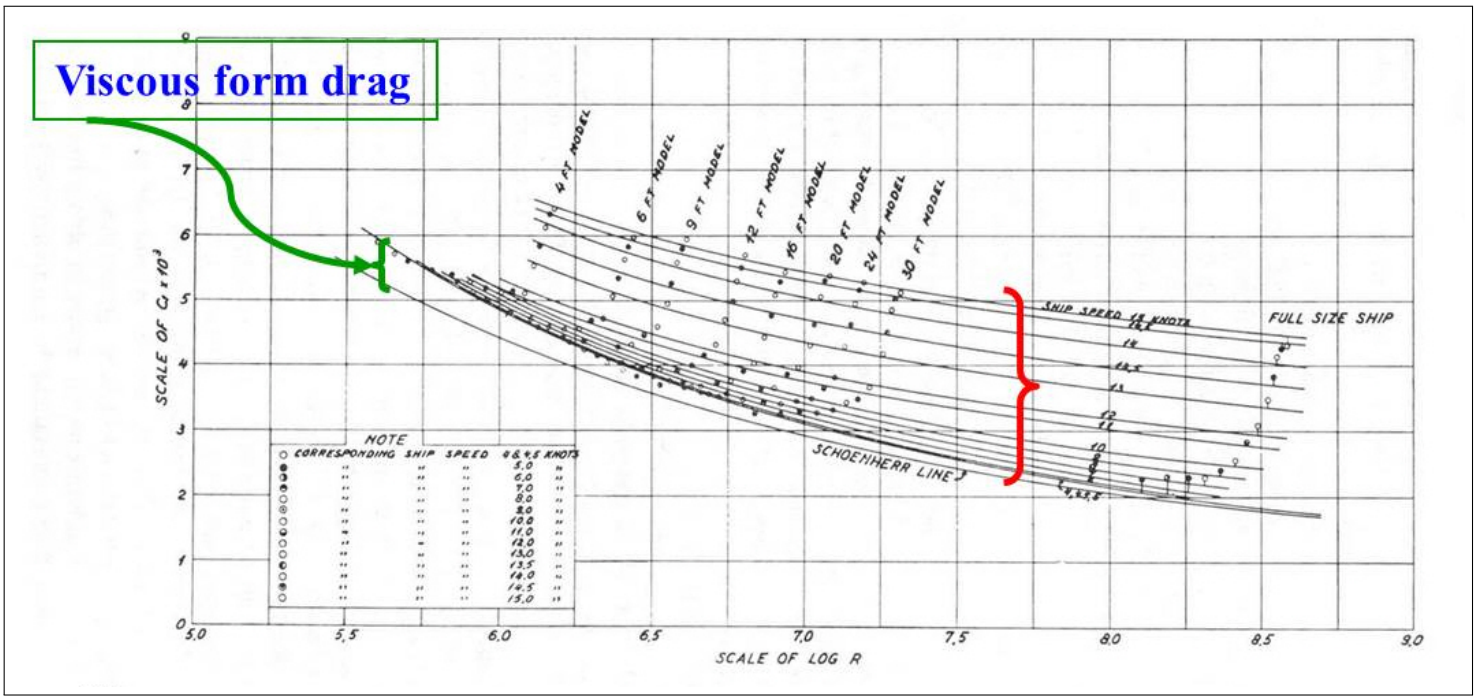

Figure 2.43 Total drag coefficients of geosim models: Larger models effect. (From Newman 1977)

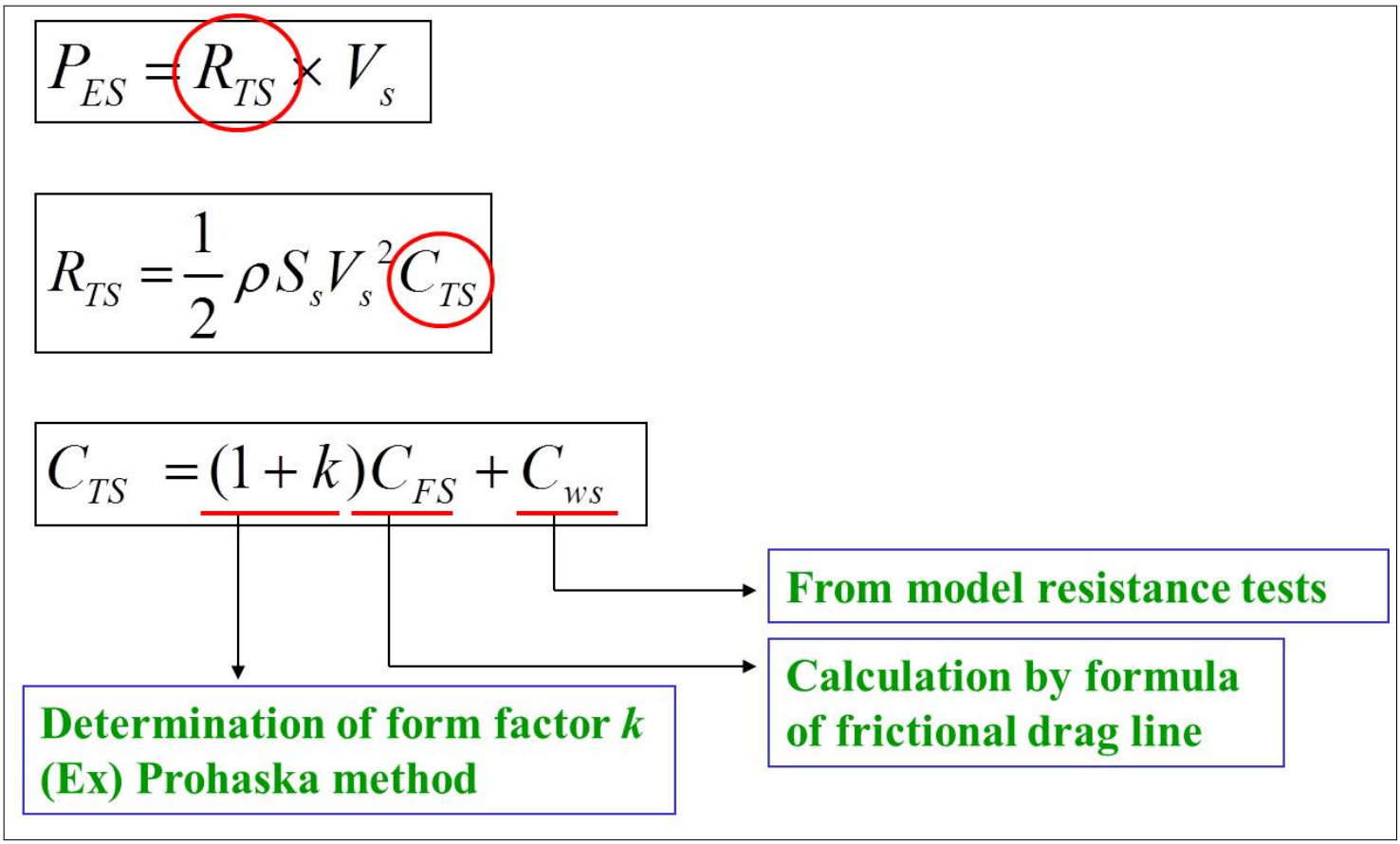

Figure 2.44 Extrapolation using form factor k.

– Quasi-propulsive efficiency

$$\eta = \frac{R_T\, V}{2\pi n\, Q} = \frac{(1-t)\, V\, K_T}{2\pi n\, D\, (K_Q)_{SP}} = \frac{(1-t)}{(1-w_T)}\, \eta_P\, \eta_R \tag{2.34}$$

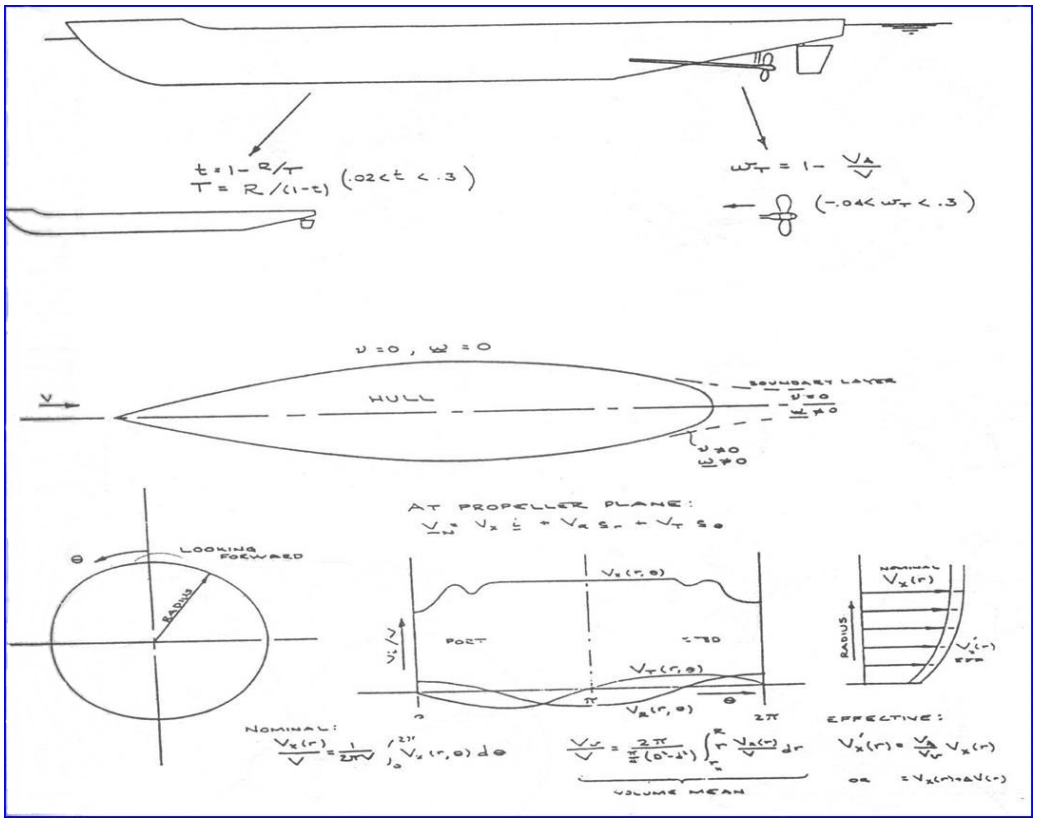

Figure 2.45 Schematic diagram of propeller-hull interaction. (From Brockett 1988)

2.8.1 Propeller and Ship Powering

- Shaft Power, SHP or Brake Power, BHP
  - Power output at the prime mover is higher than delivered power.
  - It is usually called shaft power (P_S or SHP) for gas turbines and brake power(P_B or BHP) for diesel engines.
  - Occasionally P_S is the power immediately fore of the stern tube bearing, and P_B is the power right at the prime mover.
- Delivered Power, DHP

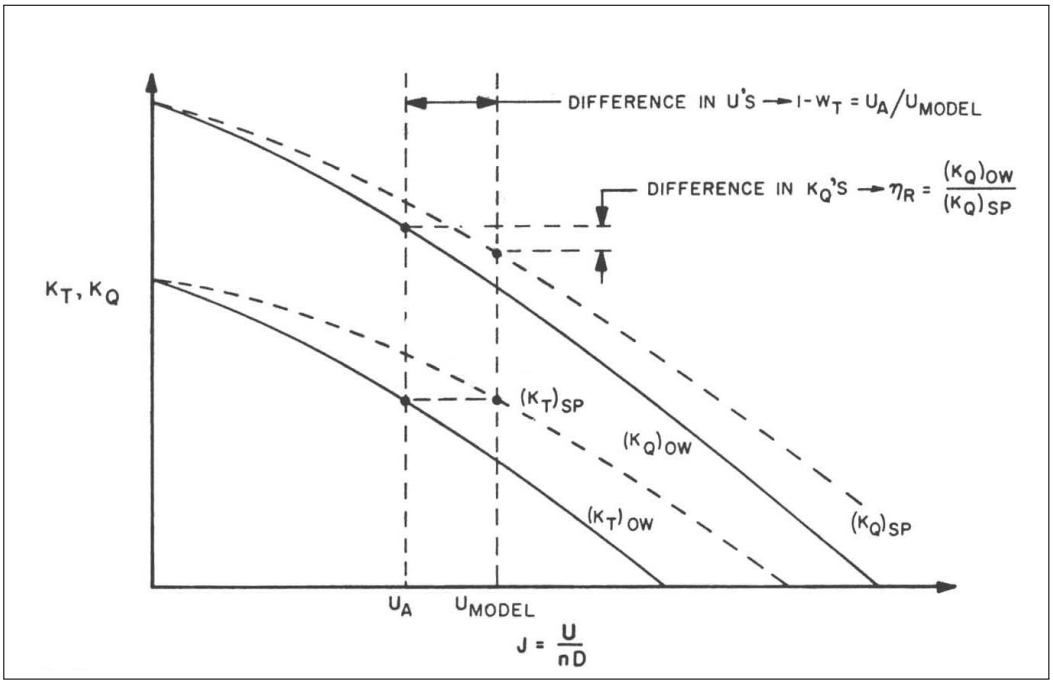

Figure 2.46 Thrust identity condition between open-water propeller test and self-propulsion test. (From Newman 1977) (Note: Here $U_A = V_A$, $U_{\text{Model}} = V_{\text{Model}}$ and $U = V$.)

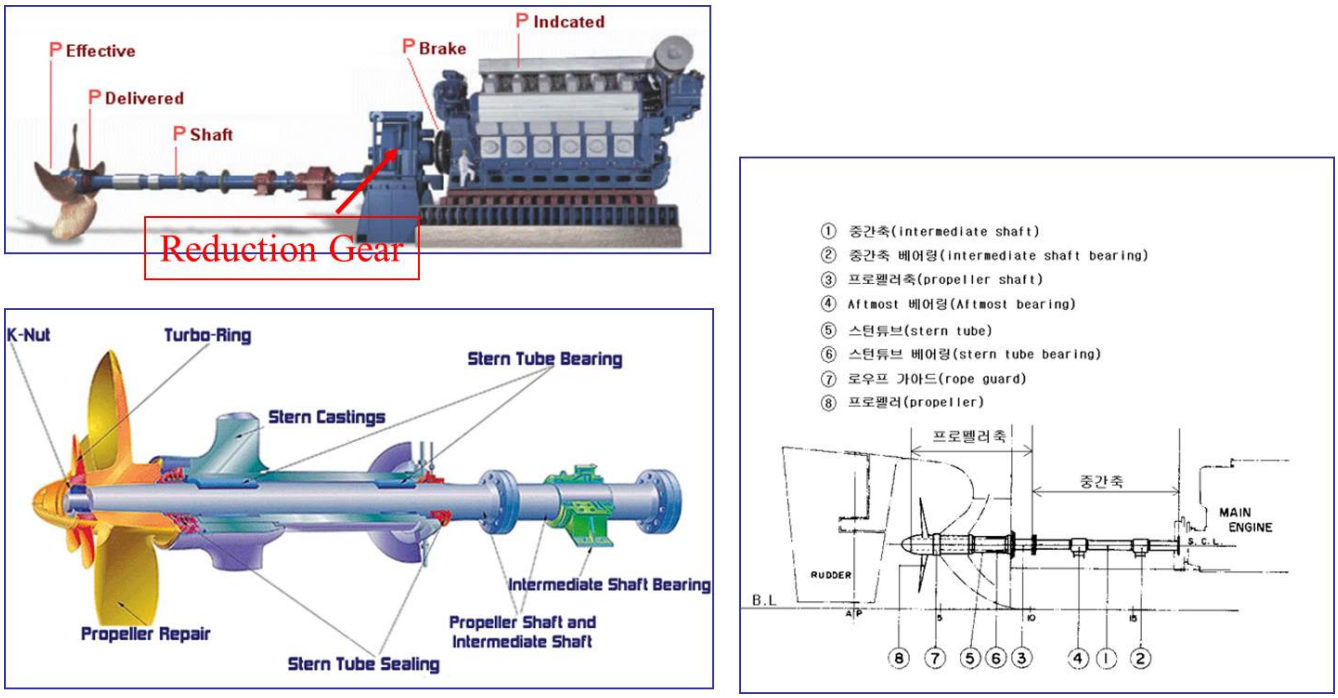

Figure 2.47 Components of a typical marine propulsion system. (출처: 삼성중공업 2004)

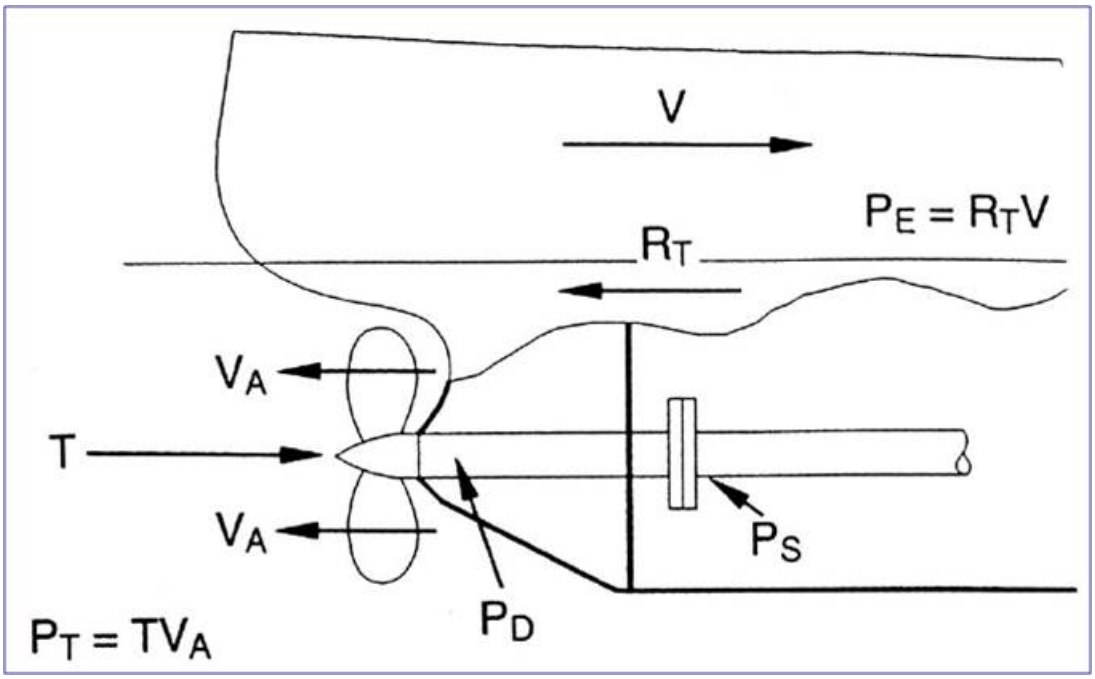

Figure 2.48 Schematic diagram of propeller and ship powering.

- P_D or DHP is power delivered to the propeller by the prime mover.

$$P_D = 2\pi n Q_D \tag{2.35}$$

where n = revolutions per second of shaft or propeller and Q_D = torque delivered to the propeller.

- Propeller converts rotating power to thrust power.

- Thrust Power, THP
  - Propeller is producing thrust T at a speed of advance V_A.

$$P_T = TV_A \tag{2.36}$$

where $T \neq R_T$, $V_A \neq V$.

  - Useful power output of the propeller is called the thrust power P_T or THP.

- Effective Power, EHP
  - P_E or EHP is power needed to tow ship at a given speed in calm water

or power to overcome total resistance force R_T at ship speed V.

$$P_E = R_T V \tag{2.37}$$

where R_T is total resistance and V is ship speed.

- Shaft Transmission Efficiency, $\eta_S = \dfrac{P_D}{P_S}$
  - Occasionally, more than one transmission (or mechanical) efficiencies are defined.
  - the overall transmission efficiency will then be the product of the individual components.

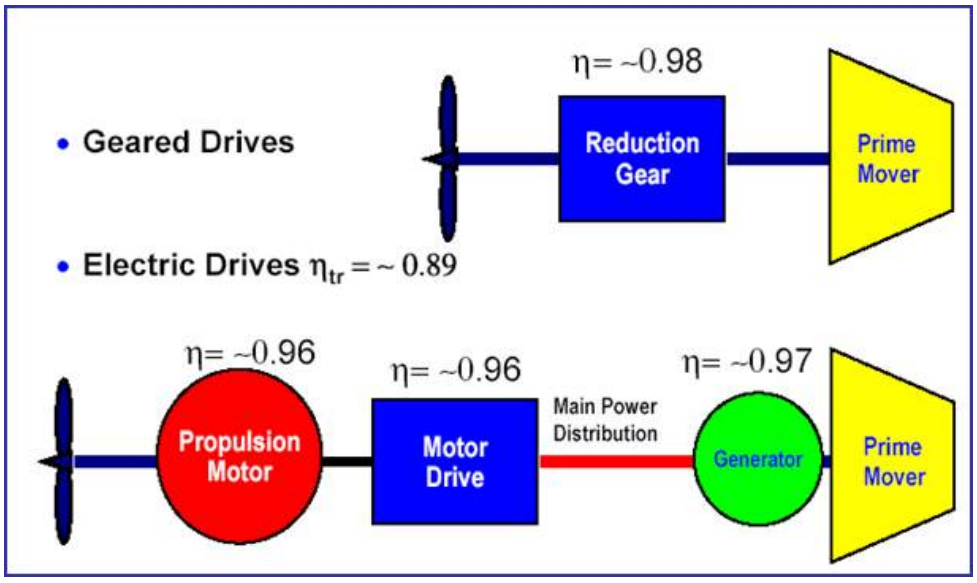

Figure 2.49 Transmission efficiency of mechanical drives and electric drives.

- Propeller Efficiency
  - Power conversion between P_D and P_T is the major loss in power.
  - Depending on where the propeller torque is measured,
    - Efficiency of propeller behind the ship, η_B:

$$\eta_B = \frac{P_T}{P_D} = \frac{TV_A}{2\pi n Q_B} \tag{2.38}$$

where Q_B = Torque required by the propeller to deliver T and V_A behind the ship.

* Efficiency of propeller in open water, η_0:

$$\eta_0 = \frac{P_T}{P_D} = \frac{T\,V_A}{2\pi n\,Q_0} \tag{2.39}$$

where Q_0 = Torque required by the propeller to deliver T and V_A in open water.

- Relative Rotating Efficiency, η_R

$$\eta_R = \frac{\eta_B}{\eta_0} = \frac{Q_0}{Q_B} \tag{2.40}$$

  - It is not a "true" efficiency (not a ratio of powers).
  - It can be greater than one. Usual values around one.

- Hull Efficiency, η_H

$$\eta_H = \frac{P_E}{P_T} = \frac{R_T\,V}{T\,V_A} \tag{2.41}$$

  - A measure of hull form (stern) design to suit propulsor arrangement.
  - It does not involve power conversion, so it is not a "true" efficiency.
  - It can be greater than one, usual numbers around 1.05.

- Overall Efficiency (Propulsive Efficiency), η_P

$$\eta_P = \frac{P_E}{P_S} = \frac{P_E}{P_T} \times \frac{P_T}{P_D} \times \frac{P_D}{P_S} = \eta_H\,\eta_B\,\eta_S = \eta_H\,\eta_0\,\eta_R\,\eta_S \tag{2.42}$$

  - While η_S depends on mechanical efficiencies, η_H, η_0 and η_R depend on hydrodynamics, where η_0 is the major loss in power.
  - The powering problem is how to maximize η_P in design stage.

2.9 Unsteady Force on an Accelerating Body

- Development of unsteady flows [10]
  1. Symmetrical attached flow: ideal flow behavior
  2. Increase of viscous effects: growth of boundary layer
  3. Wake separates downstream
  4. Two symmetric vortices: grow in strength
  5. Shedding vortex unstable
  6. Alternating shedding vortex

- In the case of a body accelerated impulsively from a state of rest, the hydrodynamic force $F(t)$ will vary with time.

- Force in the direction opposite to the body motion:

$$\frac{F}{\frac{1}{2}\rho U^2 l^2} = C_F(R, Ut/l) \tag{2.43}$$

- Case 1: Large values of time

  – Steady-state drag coefficient

$$C_F(R, Ut/l) \simeq C_D(R) \quad \text{for } Ut/l \gg 1 \tag{2.44}$$

- Case 2: Small time (Initial stage of rapid acceleration) [11]

  – Inertia force dominates viscous force: inviscid limit of high Reynolds number

$$C_F(R, Ut/l) \simeq C_D(\infty, Ut/l) \quad \text{for } Ut/l \ll 1 \tag{2.45}$$

[10] Movie: Unsteady flows of impulsive started circular cylinder(Exp.)
./mmfm_movies/2_05005.mov

[11] Movie: Initial stage of impulsive started circular cylinder(CFD)
./mmfm_movies/Cyl.mov

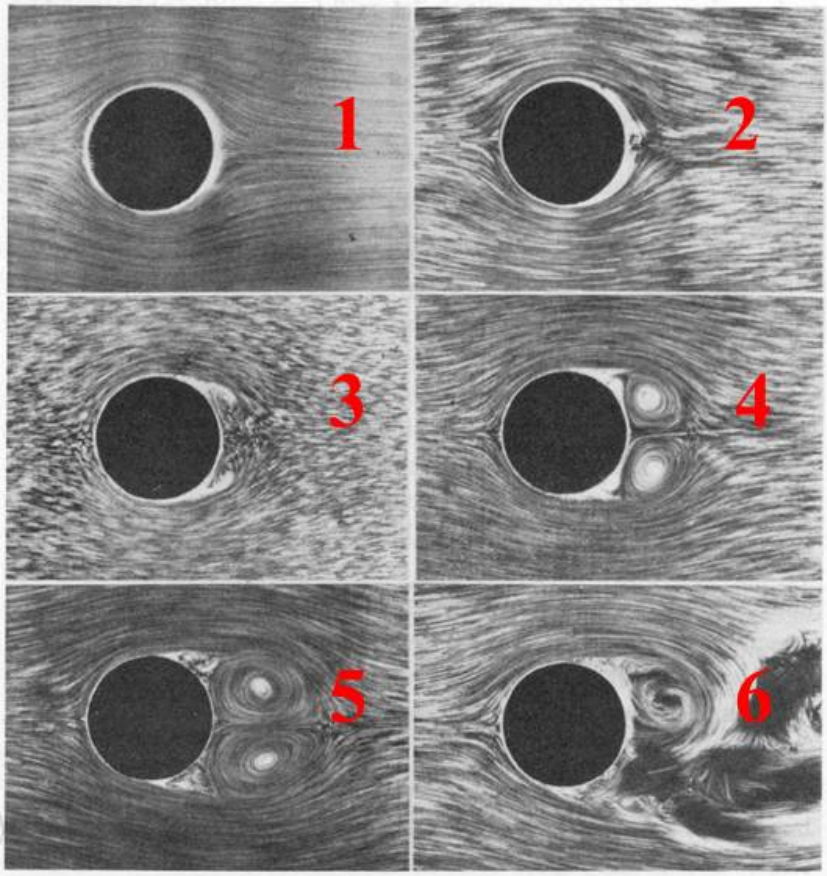

2.14
Initial stages of the flow past a circular cylinder which is accelerated impulsively from a state of rest to constant velocity. (From Prandtl 1927)

Figure 2.50 Development of unsteady flows about an impulsively started circular cylinder. (From Newman 1977)

2.9.1 Added Mass

- Initial Stage: Viscous forces are negligible, the hydrodynamic force:

$$F = -m_{11}\,\dot{U} \tag{2.46}$$

  where $\dot{U}$ denotes the acceleration. Force coefficient:

$$C_F(\infty, U\,t/l) = \frac{m_{11}\,\dot{U}}{\frac{1}{2}\,\rho\,U^2 l^2} \tag{2.47}$$

- Relative magnitudes of viscous force and added mass force are, since the added mass is proportional to l^3,

$$\frac{C_F(R,\infty)}{C_F(\infty, U\,t/l)} = \frac{\frac{1}{2}\,\rho\,U^2 l^2 C_D(R)}{m_{11}\,\dot{U}} \propto \frac{U^2}{\dot{U} l} \tag{2.48}$$

  – The parameter $U^2/\dot{U}l$ is small during the period of acceleration and large subsequently.

- Gradual transition of the force coefficient

  – Added-mass forces will dominate initially and viscous forces subsequently.

2.10 Vortex Shedding

- Karman Vortex Street [12]

  – Oscillatory shedding of vortices into the wake in a staggered configuration as predicted from a stability analysis.

  – The small-scale vortices lie between the separation having the initial instability and the initial formation of large-scale Karman vortex.

- Phenomena of Vortex Shedding in Nature

[12] Movie: Vortex shedding of circular cylinder wake
./mmfm_movies/Cylinder.mov

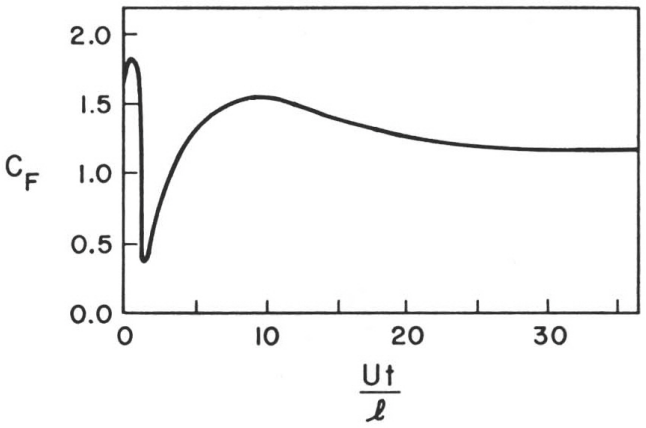

2.15
Force coefficient for a circular cylinder accelerated from an initial state of rest to a constant velocity U, based on experiments of Sarpkaya (1966).

Figure 2.51 Force coefficient for an impulsively started circular cylinder. (From Newman 1977)

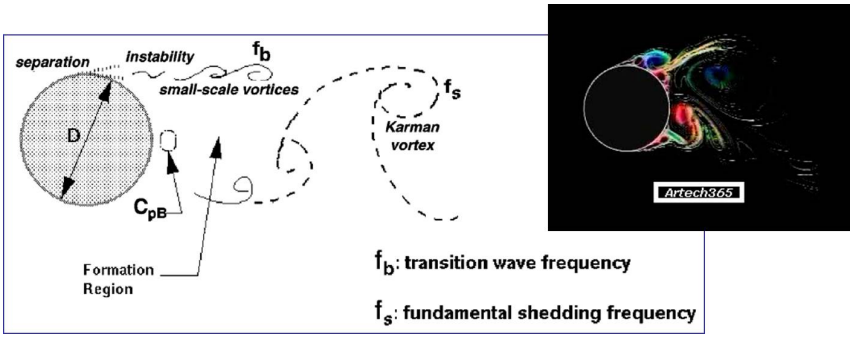

Figure 2.52 Karman vortex street.

Figure 2.53 Karman vortex street in nature. Cloud formation caused by steady wind downstream of an island (Madeira) at 2.4km height above the island.

- Lateral lift force and shedding frequency

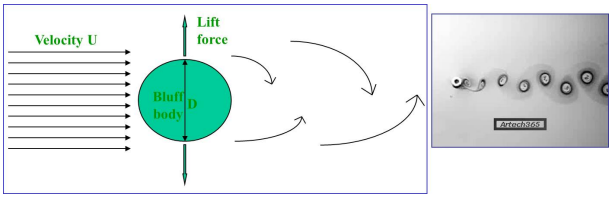

Figure 2.54 Lateral lift force and shedding frequency.

  - Nondimensional magnitude of the lift force and shedding frequency: [13]

$$\boxed{L_{\max}/\frac{1}{2}\rho U^2 l = C_L(R),} \quad \boxed{f\,l/U = S(R)} \tag{2.49}$$

    where $L_{\max}$ denotes the maximum value of the lift force per unit length along the cylinder, and S is the Strouhal number. For circular cylinders, C_L is typically 0.5.

  - For Reynolds numbers in the laminar regime (i.e., for low Reynolds numbers) for circular cylinders, the Strouhal number S is about $0.20 \sim 0.22$.

[13] Movie: Vortex shedding of circular cylinder wake(Re=200)
./mmfm_movies/Cyl200.mov

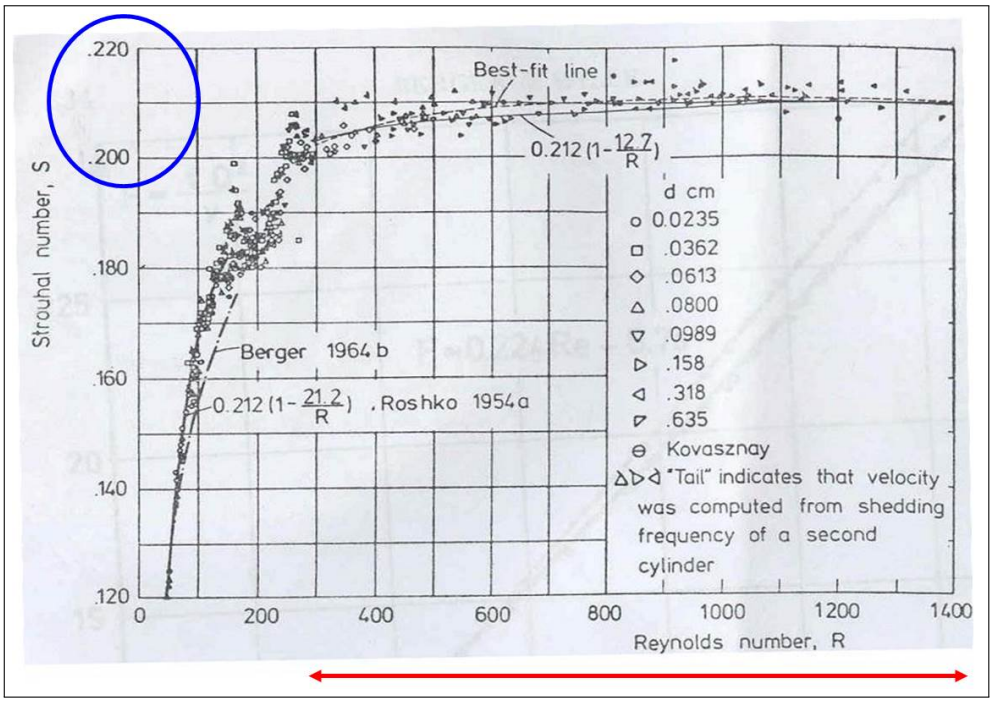

Figure 2.55 Strouhal number for a circular cylinder at low Reynolds numbers.

– For moderate and high Reynolds numbers ($10^2 < R < 10^7$), the Strouhal number is approximated by $S = 0.23/C_D$.

- Hydroelastic resonance: Lift force induces vibration [14]

– The well-known *lock-in* phenomena between the Strouhal frequency and the structural mode of vibration of the body.

– This VIV (Vortex Induced Vibration) problems may occur on cables, risers, pilings and other fixed structures in a current. [15]

[14] Movie: Vortex shedding of freely oscillating circular cylinder
./mmfm_movies/free_cylinder2.mov

[15] Movie: Tacoma bridge
./mmfm_movies/tnb.mov

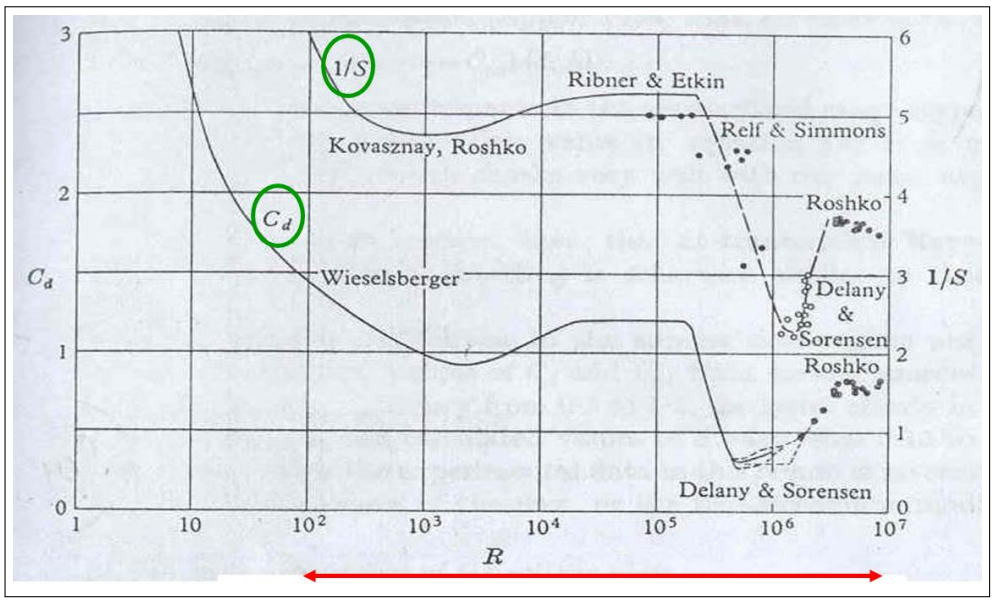

Figure 2.56 Drag coefficient and Strouhal number for a circular cylinder at moderate and high Reynolds numbers. Note: Experiments are available for very high Reynolds numbers.

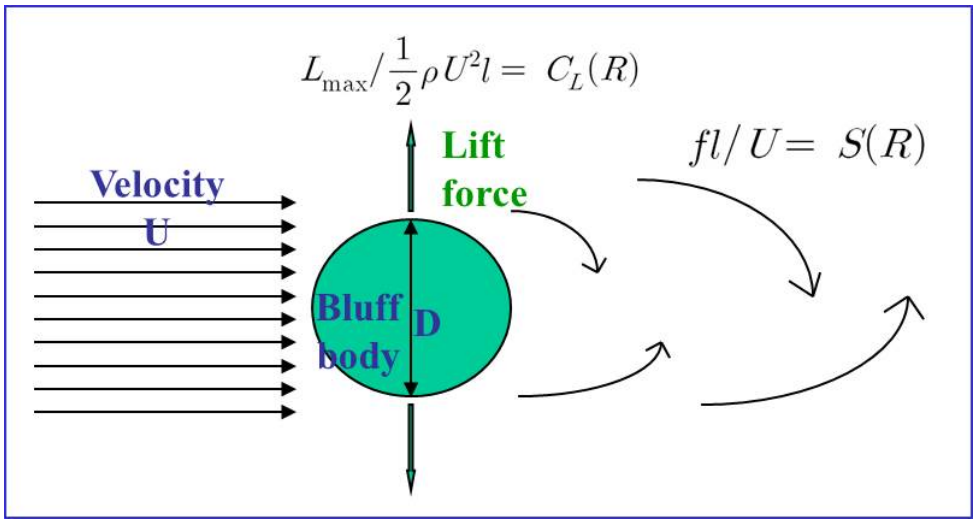

Figure 2.57 Lock-in phenomena between the lateral lift force and vortex-shedding frequency.

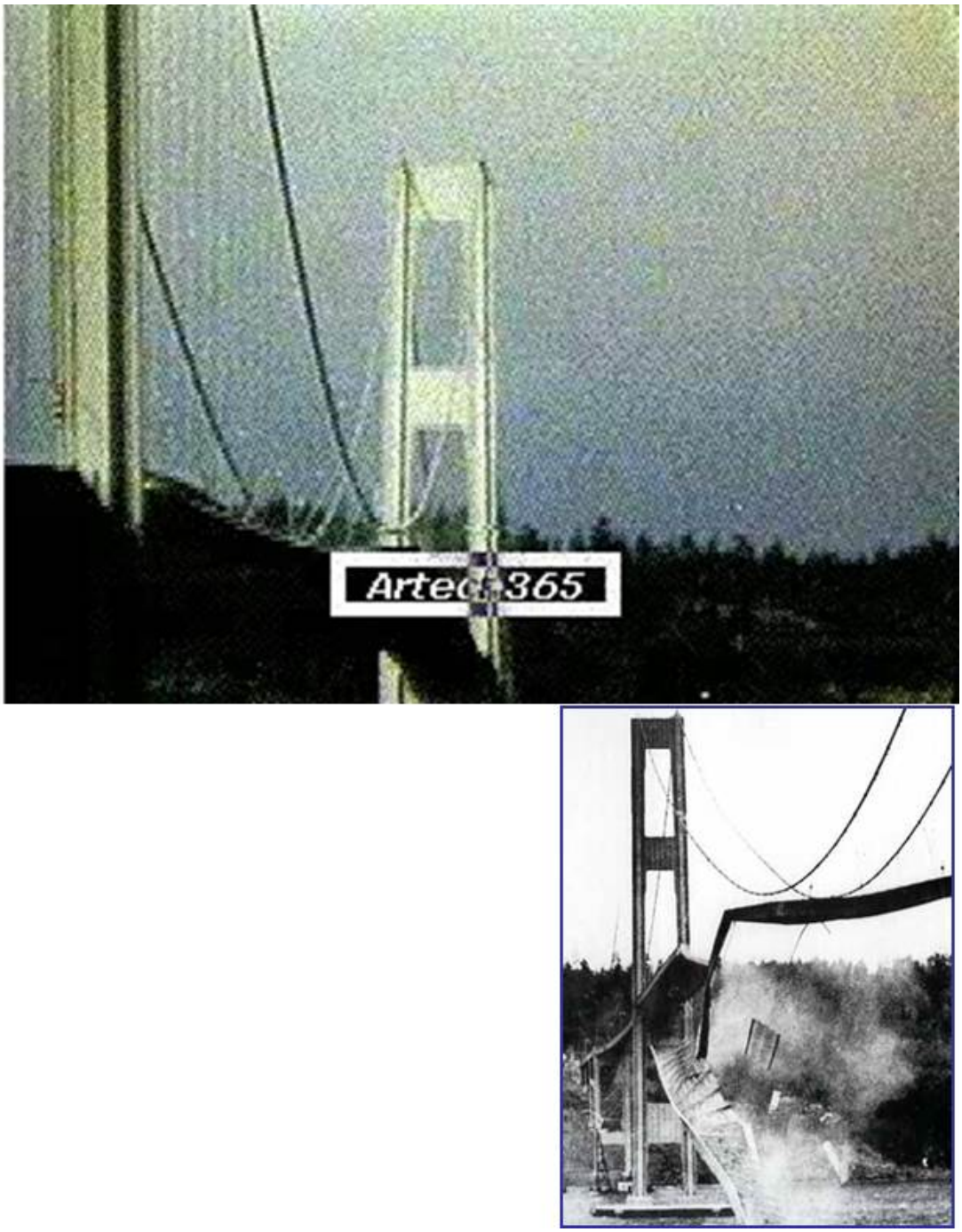

Figure 2.58 Example of VIV(Vortex Induced Vibration) phenomena: Collapse of the Tacoma bridge.

2.11 Water Waves

2.11.1 Dispersion Relation of a Progressive Wave in Infinite Depth

- Periodic progressive wave system is characterized by amplitude A, wavelength λ , period T (or frequency $\omega = 2\pi/T$)
- Phase velocity: $V_p \equiv \omega/k \equiv \omega\lambda/2\pi$
  - $\eta(x,t) = A\cos(kx - \omega t + \epsilon)$ with $\epsilon =$ phase
  - Wave number $k \equiv 2\pi/\lambda = \omega/V_p$

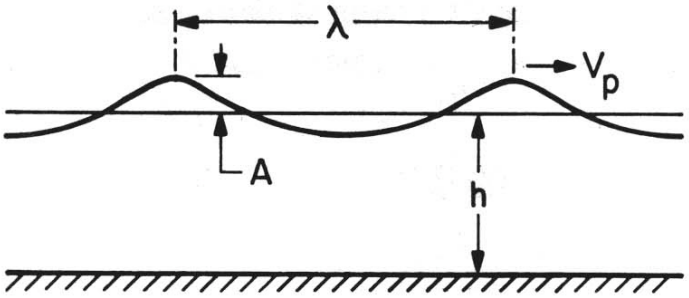

2.1
Sketch of a periodic progressive wave in a fluid of mean depth *h*. Note that λ is the wavelength, *A* the wave amplitude, and the wave translates with phase velocity V_p in the direction shown by this vector.

Figure 2.59 Sketch of a periodic progressive wave in a fluid of mean depth h. (From Newman 1977)

- Wave period T must be a function of amplitude A, wavelength λ , density ρ , gravitational acceleration g, and depth h.
- Frequency ω and phase velocity V_p can be replaced by period T and wavelength λ .
- The density of fluid ρ is only one parameter containing units of mass, so that the parameter ρ can be deleted from the dimensional analysis.

- Five dimensional parameters (T, λ, A, g, h) remain and a nondimensional form for period T is

$$\boxed{T(g/\lambda)^{1/2} = f(A/\lambda, h/\lambda)} \tag{2.50}$$

where nondimensional amplitude ratio A/λ is analogous to the maximum pendulum swing angle θ_0 in pendulum .

- If the wave amplitude is sufficiently small compared to the wavelength, a *linearized* result is

$$\boxed{T(g/\lambda)^{1/2} \simeq f(0, h/\lambda)} \quad \text{for } A/\lambda \ll 1 \tag{2.51}$$

- If fluid depth is very large compared to the wavelength (as in *deep ocean*), the form is

$$\boxed{T(g/\lambda)^{1/2} \simeq f(A/\lambda, \infty)} \quad \text{for } \lambda/h \ll 1 \tag{2.52}$$

- For small amplitude waves in deep water, i.e., $A/\lambda \ll 1$ and $\lambda/h \ll 1$,

$$\boxed{T(g/\lambda)^{1/2} \simeq f(0, \infty) = constant} \tag{2.53}$$

where *constant (C)* cannot be determined from dimensional analysis. From a more complicated analysis, [16] we have $C = (2\pi)^{1/2}$ and conse-

[16] By using the potential flow analysis (inviscid irrotational flow analysis), we have the linearized result for plane progressive waves in deep water: (see Newman (1977), Chapter 6 for details)

$$\phi = \frac{gA}{\omega} e^{ky} \sin(kx - \omega t). \tag{2.54}$$

With the velocity potential ϕ, the linearized free surface boundary condition $\frac{\partial^2 \phi}{\partial t^2} + g\frac{\partial \phi}{\partial y} = 0$ is applied to have $\omega^2 = gk$, from which the constant $C = (2\pi)^{1/2}$ can be derived. The corresponding velocity field $\underline{u} = (u, v)$ is, then,

$$u = \frac{\partial \phi}{\partial x} = \omega A e^{ky} \cos(kx - \omega t), \quad v = \frac{\partial \phi}{\partial y} = \omega A e^{ky} \sin(kx - \omega t). \tag{2.55}$$

An instantaneous velocity field is depicted in Figure 2.60 .

quently

$$\begin{aligned} & T(g/\lambda)^{1/2} = (2\pi)^{1/2} \\ \Longrightarrow\ & (2\pi/\omega)(g/\lambda)^{1/2} = (2\pi)^{1/2} \\ \Longrightarrow\ & \omega = \left(\frac{2\pi g}{\lambda}\right)^{1/2} \\ \Longrightarrow\ & \omega^2 = gk \end{aligned} \tag{2.56}$$

The phase velocity

$$\begin{aligned} V_p\ (\equiv \omega/k \equiv \lambda/T) &= g/\omega \\ \text{or} &= (g/k)^{1/2} \\ \text{or} &= (g\lambda/2\pi)^{1/2} \end{aligned} \tag{2.57}$$

- Period T is proportional to $\lambda^{1/2}$ and from $V_p \equiv \lambda/T$, the phase velocity V_p is proportional to $\lambda^{1/2}$:

$$V_p = \sqrt{\frac{g}{k}} = \sqrt{\frac{\lambda g}{2\pi}} \tag{2.58}$$

  - Dispersive relation: water waves of different wavelengths or periods will propagate at different phase velocities. See Table 2.2 for example.

Table 2.2 Dispersive relation of deep water ocean waves

Wavelength λ	Phase Velocity V_p
30 m	24 km/h
150 m	56 km/h
300 m	80 km/h

  - Long waves will travel faster than short waves, and a spectrum of waves will constantly change its appearance.
  - The monochromatic wave system is an exception because only one wavelength is present.

- Velocity field for plane progressive waves in deep water

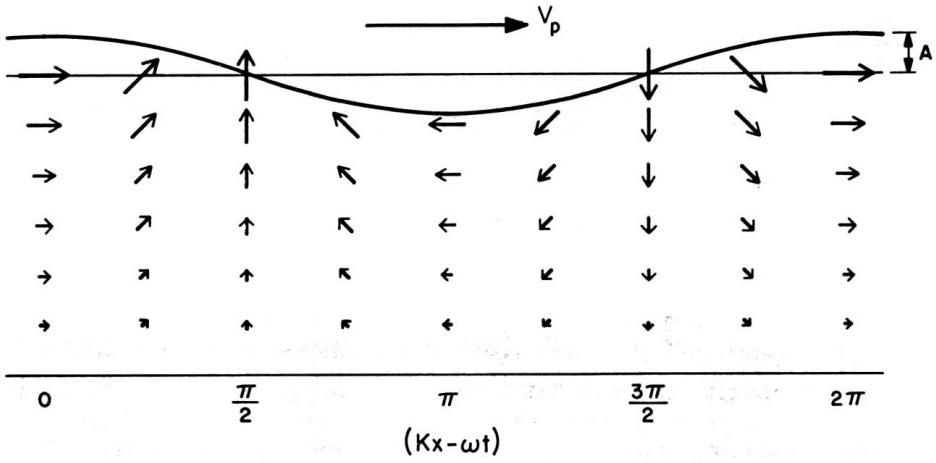

6.1
Velocity field of a plane progressive wave in deep water. The phase velocity and fluid velocity vectors are to the same scale. This example corresponds to the case $A/\lambda = 1/20$.

Figure 2.60 Velocity field of a plane progressive wave in deep water. (From Newman 1977)

2.11.2 Secondary Effects: Viscosity, Air, Surface tension, Nonlinear Effects

- The water viscosity exerts a small dissipative effect, typical water waves can travel for hundreds or thousands of wavelengths.
  A non-dimensional viscosity ratio:

$$\frac{\text{Viscous Force}}{\text{Gravitational Force}} = \frac{\mu\, V_p\, \lambda}{\rho\, g\, \lambda^3} = \frac{\nu\sqrt{g\,\lambda}}{g\,\lambda^2} = \frac{\nu}{g^{1/2}\,\lambda^{3/2}} \simeq 3 \times 10^{-7} \quad \text{for } \lambda = 1m \text{ (for example)} \tag{2.59}$$

- Air effects can be ignored on water waves since the air density is about 1/800 of the water density.

$$\frac{\rho_{\text{air}}}{\rho_{\text{water}}} \sim O\left(10^{-3}\right) \tag{2.60}$$

Exception is the process by which ocean waves are generated by the wind.

- Surface Tension effects
  - Surface tension is due to the inter molecular forces attraction forces in the fluid: Surface tension σ = Tension force/Length = Surface energy/Area. For a water-air interface, it is about 0.07 Newton/m. [17]
  - On an interface surface between two fluids (i.e., stratified fluids), the continuity of the stress:

$$\underline{n} \cdot \left(\underline{\underline{T}}^{(i)} - \underline{\underline{T}}^{(o)} \right) = \sigma \left(\frac{1}{R_1} + \frac{1}{R_2} \right) \underline{n} \tag{2.61}$$

    where $\underline{\underline{T}}$ is the stress tensor, $\underline{n}$ is the unit normal vector, R_1 and R_2 are the principal radii of curvature of the interface.
  - When the two fluids are stationary, only the pressure terms:

$$\underline{n} \cdot \left(p^{(i)} - p^{(o)} \right) = \sigma \left(\frac{1}{R_1} + \frac{1}{R_2} \right) \tag{2.62}$$

  - (Example) Two stationary fluids in 2-dimensions At the interface of two fluids, surface tension implies in a pressure jump across the interface from force equilibrium:

$$\begin{aligned} &\cos\left(\frac{d\theta}{2}\right)(\triangle p)(R\,d\theta) = 2\,\sigma \sin\left(\frac{d\theta}{2}\right) \\ &\Longrightarrow (1)(\triangle p)(R\,d\theta) = 2\,\sigma\left(\frac{d\theta}{2}\right) \Longrightarrow \triangle p = \frac{\sigma}{R} \end{aligned} \tag{2.63}$$

    We have used $\cos\left(\frac{d\theta}{2}\right) \approx 1$ and $\sin\left(\frac{d\theta}{2}\right) \approx \left(\frac{d\theta}{2}\right)$ for $d\theta \ll 1$.
  - (Example) For a stationary spherical bubble,

$$\boxed{p^{(i)} - p^{(o)} = 2\sigma/R} \tag{2.64}$$

  - A suitable nondimensional parameter is related to Weber number, e.g.,

[17] Movie: Surface tension
./mmfm_movies/5171.mov

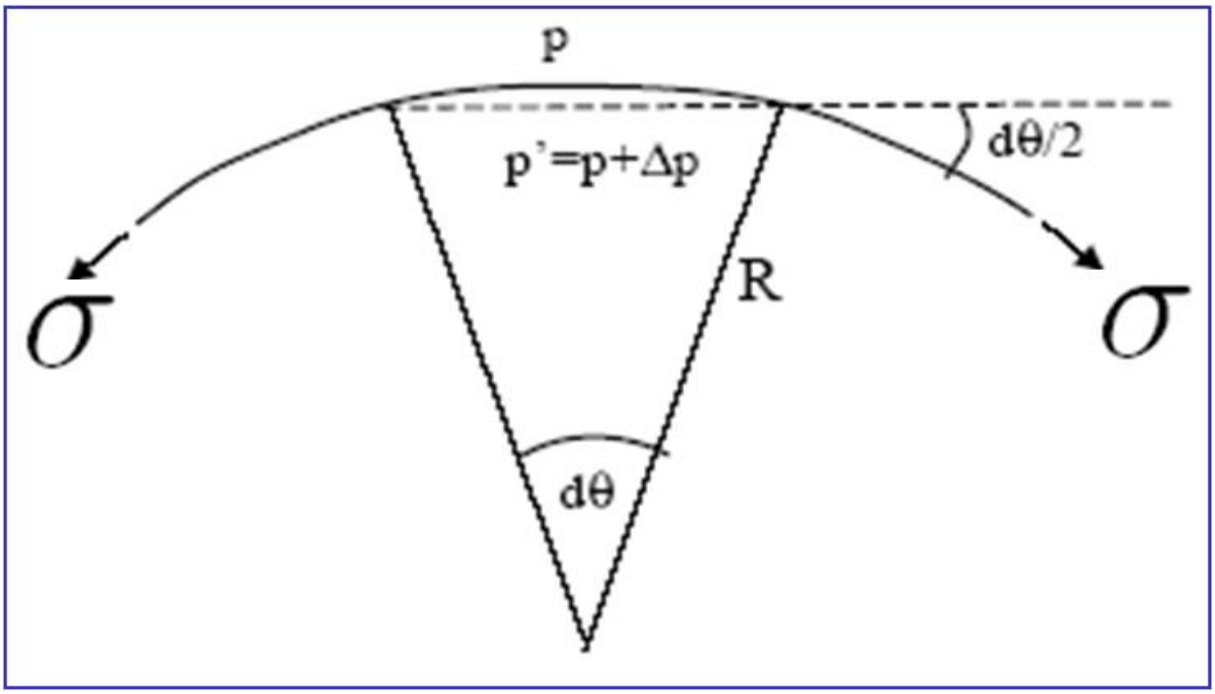

Figure 2.61 Surface tension for two stationary fluids in 2-dimensions.

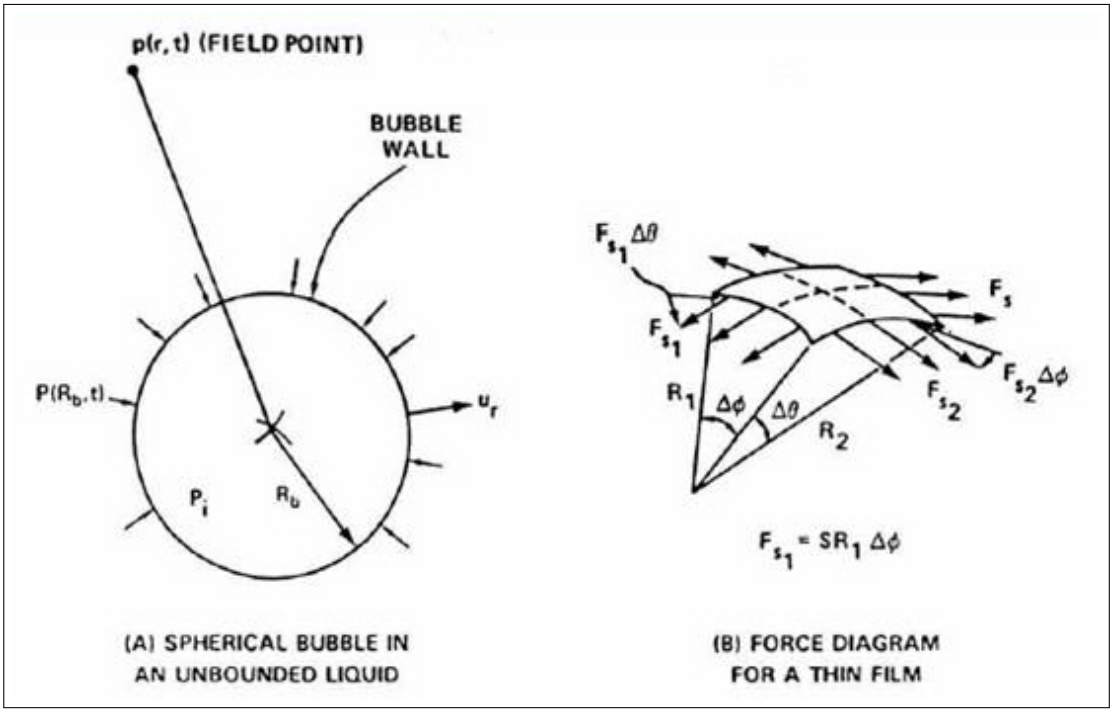

Figure 2.62 Surface tension for a stationary spherical bubble.

for water waves:

$$\frac{\text{Surface Tension Forces}}{\text{Gravitational Force}} = \frac{\sigma\lambda}{\rho\, g\, \lambda^3} = \sigma/(\rho\, g\, \lambda^2) \tag{2.65}$$
$$\sim \; O\left(10^{-6}\right) \quad \text{for } \lambda = 1\, m \text{ and } \sigma = 0.07\, N/m \text{ (for example)}$$

– Surface tension effects are negligible for long waves. However, the effects must be included in flow analysis involved in the shortest waves or micro-bubbles. [18]

- Nonlinear effects

– Steepest wave slope: 1 / 7, Max. crest angle: 120^0.

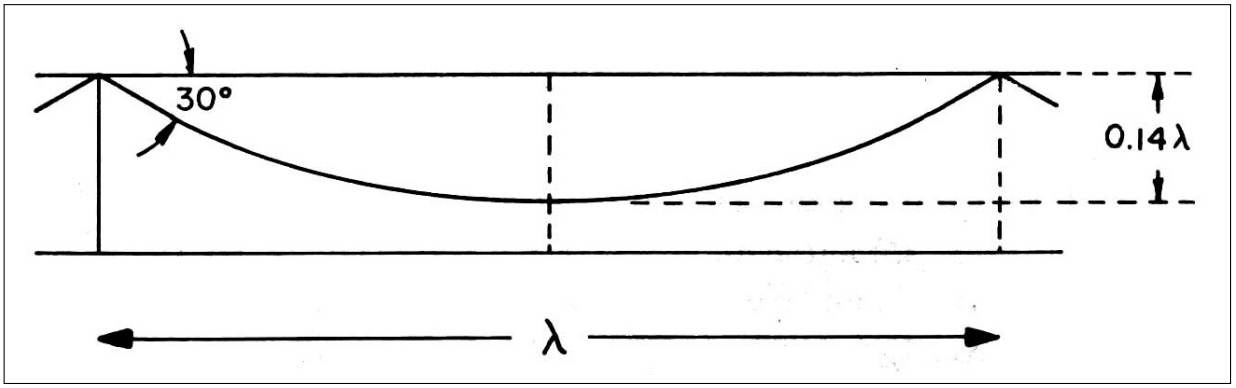

Figure 2.63 The "steepest wave" profile of nonlinear waves. (From Newman 1977)

– Wave profile

$$\eta = A\cos(kx-\omega t)+\frac{1}{2}kA^2\cos 2(kx-\omega t)+\frac{17}{24}k^3A^4\cos 2(kx-\omega t)+\cdots \tag{2.66}$$

[18] Movie: Water drop in cup; Water Strider on surface
./mmfm_movies/5444.mov ./mmfm_movies/strider.mov

Table 2.3 Relative effect of nonlinear waves

Wave Slope $2A/\lambda$	Ratio of the second term (nonlinear term) in Eq. (2.66) to the first term(linear term) $\frac{1}{2}kA$
1/80	0.0196
1/40	0.0393
1/20	0.0785

2.11.3 Solutions for Finite Depth

- The solution of the linearized potential flow problem for a plane progressive wave in finite depth: [19]

$$\phi = \frac{gA}{\omega}\frac{\cosh\{k(y+h)\}}{\cosh(kh)}\sin(kx-\omega t). \tag{2.67}$$

The corresponding velocity field $\underline{u} = (u, v)$ is, then,

$$u = \frac{\partial\phi}{\partial x} = \frac{\omega Ak}{\omega}\frac{\cosh\{k(y+h)\}}{\cosh(kh)}\cos(kx-\omega t), \tag{2.68}$$

$$v = \frac{\partial\phi}{\partial y} = \frac{\omega Ak}{\omega}\frac{\sinh\{k(y+h)\}}{\cosh(kh)}\sin(kx-\omega t). \tag{2.69}$$

An instantaneous velocity field for plane progressive waves in finite depth is shown in Figure **2.64** and Figure **2.65** (a).

- With this solution for ϕ, the linearized free surface boundary condition

[19] Like the case of a plane progressive waves in deep water, we have the linearized result. See Newman (1977), Chapter 6 for details.

$\frac{\partial^2\phi}{\partial t^2} + g\frac{\partial\phi}{\partial y} = 0$ is again applied to derive the dispersion relation. [20] This dispersion relation is an implicit equation:

$$k\,\tanh(kh) = \omega^2/g \implies V_p = \omega/k = [(g/k)\tanh(kh)]^{1/2} \tag{2.73}$$

The ratio of the phase velocity to the infinite-depth limit V_p/V_{p_∞} is plotted in Figure **2.66** , together with the depth-wavelength ratio h/λ.

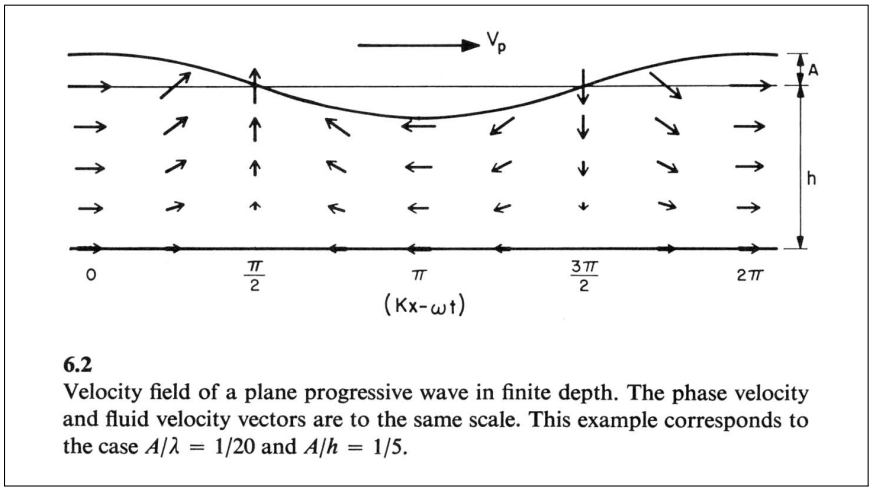

6.2
Velocity field of a plane progressive wave in finite depth. The phase velocity and fluid velocity vectors are to the same scale. This example corresponds to the case $A/\lambda = 1/20$ and $A/h = 1/5$.

Figure 2.64 Velocity field of a plane progressive wave in finite depth. (From Newman 1977)

2.11.4 Shallow Water Limit

- While the waves for infinite (even finite) water depth are dispersive, the shallow-water limit is nondispersive.

$$V_p \simeq (gh)^{1/2} \quad \text{for } kh \ll 1 \tag{2.74}$$

[20] For a fixed value of ω for all depths, i.e., $\omega = \omega_\infty$, we have

$$\omega^2 = g\,k_\infty = \frac{2\pi g}{\lambda_\infty} \implies \frac{\omega^2 h}{g} = 2\pi\frac{h}{\lambda_\infty} \tag{2.70}$$

$$V_p = \frac{\omega}{k} = \frac{\omega\,\lambda}{2\pi} \implies \frac{V_p}{V_{p_\infty}} = \frac{\lambda}{\lambda_\infty} \tag{2.71}$$

$$\omega^2 = \omega_\infty^2 \implies g\,k\,\tanh(kh) = gk_\infty$$
$$\implies \frac{\lambda}{\lambda_\infty} = \tanh\left(\frac{2\pi h}{\lambda_\infty}\frac{\lambda_\infty}{\lambda}\right) \tag{2.72}$$

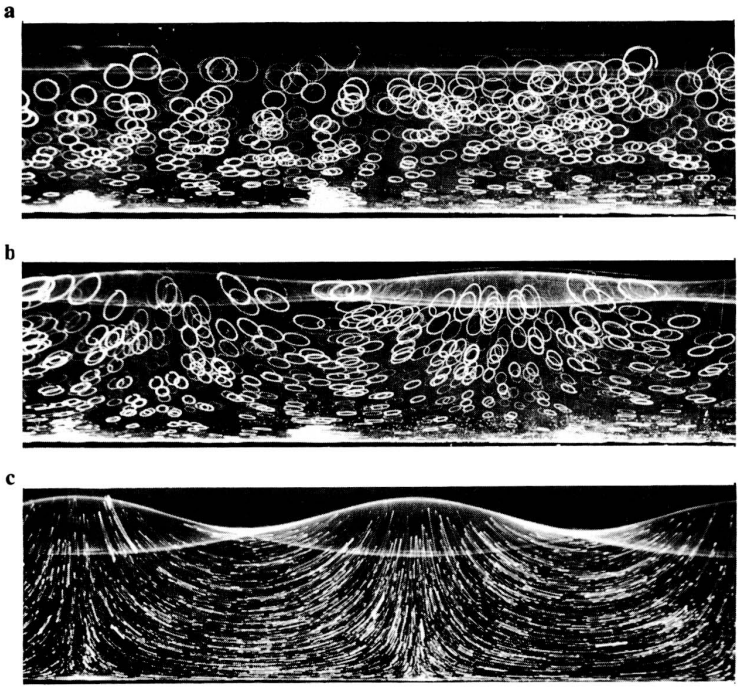

6.7
Particle trajectories in a plane progressive wave (a), a partial reflected wave (b), and a standing wave (c). These correspond respectively to a reflection coefficient of 0, 0.38, and 1.0 in equation (56). Note that the reflection coefficient can be measured from the maximum and minimum of the envelope, using (56). These photographs are based on time exposures, and are reproduced from a more extensive series of observations made by Ruellan and Wallet (1950).

Figure 2.65 Particle trajectories of a plane progressive wave in finite depth. (From Newman 1977)

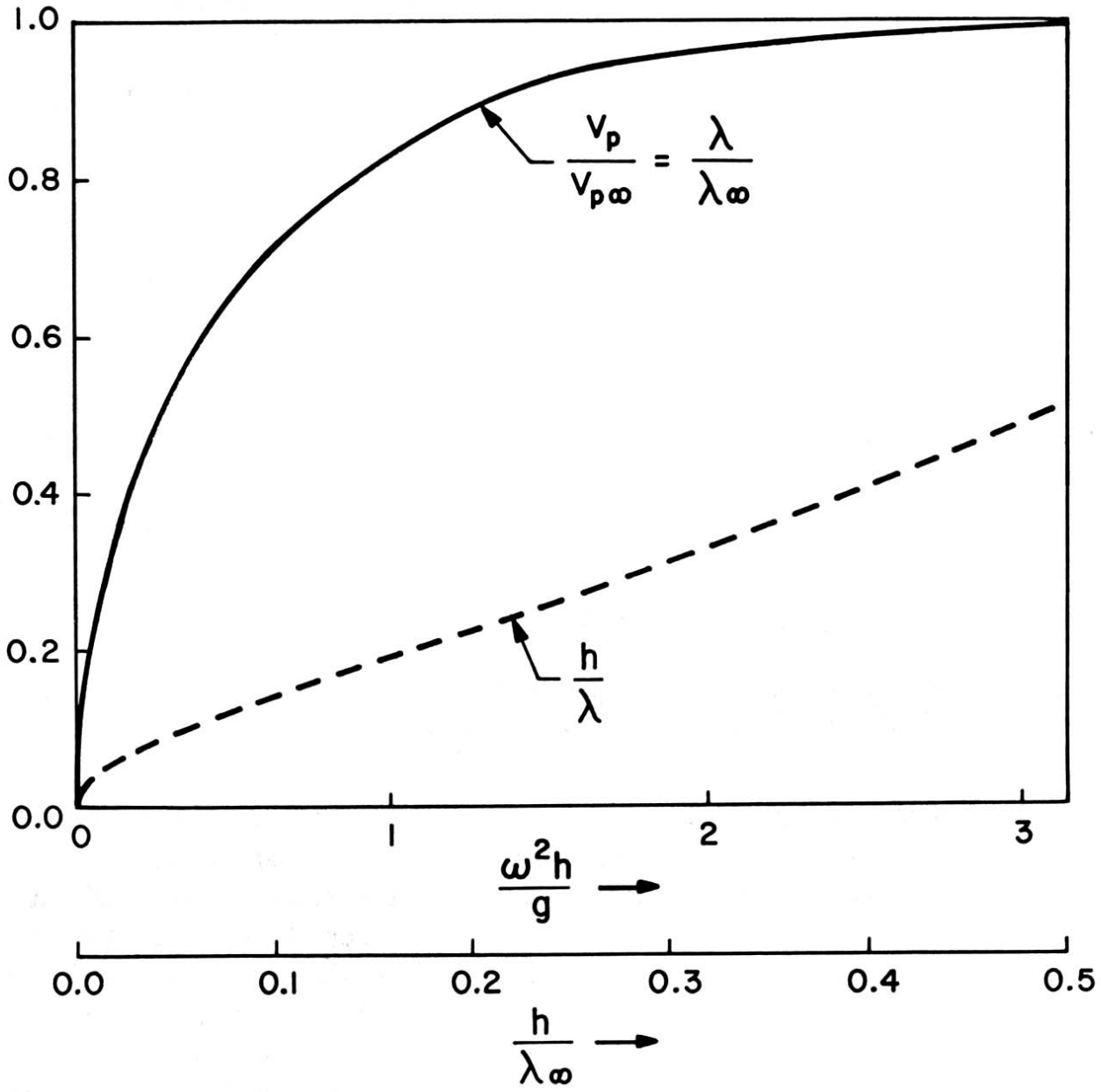

6.3
Phase velocity, wavelength, and depth ratios of a plane progressive wave. The deep-water limiting values $V_{p\infty}$ and λ_∞ can be determined from equation (18).

Figure 2.66 Phase velocity, wave length, and depth ratios of a plane progressive wave in finite depth. (From Newman 1977)

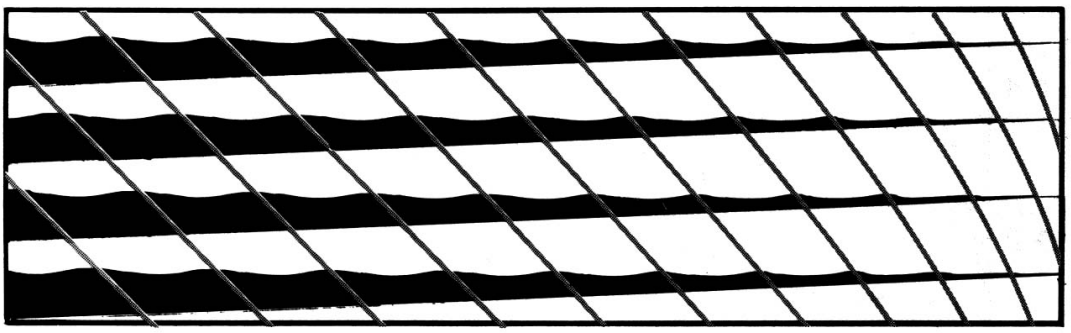

6.4
Sequence of photographs, taken through the transparent side of a wave tank, showing the propagation of plane progressive waves into shallow water. The water is darkened with dye, and the waves are generated by an oscillating vertical wedge at the left side of the tank. Each wave crest is connected in successive photographs by gray diagonal lines, which advance in time with the phase velocity. Both the phase velocity and wavelength are reduced as the waves propagate toward the shallow end of the tank. The interval between successive photographs is 0.25 s, and the wave period is 0.4s. The water depth is 0.11 m at the left end, decreasing to zero at the right. Nonlinear distortion occurs when the depth is comparable to the wave height.

Figure 2.67 Propagation of plane progressive waves into shallow water. (From Newman 1977)

- Example: Speed of a Tsunami (Propagation of the Indian Ocean Tsunami of 26 December 2004)

  - The wave length is order of 200 km and the water depth is order of 5 km, so that the shallow water limit can be applied.
  - The wave speed would be about 200 m/s (720 km/hr) in average sense.
  - At this speed it took only about 15 minutes to reach the nearest Sumatran coast and 28 minutes the city of Banda Aceh.

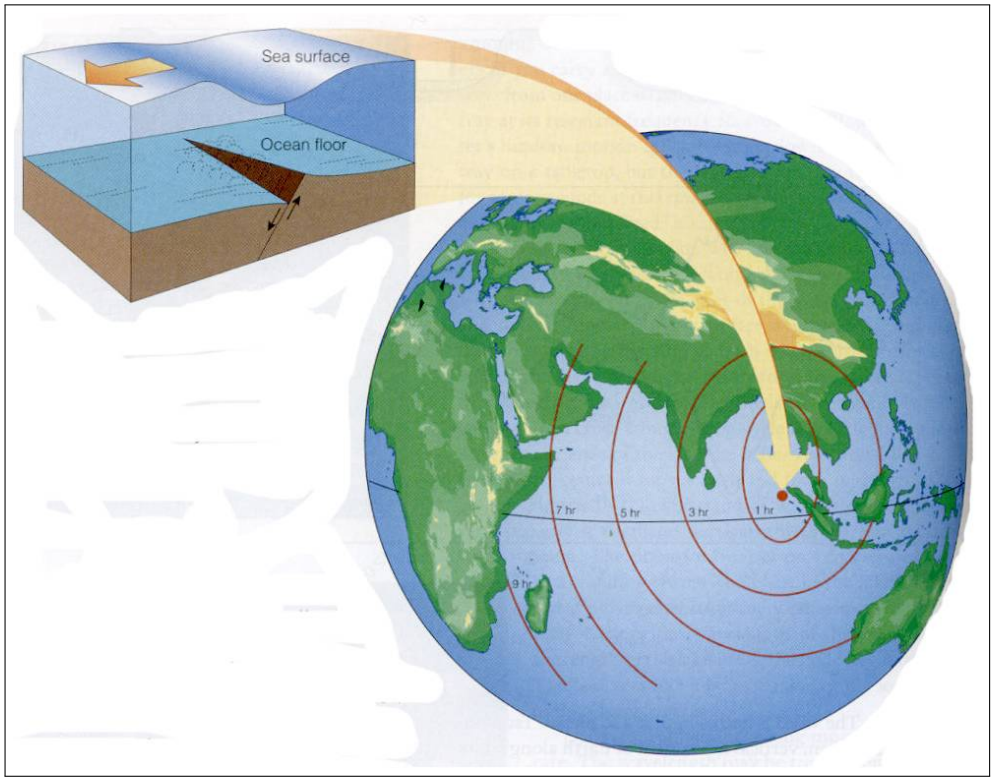

Figure 2.68 Propagation of the Indian Ocean Tsunami of 26 December 2004. (From Garrison 2007)

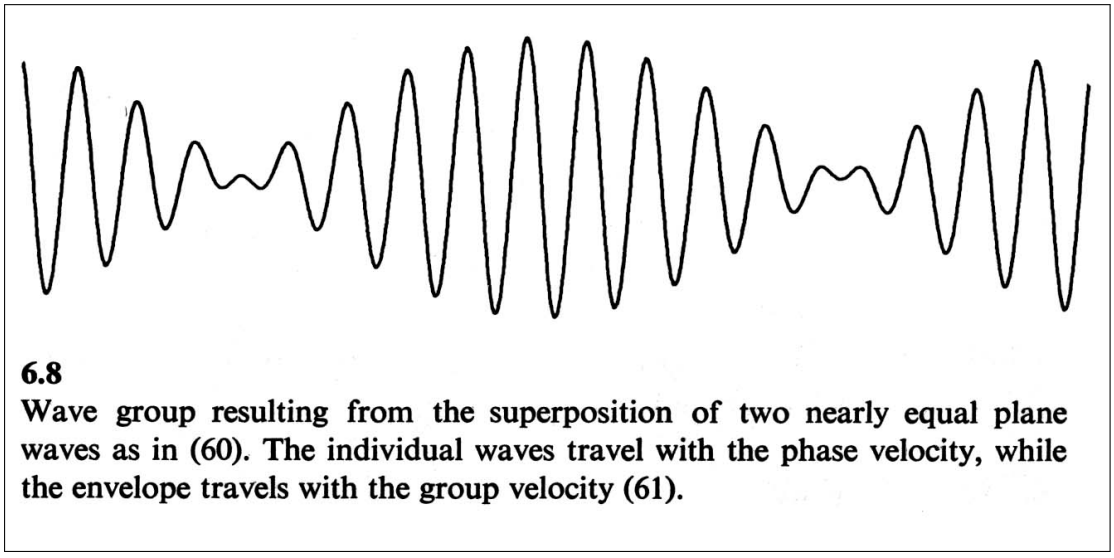

6.8
Wave group resulting from the superposition of two nearly equal plane waves as in (60). The individual waves travel with the phase velocity, while the envelope travels with the group velocity (61).

Figure 2.69 Wave group resulting from the superposition of two nearly equal plane waves. (From Newman 1977)

2.11.5 Superposition of Waves: Group Velocity

- The individual waves travel with the phase velocity, while the envelope travels with the group velocity V_g:

$$V_g \equiv \frac{\delta\omega}{\delta k} = \frac{d\omega}{dk} = \left(\frac{1}{2} + \frac{kh}{\sinh(2kh)}\right) V_p \tag{2.75}$$

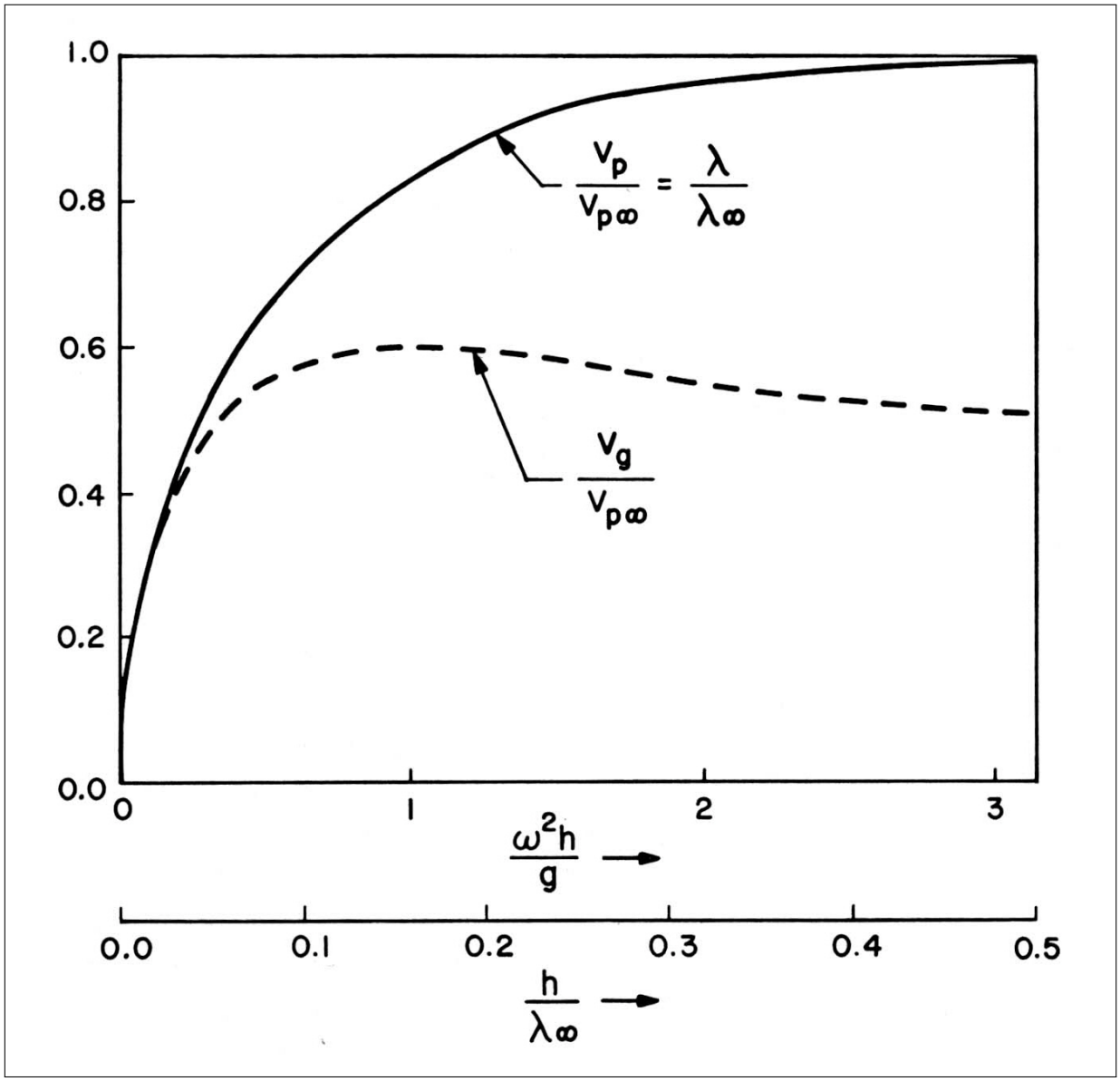

Figure 2.70 Phase velocity and group velocity ratios for a plane progressive wave as a function of the water depth. (From Newman 1977)

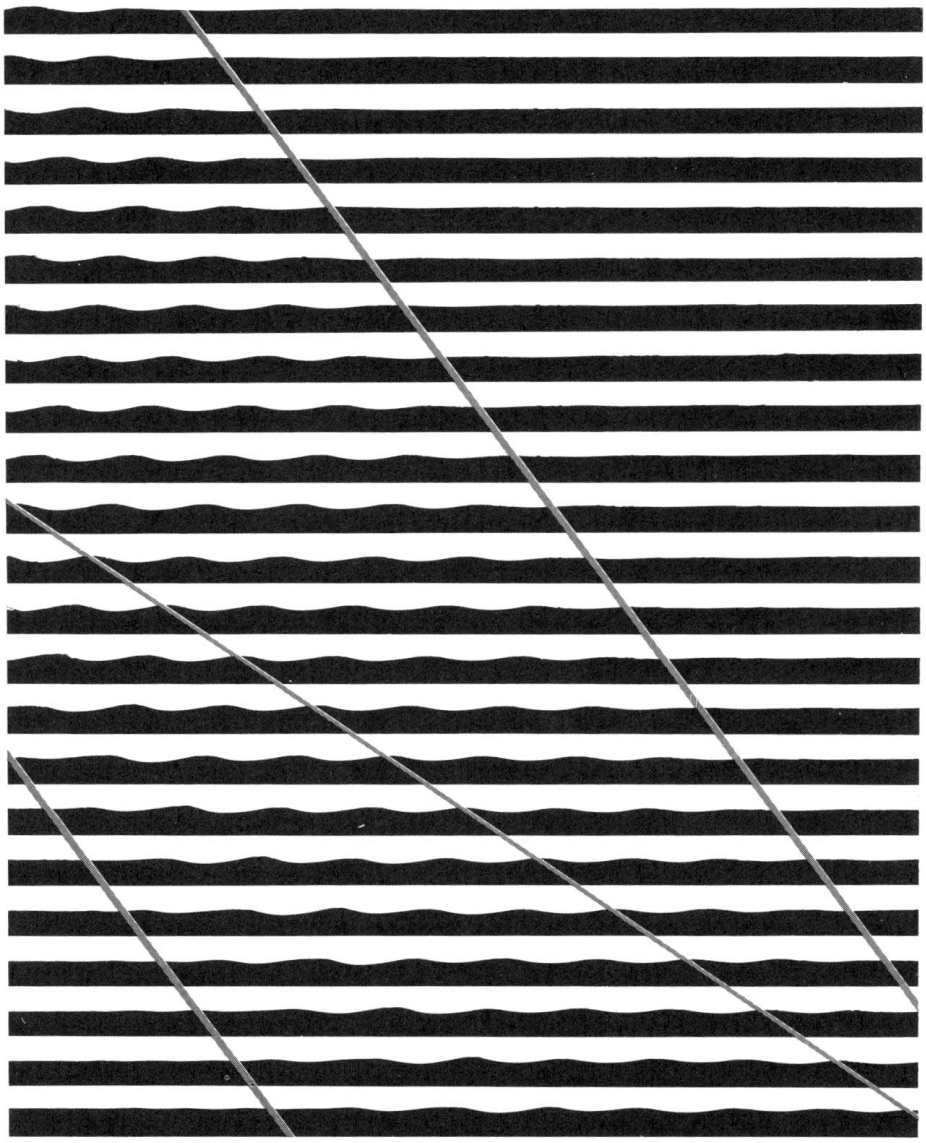

6.10
Sequence of photographs showing a plane progressive wave system advancing into calm water. The water is darkened with dye, and the lower half of the water depth is not shown. The wave energy is contained within the heavy diagonal lines, and propagates with the group velocity. (The boundaries of the wave group diffuse slowly with time, due to dispersion.) The position of one wave crest is connected in successive photographs by the light line, which advances with the phase velocity. Each wave crest moves with the phase velocity, equal to twice the group velocity of the boundaries. Thus each wave crest vanishes at the front end and, after the wavemaker is turned off, arises from calm water at the back. The interval between successive photographs is 0.25 s and the wave period is 0.36 s. The wavelength is 0.23 m and the water depth is 0.11m.

Figure 2.71 Sequence of photograpghs showing the phase velocity and the group velocity for a plane progressive wave system advancing into calm water. (From Newman 1977)

2.11.6 Wave Force on a Stationary Body

- Unsteady wave force F on a restrained body
  - Magnitude depends on 9 dimensional quantities

$$F = f(\rho, g, \nu, A, \lambda, \beta, h, l, t) \tag{2.76}$$

  - Nondimensional force with 7 parameters

$$\frac{F}{\rho\, g\, l^3} = C_F(A/\lambda, h/\lambda, l/\lambda, \beta, R, \omega t) \tag{2.77}$$

    Here wave frequency $\omega(\equiv\ 2\pi/T)$ is related to $g, A, h,$ and λ by $T(g/\lambda)^{1/2} = f(A/\lambda, h/\lambda)$.

- In model test the Reynolds number can not be scaled properly, since it follows that $R \propto l^{3/2}$, namely,

$$R = \omega\, A\, l/\nu \sim \frac{1}{\lambda^{1/2}} A\, l \sim \left(\frac{l}{\lambda}\right)^{1/2} \frac{A}{l}\, l^{3/2} \sim l^{3/2}. \tag{2.78}$$

- Relative magnitude of viscous forces and inertial forces as in the impulsively started cylinder problems before,

$$\frac{C_F(R, \infty)}{C_F(\infty, U\, t/l)} = \frac{\frac{1}{2}\rho\, U^2 l^2\, C_D(R)}{m_{11}\, \dot{U}} \propto U^2/\dot{U}\, l \tag{2.79}$$

  With U replaced by ωA and the fluid acceleration $\dot{U}$ by $\omega^2 A$, the ratio of viscous forces to inertial forces is

$$U^2/\dot{U}\, l = A/l \tag{2.80}$$

- Let us consider 3 cases:
  - Case of a large structure or a ship where the ratio A/l is small.
  - Case of a small body where the ratio A/l is large.
  - The intermediate case where the ratio A/l is of order one.

(1) Case of Large Structure (small A/l)

- Viscous force is negligible. Additionally, if wave amplitude A is assumed to be small compared to the wavelength λ and depth h, then the linearized fluid motion is sinusoidal in time:

$$C_F = C_{F0} \cos(\omega t + \epsilon) \tag{2.81}$$

  where ϵ is a phase angle, C_{F0} a force coefficient, and both depend on h/λ, l/λ, and β but not on time.

- Decomposition into velocity and acceleration parts:

$$C_F = C_M \dot{U} + C_d U \tag{2.82}$$

  where C_M and C_d are *apparent mass* and *apparent damping* coefficients, respectively.

- For body that is small compared with wavelength, $l/\lambda \ll 1$, i.e., if $A \ll l \ll \lambda$, then $C_M = (m_{11} + \rho \mathbf{V})/(\rho g l^3)$, $C_d \simeq 0$, and thus

$$\boxed{F \simeq (m_{11} + \rho \mathbf{V}) \dot{U}} \tag{2.83}$$

(2) Case of Small Structure (large A/l)

- Viscous force is dominant, and acts in the same direction as the fluid velocity:

$$\boxed{F = \frac{1}{2} \rho l^2 U |U| C_D(R)} \tag{2.84}$$

- For bluff bodies, viscous drag coefficient is not sensitive to the Reynolds number.

(3) Intermediate Case ($A/l \sim O(1)$)

- Viscous and inertial effects are of comparable magnitude. Morison's formula

$$\boxed{F = (m_{11} + \rho \mathbf{V}) \dot{U} + \frac{1}{2} \rho l^2 U |U| C_D(R)} \tag{2.85}$$

2.11.7 Body Motions in Waves

- For heave motion of an unrestrained (freely floating) body in waves, nondimensional form with physical parameters:

$$y/A = f(A/\lambda, h/\lambda, l/\lambda, \beta, R, \omega\, t, m/\rho\, l^3) \tag{2.86}$$

  - Since the body mass m is equal to the displaced mass of water $m = \rho \times$ (volume), the last parameter is equal to (volume)$/l^3$.
  - The mass parameter is deleted since it is independent of length scale for a prescribed body shape.
  - Again, the Reynolds number cannot be scaled properly. Its dependence is a key source of fundamental problems for model testing.

- If the viscosity is neglected, and thus deleting the Reynolds number parameter R:

$$y/A = f(A/\lambda, h/\lambda, l/\lambda, \beta, \omega\, t) \tag{2.87}$$

- If the wave amplitude is small compared to the wavelength and depth (namely, if $A/\lambda \ll 1$ and $A/h \ll 1$), nonlinear effects can be then neglected.
  The linearized approximation gives

$$y/A = f(0, h/\lambda, l/\lambda, \beta, \omega\, t) = f_0(h/\lambda, l/\lambda, \beta)\cos(\omega\, t + \epsilon) \tag{2.88}$$

  where for a prescribed body shape, the amplitude f_0 and phase angle ϵ depend only on h/λ, l/λ and β.

- In deep water, there is no dependence on depth ratio h/λ.

$$y/A = f_0(\infty, l/\lambda, \beta)\cos(\omega\, t + \epsilon) \tag{2.89}$$

- For axisymmetric bodies, the heave response is independent of the angle of incidence β.

$$y/A = f_0(\infty, l/\lambda)\cos(\omega\, t + \epsilon) \tag{2.90}$$

- The heave-amplitude ratio for a slender spar buoy of draft T in deep water where the draft T corresponds to the length scale l (see Figure **2.72**):
  (a) In the limit of $\lambda/T \gg 1$, $f_0 \to 1$.
    * Very small body moves with the same velocity as the fluid.
  (b) In the limit of $\lambda/T \ll 1$, $f_0 \to 0$.
  (c) At wavelength of $\lambda/T \approx 6$,
    * A sharp resonance occurs, analogous to the motion of weakly-damped oscillator.
    * This severe resonant motion is a consequence of vertical slenderness.

2.11.8 Ship Motions in Waves

- Additional physical parameter: ship speed U
  – Corresponding Froude number: $F_n = U/(g\,l)^{1/2}$.
- Viscous effects are negligible and wave amplitude is assumed to be small for linearization.
- Heave-amplitude ratio

$$y/A = f_0\left(h/\lambda, l/\lambda, \beta, U/(g\,l)^{1/2}\right)\cos(\omega\,t + \epsilon) \tag{2.91}$$

- Typical Roll and Pitch Response
  – Froude number $F_n = 0.23$.
  – Ship speed: $U = 25$ knots.
  – Roll response is similar to the spar buoy response.
  – For stern quartering sea, the peak values of roll response appear due to continuously tracing (following) waves with ship.

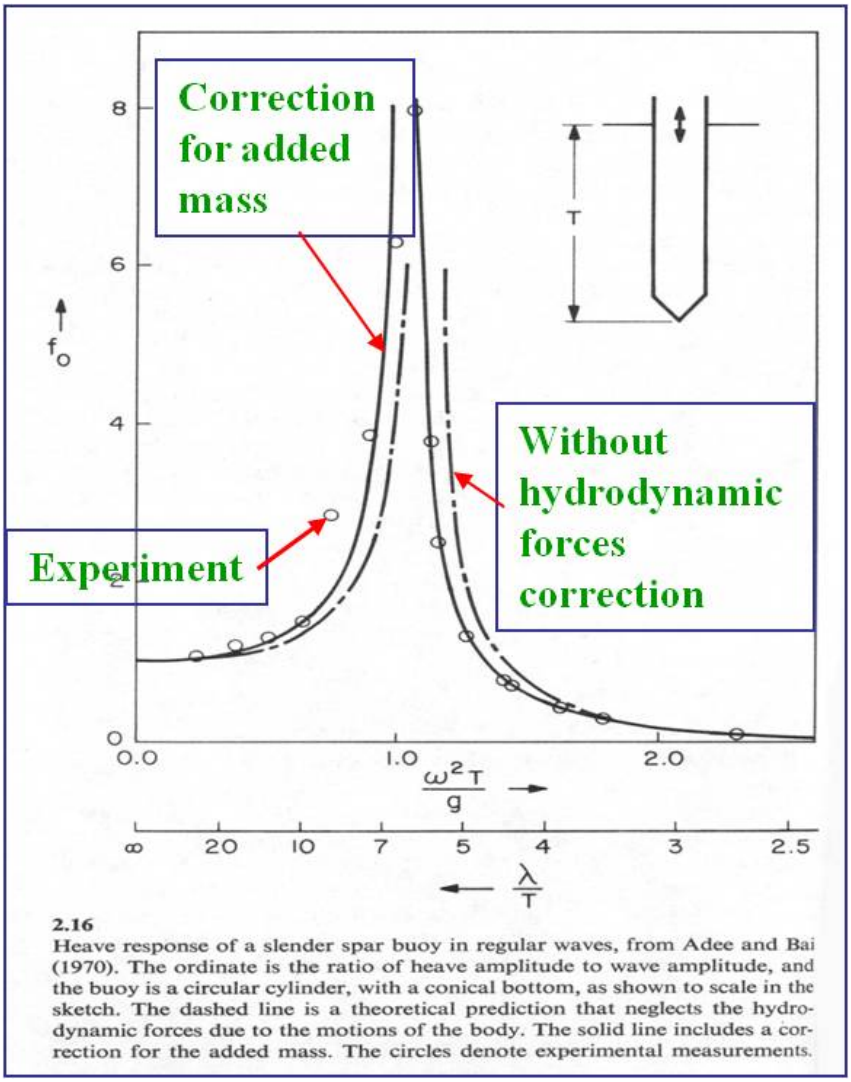

2.16
Heave response of a slender spar buoy in regular waves, from Adee and Bai (1970). The ordinate is the ratio of heave amplitude to wave amplitude, and the buoy is a circular cylinder, with a conical bottom, as shown to scale in the sketch. The dashed line is a theoretical prediction that neglects the hydrodynamic forces due to the motions of the body. The solid line includes a correction for the added mass. The circles denote experimental measurements.

Figure 2.72 Heave response of slender spar buoy in regular waves. (From Newman 1977)

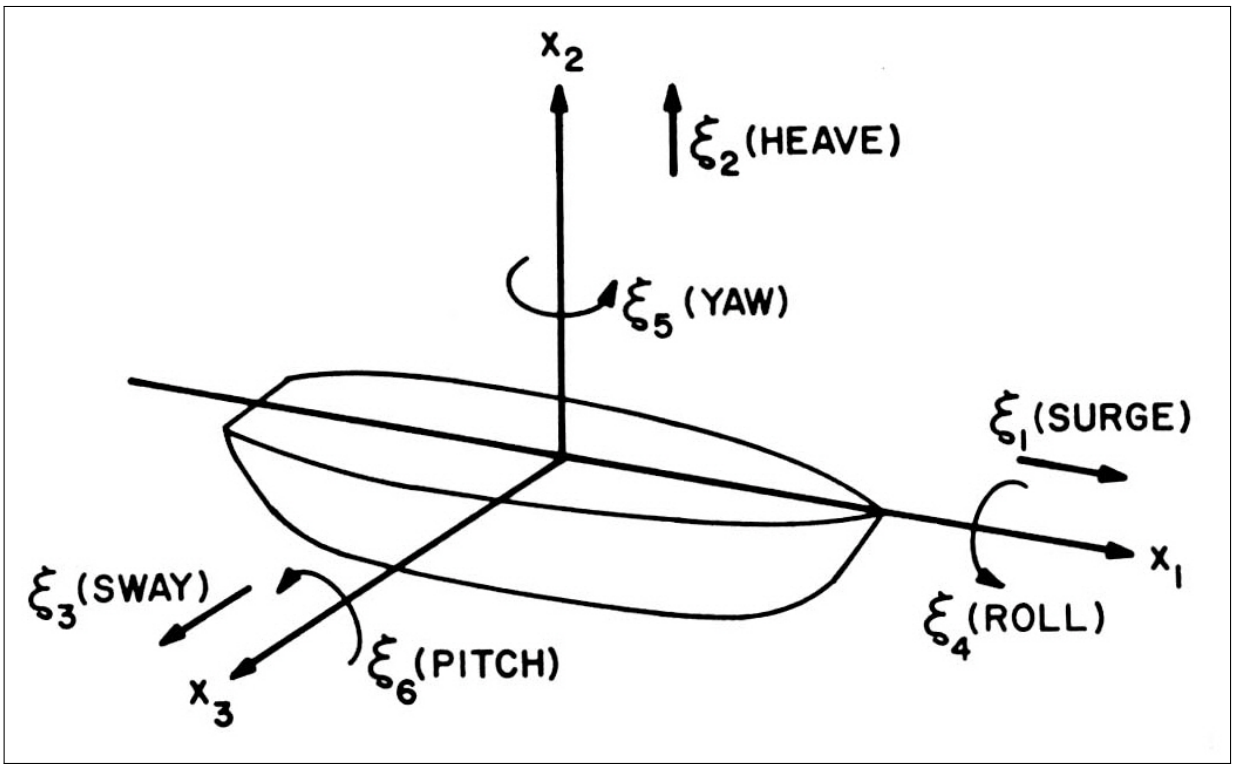

Figure 2.73 Ship motions in 6 degrees of freedom. (From Newman 1977)

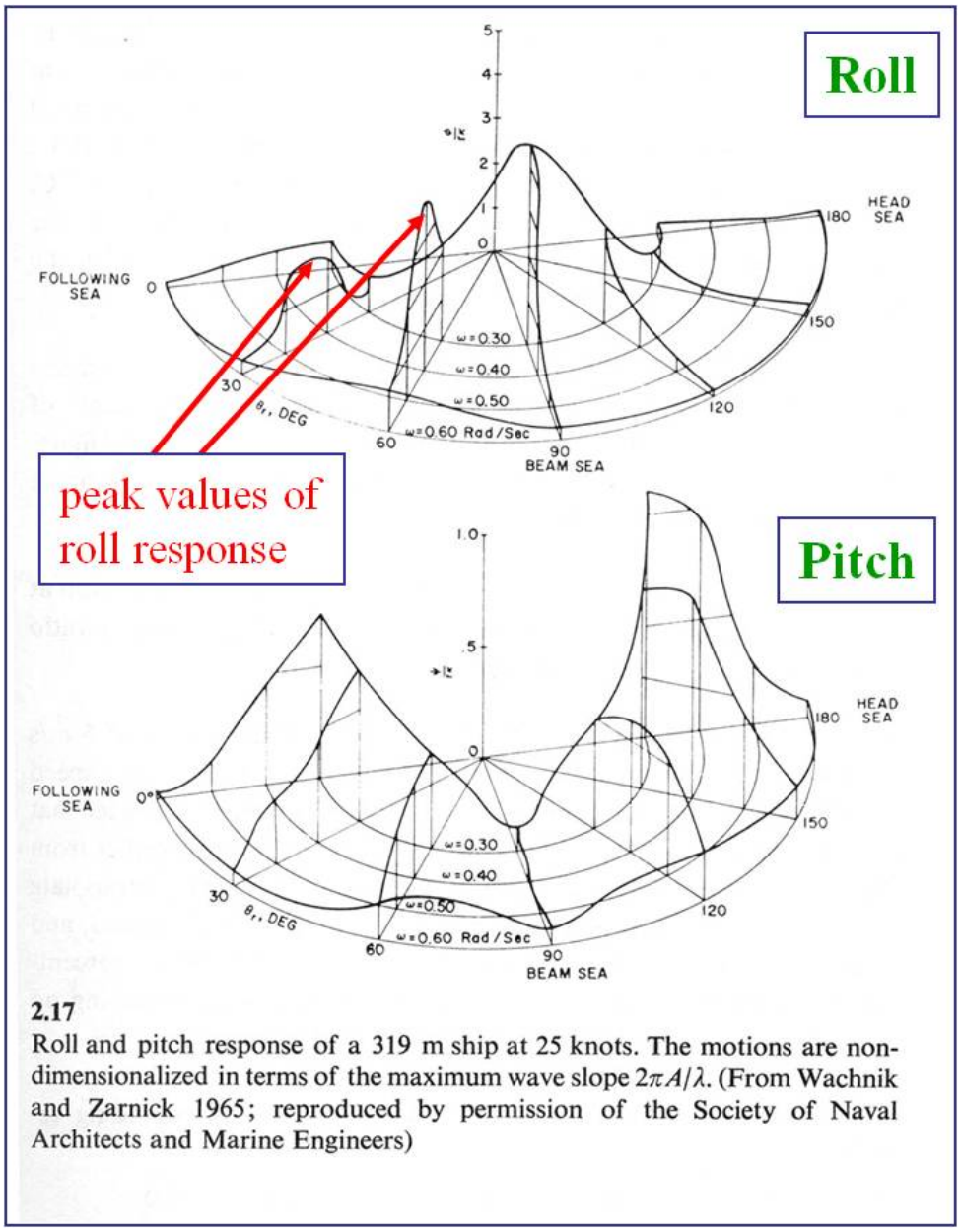

2.17
Roll and pitch response of a 319 m ship at 25 knots. The motions are non-dimensionalized in terms of the maximum wave slope $2\pi A/\lambda$. (From Wachnik and Zarnick 1965; reproduced by permission of the Society of Naval Architects and Marine Engineers)

Figure 2.74 Roll and pitch response of a 319 m ship. (From Newman 1977)